2016•2017

Faculteit Industriële ingenieurswetenschappen

master in de industriële wetenschappen: nucleaire technologie

Masterthesis

Fabrication and calibration of superheated droplet detectors (SDDs) for neutron dosimetry

PROMOTOR :

Prof. dr. Brigitte RENIERS

PROMOTOR :

Phd. Marijke DE SAINT-HUBERT

Stef Mommen

Scriptie ingediend tot het behalen van de graad van master in de industriële wetenschappen: nucleaire technologie, afstudeerrichting nucleaire technieken / medisch nucleaire technieken

De transnationale Universiteit Limburg is een uniek samenwerkingsverband van twee universiteiten in twee landen: de Universiteit Hasselt en Maastricht University.

Universiteit Hasselt | Campus Diepenbeek | Agoralaan Gebouw D | BE-3590 Diepenbeek

Universiteit Hasselt | Campus Hasselt | Martelarenlaan 42 | BE-3500 Hasselt

2016 • 2017

Faculteit Industriële ingenieurswetenschappen

master in de industriële wetenschappen: nucleaire technologie

Masterthesis

Fabrication and calibration of superheated droplet detectors (SDDs) for neutron dosimetry

PROMOTOR :

Prof. dr. Brigitte RENIERS

PROMOTOR :

Phd. Marijke DE SAINT-HUBERT

Stef Mommen

Scriptie ingediend tot het behalen van de graad van master in de industriële wetenschappen: nucleaire technologie, afstudeerrichting nucleaire technieken / medisch nucleaire technieken

UHASSELT

KU LEUVEN

Acknowledgements

In the search for a subject for a master's thesis, I contacted dr. Sarah Baatout of the SCK•CEN in Mol. She brought me in further contact with PhD Lara Struelens and PhD Marijke De-Saint Hubert who introduced me to the idea of using a bubble dosimeter to assess secondary neutron doses in anthropomorphic phantoms during proton radiotherapy. I was introduced to the Research in Dosimetric Applications (RDA) unit and was able to use their knowledge and facilities to accomplish my master's thesis.

Therefore, I would like to thank everyone who has helped me to achieve this. Above all, I would like to thank my mentor or external promotor PhD Marijke De Saint-Hubert and internal promotor prof. dr. Brigitte Reniers for the support on my master's thesis, for their patience, effort and sharing of their knowledge and experience. A special thanks goes to Prasanna Mondal for the many emails about his experience with fabricating SDDs.

Furthermore, I would like to thank PhD Olivier Van Hoey for the irradiations at BR1 and temporary follow-up, Jo Boekx for the optimisation of the LabVIEW program and Bart Marlein for the irradiations at LNK. A final thanks goes to my family, friends and girlfriend for the support throughout the year.

Table of contents

List of tables

List of figures

Abstract

The RDA unit of SCK•CEN in Mol performs research in the development of neutron dosimeters. There is a major concern about the carcinogenic risk of secondary neutrons which are inevitably present in proton therapy. In order to measure the secondary neutron dose, commercial bubble detectors can be used. However, these detectors take a lot of space, are very expensive and have limited life time and therefore small SDDs need to be developed to measure the neutron dose in vivo by using a phantom. This master's thesis aims to improve an existing fabrication protocol to achieve a stable detector to assess neutron doses in anthropomorphic phantoms during proton radiotherapy. Thereafter, the detectors must be characterized and a reproducible calibration method has to be sought.

In this thesis, a new fabrication protocol has been developed that must be followed very carefully. The SDDs are irradiated with a ^{252}Cf neutron source and read through an acoustic detection system. Afterwards, registered pulses are analyzed through an optimized software program to provide an objective analysis.

To conclude, the SDDs must be manufactured by strictly following a dedicated protocol. The sensitivity of the SDDs can be increased by increasing the amount of added Freon. However, these detectors are limited in sensitivity because of the limited volume. Finally, a reproducible calibration method was obtained by resetting (applying pressure on the vial) the SDDs after each irradiation and with the software analysis of the acoustic pulses.

Abstract in Dutch

De RDA groep van het SCK•CEN te Mol doet onderzoek naar de ontwikkeling van neutronen dosimeters. Er bestaat een grote zorg omtrent het carcinogene risico van secundaire neutronen die onvermijdelijk aanwezig zijn bij protontherapie. Commerciële bubbeldetectoren kunnen de secundaire neutronendosis te meten, maar ze nemen echter veel plaats in, zijn zeer duur en hebben een beperkte levensduur waardoor er nood is aan kleine SDD's om de neutronendosis in vivo te meten met een fantoom. Deze masterproef heeft als doel een bestaand fabricage protocol te verbeteren om zo een stabiele detector te bekomen om neutronendosissen te meten in antropomorfe fantomen tijdens protontherapie. Nadien worden de detectoren gekarakteriseerd en wordt er een reproduceerbare kalibratiemethode ontwikkeld.

Een nieuw fabricage protocol werd opgesteld dat zeer nauwgezet gevolgd moet worden. De SDD's worden bestraald met een ^{252}Cf neutronenbron en via een akoestisch detectiesysteem uitgelezen. Nadien worden geregistreerde pulsen via een geoptimaliseerd software programma geanalyseerd om zo tot een objectieve beoordeling te komen.

Tot besluit, om een SDD te maken moet een duidelijk protocol strikt gevolgd worden. De gevoeligheid van de SDD's kan worden verhoogd door de hoeveelheid Freon te laten toenemen. Deze detectoren hebben echter een beperkte gevoeligheid omwille van het beperkt volume. Ten slotte werd een reproduceerbare kalibratiemethode verkregen door de SDD's na elke bestraling te resetten en met de software analyse van de akoestische pulsen.

Introduction

The conducted research is completed in association with the Research in Dosimetric Applications (RDA) unit of SCK•CEN in Mol. This unit performs research in several fields such as the development of neutron dosimeters.

Proton therapy is becoming one of the most attractive approaches in the treatment of cancer. This technique has the advantage of depositing the dose over a narrow range in the tumor. In this way surrounding tissue and the skin of the patient will receive less dose compared with other conventional techniques. Nevertheless, there is a major concern about the carcinogenic risk of secondary neutrons, which are inevitably present in proton therapy. Commercial bubble detectors are able to measure the dose derived from these secondary neutrons. However, these detectors take a lot of space, are very expensive and have limited life time which makes it necessary to develop small SDDs to measure the neutron dose in vivo by using a phantom.

The main objectives of this master's thesis are to improve an existing fabrication protocol to achieve a stable detector to assess neutron doses in anthropomorphic phantoms during proton radiotherapy. Thereafter, the detectors must be characterized and a reproducible calibration method has to be sought.

Firstly, a great practical aspect was addressed to achieve this. Many attempts were made to manufacture the detector and after improvements and clear follow-up of a step-by-step plan, a stable SDD could be made. In order to verify if the fabricated detector also worked properly, the SDD should of course be characterized. The SDDs were able to measure neutrons from a ^{252}Cf neutron source as measured with an acoustic detection system. The development of an optimized LabVIEW program provided a step towards a reproducible calibration method. LabVIEW is systems engineering software for applications that require test, measurement, and control with rapid access to hardware and data insights.

The first two chapters of this dissertation discuss the need of a neutron dosimeter. A brief introduction to the problem of secondary neutrons is given as well a general discussion on neutron dosimetry. Chapter 3 introduces the bubble dosimeter and the next three sections explain how the SDD is fabricated, how the data acquisition happens and how the detector is calibrated. Finally, the results are studied with in-depth analysis, the most important conclusions and a future perspective are given.

1 Secondary neutrons

1.1 Proton therapy

Proton therapy is a form of external beam radiotherapy using energetic protons for cancer treatment. It is becoming one of the most attractive approaches in the treatment of cancer because the dose is deposited over a narrow range in the tumor. In this way surrounding tissue will receive less dose compared with other conventional techniques. Figure 1 shows the Bragg-peak of 18 MV photons, 135 MeV protons and 254 MeV/u carbon ions.

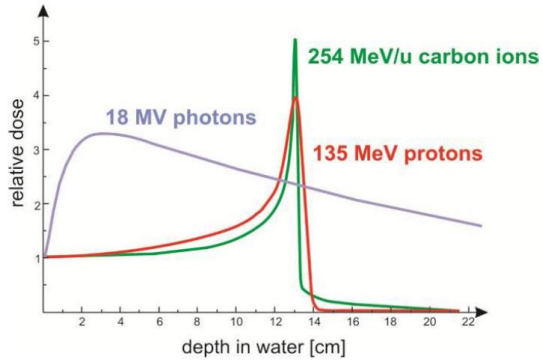

Figure 1: The Bragg-peak of 18 MV photons, 135 MeV protons and 254 MeV/u carbon ion, the relative dose [/] is presented in function of the depth in water [cm].

Figure 1 illustrates that for protons the dose is deposited over a much narrower range than for photons. Another big advantage of proton therapy is the relatively low entrance dose (a plateau can be seen in Figure 1 and 2). The skin of the patient will receive a lot less dose than the tumor or target volume. This is illustrates in Figure 2 and 3.

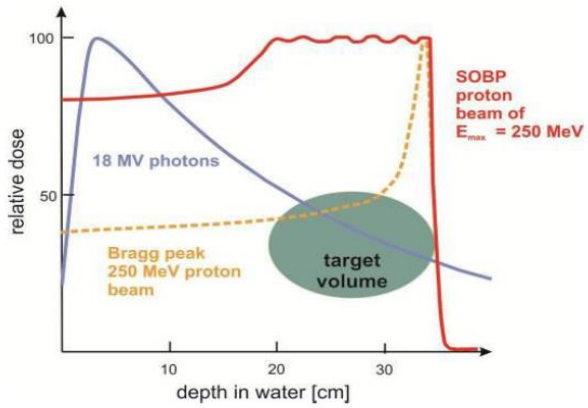

Figure 2: Bragg-peak of 18 MV photons, 250 MeV proton beam and the Spread Out Bragg-peak (SOBP) of the proton beam.

Figure 2 shows that by using proton therapy the skin will receive less dose while the tumor will receive 100 % of the dose. The maximum dose is given at depth which can be seen by

looking at the shape of the Bragg-peak. For conventional treatment with photons this is not the case. An advantage of using a proton beam as well is the rapid distal dose fall-off, the red and yellow line (proton beam) in Figure 2 fall more rapidly than the blue line (photon beam). The spread out Bragg Peak (SOBP) is the sum of several individual Bragg peaks at staggered depths. Figure 3 shows the advantage of proton therapy as well as the dose given to different tissues.

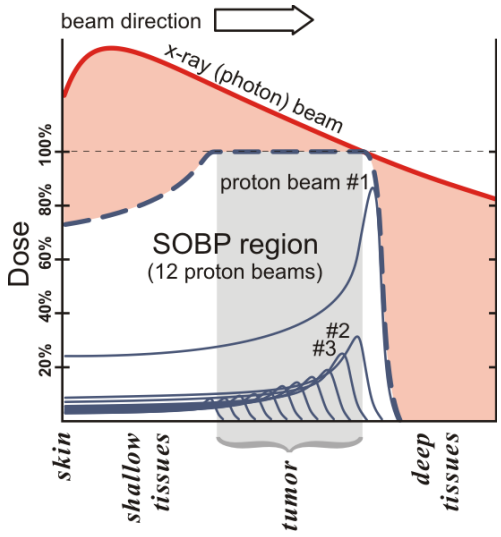

Figure 3: Individual (thin blue lines) Bragg-peaks and the SOBP of a proton beam. The red line represents the dose in function of the depth for a photon beam.

In a typical treatment plan for proton therapy, the SOBP (dashed blue line) is the therapeutic radiation distribution. The SOBP is the sum of several individual Bragg peaks (thin blue lines) at staggered depths. The depth-dose plot of an X-ray beam (red line) is provided for comparison.

For the reasons given above proton therapy is becoming one of the most attractive approaches in the treatment of cancer. The reduction of the dose burden is particularly important for children because long-term survivors of childhood cancer receiving radiotherapy are at a significantly increased risk of second malignant neoplasms (SMNs) [1].

1.2 Secondary neutrons

Nevertheless there is a major concern related to the carcinogenic risk from secondary neutrons, which are unavoidably present with particle treatments [2]. Proton therapy uses high energy protons which will cause interactions in matter. The most concerning proton interaction mechanism is the removal of a primary proton and creation of secondary particles via non-elastic nuclear interaction, this is illustrated in Figure 4 [3].

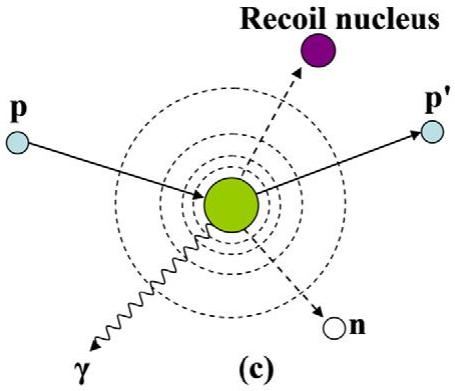

Figure 4: Removal of primary proton and creation of secondary particles via non-elastic nuclear interaction (p: proton, e: electron, n: neutron, γ: gamma rays).

As can be seen in Figure 4 high energy protons will form possibly harmful secondary neutrons inside the human body. For a non-elastic nuclear interaction a proton will interact with the atomic nucleus creating secondary neutrons. This will cause a removal of primary protons from the beam.

Different techniques can be used for the detection of stray neutrons. Passive detectors (track detectors, bubble detectors, activation foils, TLDs with ^{6}Li and ^{7}Li and semiconductor detectors), active detectors (rem counters, TEPC, recombination chambers and Bonner spheres) and Monte Carlo simulations can be used. It is clear that there are several methods of neutron dosimetry in the secondary radiation field, but the problem lies with in vivo neutron dosimetry.

Currently in vivo neutron doses in particle therapy are not performed routinely and are limited to Monte Carlo simulations or the use of bubble detectors. A possible method is the use of track etch detectors but these require simulation input or an automatic counting system. Additionally there is a lack of measured data in anthropomorphic phantoms [4]. The use of bubble detectors has been proposed to estimate the patient secondary neutron doses by irradiation in anthropomorphic phantoms. The current existing commercial bubble detectors have the disadvantage of consuming a lot of space due to their large volume. Therefore there is a need for small detectors to measure the neutron doses in vivo by using a phantom.

The risk of developing a second cancer following radiotherapy is a major concern and although proton therapy has a major advantage of sparing healthy tissue in the organs surrounding the tumor, we have to consider the presence of secondary neutrons which are effective at causing biological damage in the body. Therefore it is important to study more about neutron doses in as many as possible different organs using anthropomorphic phantoms.

2 Neutron dosimetry

2.1 Problem

Neutron dosimetry is still far less developed than gamma dosimetry, the existing neutron dosimeters are less accurate than the gamma dosimeters. Neutrons are non-charged particles that interact less and in a different way compared to gammas or charged particles, this is why they are more difficult to detect. Neutrons can travel through many centimeters of matter without any type of interaction and thus can be totally invisible to a detector of common size or composition.

However, in particular neutrons are believed to be harmful radiation for the body because they are highly biological effective with regard to cancer induction and thus even a very small absorbed dose might cause side effects [5]. Therefore assessment of neutron doses in clinical proton therapy requires special attention for radiation protection and prevention of SMNs.

Neutrons produce high LET (Linear Energy Transfer) radiation and will cause single- and double-strand breaks in DNA. For practical purposes of assessing and regulating the hazards of ionizing radiation to workers and the general population, weighting factors defined by the ICRP are used. A radiation weighting factor is an estimate of the effectiveness per unit dose of the given radiation relative to a low-LET standard. Weighting factors are dimensionless multiplicative factors used to convert physical dose (Gy) to equivalent dose (Sv), i.e. to place biological effects from exposure to different types of radiation on a common scale.

In 2007 ICRP published a new set of radiation weighting factors [6].

$$w_R = \begin{cases} 2.5 + 18.2e^{-[\ln(E_n)]^2/6}, & E_n < 1 \text{ MeV} \\ 5.0 + 17.0e^{-[\ln(2E_n)]^2/6}, & 1 \text{ MeV} \leqslant E_n \leqslant 50 \text{ MeV} \\ 2.5 + 3.25e^{-[\ln(0.04E_n)]^2/6}, & E_n > 50 \text{ MeV} \end{cases}$$

This is a continuous function in neutron energy, E_n [MeV], for the calculation of radiation weighting factors for neutrons.

It is a big challenge to monitor neutron doses because both the biological effect of neutrons and the neutron detection efficiency of most neutron detectors are largely depending on neutron energies. Because of the wide range of neutron energies to be covered and because of the large variation in linear energy transfer (LET) from neutron induced reactions, a good neutron dosimeter is difficult to find [7]. In order to get a complete picture of the energy spectrum there is a need for a large amount of equipment which will hamper neutron dose monitoring in a small area. Another complex problem is that the neutron radiation usually occurs together with strong gamma fields, which makes it difficult to measure the neutron flux separately.

Because of the complexity with which neutrons interact with the environment, precise determination of the neutron energy is quite difficult. Bonner sphere spectroscopy (BSS) is one of the few methods that provide an accurate measure of the neutron spectrum, it uses a small lithium iodide (LiI) scintillator or 3He proportional counter placed at the center of polyethylene moderating spheres of different diameters. Figure 5 shows the complexity as well as the size of the set-up for the measurement.

Figure 5: Bonner Sphere Spectroscopy set-up.

2.2 Interaction of neutrons

Neutrons carry no charge and therefore cannot interact in matter by means of the Coulomb force, which dominates the energy loss mechanism for charged particles. When a neutron does undergo interaction, it is with a nucleus of the absorbing material. As a result of the interaction, the neutron may either totally disappear and be replaced by one or more secondary radiations, or else the energy or direction of the neutron is changed significantly [8].

There are several possible interaction mechanisms of neutrons with matter, given in Table 1.

Table 1: Possible neutron interaction mechanisms with matter.

Before the reaction	After the reaction	Name	Symbol
${}^{A}_{Z}X + {}^{1}_{0}n$	${}^{A}_{Z}X + {}^{1}_{0}n$	Elastic scattering	(n,n)
	${}^{A}_{Z}X + {}^{1}_{0}n' + \gamma$	Inelastic scattering	(n,n',γ)
	${}^{A+1}_{Z}X + \gamma$	Neutron capture	(n,γ)
	${}^{A}_{Z-1}X + p$	Neutron capture with production of charged particles	(n,p)
	${}^{A-3}_{Z-2}X + \alpha$		(n,α)
	${}^{A-1}_{Z}X + 2\,{}^{1}_{0}n$	n,2n reaction	(n,2n)
	$Y + Z + \gamma$	Fission	(n,f)

The relative probabilities of the various types of neutron interaction change dramatically with neutron energy and are also dependent on the target nucleus. In somewhat of an oversimplification neutrons can be divided into two categories on the basis of their energy, either fast neutrons or slow neutrons.

The dividing line will be at about 0.5 eV, or about the energy of the abrupt drop in absorption cross section in cadmium (the cadmium cutoff energy). Elastic scattering and the capture reactions are the most important concerning radiation protection.

2.2.1 Slow neutron interactions

The significant interactions for slow neutrons include elastic scattering with absorber nuclei and a large set of neutron-induced nuclear reactions. Slow neutrons have small kinetic energy so very little energy can be transferred to the nucleus in elastic scattering. Consequently, this is not an interaction on which detectors of slow neutrons can be based. However elastic collisions tend to be very probable and often serve to bring the slow neutron into thermal equilibrium with the absorber medium before a different type of interaction takes place. These slow neutrons are often called thermal neutrons which, at room temperature, have an average energy of 0.025 eV.

More important are neutron-induced reactions that can create secondary radiations of sufficient energy because these can be detected directly. Slow neutron interactions have very low incoming energy so all such reactions must have a positive Q-value to be energetically possible. The radiative capture reaction (n,γ) is the most probable interaction for the creation of secondary radiation in most materials and plays an important part in the attenuation and shielding of neutrons. This reaction can be useful in the indirect detection of neutrons using activation foils. However, the secondary radiation takes the form a gamma rays and thus the reaction is not often applied in active neutron detectors. Instead reactions such as (n,α), (n,p) and (n,f) are much more attractive because the secondary radiations are charged particles.

Probably the most popular reaction for the conversion of slow neutrons into directly detectable particles is the $^{10}B(n,\alpha)^{7}Li$ reaction. The next most popular reaction for the detection of slow neutrons is the $^{6}Li(n,\alpha)^{3}H$ reaction, here the reaction proceeds only to the ground state of the product. The gas ^{3}He is also widely used as a detection medium for neutrons through the reaction $^{3}He(n,p)^{3}H$. The thermal neutron cross section for this reaction is 5330 barns, significantly higher than that for the boron reaction, and its value also drops off with a $1/v$ energy dependence (see Figure 5). Although ^{3}He is commercially available, its relatively high cost is a factor in some applications.

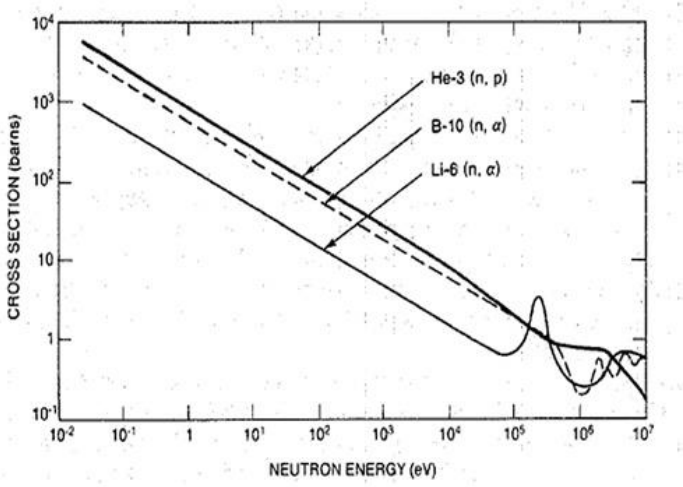

Figure 6: Cross section versus neutron energy for some reactions of interest in neutron detection.

The interactions of thermal neutrons in tissue will be mainly neutron capture by nitrogen and hydrogen by following reactions:

- $^{14}N(n,p)^{14}C$, E_{tr} = 0.62 MeV
- $^{1}H(n,\gamma)^{2}H$, $E\gamma$= 2.2 MeV

2.2.2 Fast neutron interactions

How higher the neutron energy, how greater the importance of scattering becomes because the neutron can transfer an appreciable amount of energy in one collision. With increasing neutron energy, the probability of most neutron-induced reactions potentially useful in detectors falls rapidly. Fast neutrons lose their energy by consecutive collisions, become slow neutrons and the probability of a radiative capture reaction increases. The secondary radiations in the case of fast neutrons are recoil nuclei which have picked up a detectable amount of energy from neutron collisions. At each scattering site, the neutron loses energy and is thereby moderated or slowed to lower energy. In order to slow them down elastic scattering with intermediate nuclei ($25<A<80$ e.g. tungsten) or light nuclei ($A<25$) could be used. The resulting thermal neutrons can be detected.

The most efficient moderators are hydrogen-rich materials (e.g. polyethylene, methane) because the neutron can lose up to all its energy in a single collision with a hydrogen nucleus and create fast recoil protons which can be detected. If the energy of the fast neutron

is sufficiently high, or if the absorber material shows resonances, inelastic scattering with nuclei can take place in which the recoil nucleus is elevated to one of its excited states during the collision. By emitting a gamma ray the nucleus quickly de-excites and the neutron loses a greater fraction of its energy than it would in an equivalent elastic collision. This phenomenon plays an important role in the shielding of high-energy neutrons but are an unwanted complication in the response of most fast neutron detectors based on elastic scattering.

2.3 Personal neutron dosimeters

In this section the most commonly used personal neutron dosimeters will be discussed.

1) Track detectors

Nuclear filmdosimeters were once used anywhere, they consist of a thin layer of a getalin material containing a silver compound. The tracks of the recoil protons are chemically reduced to granules of metallic silver. Disadvantages are strong fading, high gamma sensitivity and threshold energy of 0.5 MeV.

Damage track detectors use the damage that is induced in a specific medium by the neutrons. In the beginning fissile foils were used in order to produce charged particles after interaction with the neutrons. In the polycarbonate which was in contact with the fissile material one could easily detect the traces of these particles. The two most popular films were neptunium and thorium.

Through the use of electrochemical etching, and the discovery of a new more sensitive polymer CR-39, the performance of the track detectors became a lot better. Thus, it became possible to also detect recoil carbon and oxygen atoms. In CR-39 even recoil protons can be detected, in this way neutrons with an energy up to 50 keV can be measured. In this form, they are commercially available and are referred to as track etch detectors. Neutrons are detected by the path of the damaged molecules in the material. These tracks can be detected by a suitable etching process: either chemical etching (CE) or electrochemical etching (ECE), or both combined. An adequate calibration of the track density related to the neutron dose equivalent has to be performed. The major shortcomings of CR-39 are the lack of a dosimetry grade material which causes batch variations, significant angular dependence and a sensitivity that may be marginal if a change in quality factor is adopted. CR-39 also under-responds for certain neutron energy ranges (lower energy neutrons from reactors or high energy accelerator-produced neutrons). The electrochemically etched CR-39 is attractive because of the fast neutron effective response, low neutron energy threshold and photon insensitivity [9].

2) TLD detectors

The most commonly used thermoluminescent material is doped LiF, ^{6}Li has a much higher cross section for thermal neutrons than ^{7}Li. Thus thermoluminescent dosimeters (TLD) with a high concentration of ^{6}Li will detect both neutrons as gammas and those with ^{7}Li

almost exclusively gamma-radiation. The difference between the two thus gives a measure of the number of thermal neutrons.

Albedo neutron dosimetry is based on the effect of moderation and backscattering of neutrons by the human body, creating a neutron flux at the body surface in the thermal and intermediate energy range. These backscattered neutrons called albedo neutrons, can be detected by a dosimeter (usually a LiF TLD chip), placed on the body which is designed to detect thermal neutrons. The dosimeters are shielded from direct radiation, the intention was that the response was independent of the incident spectrum. However, this appears not to be the case, they are much more sensitive to the low energy neutrons.

This energy problem must be resolved by calibrations in the working environment and the use of a correction factor [10].

3 The bubble dosimeter

3.1 Superheated drop detector (SDD)

3.1.1 Introduction

A liquid maintained at a temperature above its boiling point is considered to be in a superheated state, this is a metastable state. Such superheated droplets of liquid have been used lately to detect radiation. Superheated liquid drops suspended in a visco-elastic gel (known as a superheated drop detector) or in a more rigid polymer matrix (known as a bubble detector) are known to be a useful tool in radiation physics. The first realization of the bubble detector came in 1979 when Robert Apfel presented his superheated drop detector. He managed to secure the superheated droplets in a viscous liquid or gel. Due to the influence of radiation the drops go to a gaseous state, just as in a bubble chamber [11]. The drops are placed in the gel while the temperature is lower than the boiling point and afterwards the temperature is raised to the desired level of superheating. The insertion of the droplets can also be done at higher pressure, after which the superheating is established as the ambient pressure is brought back down [12].

3.1.2 Working principle

However, unlike bubble chambers where nucleation at any point eventually consumes the whole liquid, in superheated emulsion detectors nucleation consumes only one droplet. In this detector, each droplet is in itself a miniature bubble chamber. Because the medium absorbs the shocks the evaporation of each of the droplets happens independent of each other and the rest can remain in the superheated state. In this way it is not necessary to exert pressure each time again on the bubble detector. In the drops themselves the same happens as in a bubble chamber. Ionizing radiation deposits energy and evaporates the liquid. The thus-formed bubbles will rise in the medium. At the top the gas is collected and this gas was taken as a measure for the number of formed bubbles in the first models. These drops in the superheated drop detector remain long enough in superheated state so that the whole is usable as a stable neutron dosimeter. Instead of making use of the released gas for the readout, Apfel also developed an electronic readout system. With piezo-electric sensors, it detects the acoustic waves that are associated with the generation of a bubble, this is also possible with the aid of microphones [13].

The used tissue equivalent aqueous gel consists of uniform dispersions of over-expanded halocarbon and/or hydrocarbon droplets. In particular, halocarbons with a moderate degree of superheat, i.e. a relatively small difference between their operating temperature and boiling point, can be used in neutron dosimetry and spectrometry since they are only nucleated by energetic heavy ions such as those produced by fast neutrons. More recently, halocarbons with an elevated degree of superheat have been utilized to produce emulsions that nucleate with much smaller energy deposition and detect low LET radiations, such as

photons and electrons. The energy required to trigger (nucleate) the boiling of the metastable superheated liquid is usually quite small compared to the energy required for a phase transition [14].

Although the principle of the bubble chamber has long been known, the theory has not yet been elaborated. The reason is that there are many different physical processes involved in forming a bubble. Essentially there are three steps. First, there is the production of a charged particle through the neutral neutron. This charged particle sheds its energy in the medium over a certain distance. If enough energy is deposited in a sufficiently small volume, then the third step follows, vaporizing the detector fluid into a visible bubble.

3.1.3 Neutron interaction

The used halocarbon in this work is 1,1,1,2,3,3,3-heptafluoropropane, also called heptafluoropropane (HFC-227ea, R227ea).

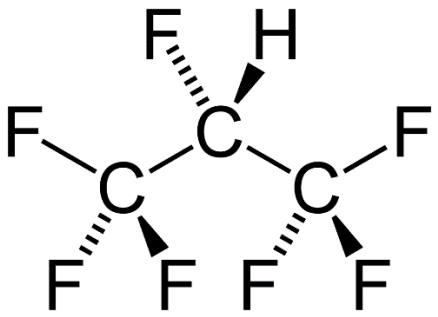

Figure 7: 1,1,1,2,3,3,3-heptafluoropropane.

The energy deposition by neutrons in HFC-227ea and the interaction with this halocarbon will be described. For neutrons the elastic scattering plays the important role in transferring maximum energy to target nuclei, while for bubble nucleation in a superheated droplet sufficient amount of energy has to be deposited within the critical volume of the active liquid (HFC-227ea). Hence we consider the elastic scattering as the important mechanism for the resulting nucleation. In the case of the neutron, the neutron deposits energy through the secondary ionizing particles produced during interaction with the nuclei of the liquid.

When a neutron of energy E_n, passing through the detector, interacts with a nucleus of atomic weight A, the energy E_r that is transferred to the nucleus through elastic scattering is given as,

$$E_r = \frac{4AE_n \cos^2\theta}{(A+1)^2}, \qquad (1)$$

where θ is the scattering angle due to the scattering.

In a single scattering event the maximum energy that can be transferred to the recoil nucleus is through the head-on elastic collision (for which $\theta = 0^o$) and is given as

$$E_r = \frac{4AE_n}{(A+1)^2}. \qquad (2)$$

Thus, due to elastic scattering the neutrons mostly create recoil ions with an ion energy distribution which extends to a maximum energy of $4AE_n/(A+1)^2$. These energetic recoil ions then move through the liquid losing its energy through Coulombic interactions until it comes to rest. The amount of energy deposited by the ions depends on the electron density of the material and is directly proportional to the square of the charge of the ions. Therefore the ions with greater charge have the larger value of stopping power dE/dx. The higher the value of dE/dx means greater amount of energy deposition in a given distance and hence greater is the probability of overcoming the barrier W. For a given neutron energy, different nuclei of the liquid will receive different amount of energy, depending on their atomic weight. The ion with highest value of dE/dx in the liquid plays the major role in nucleation. The energy deposition by massive ions is much localized close to the track and the energy deposition takes place in a much shorter length. In order to nucleate, the energy deposition $\frac{dE}{dx}r$ must exceed the energy barrier W, or in other words $\frac{dE}{dx}r \geq W$ or $\frac{dE}{dx}Kr_C \geq W$, where the distance r is expressed in critical radius r_C, and the value of K depends on the active liquid. In practice, a very small fraction of the total deposited energy is used up in the nucleation process. There are no simple analytical formulas to calculate the stopping power dE/dx. For this purpose, the cross sections should be used from nuclear databases.

The superheated HFC-227ea (C_3HF_7) is a composite material, and therefore, different nuclei will receive different amount of energy from the incident neutrons. In case of HFC-227ea recoiled C, H and F ions will be produced due to neutron interaction and they will play important role in bubble nucleation.

Carbon, fluorine and hydrogen are the only relevant elements for the neutron interactions. The probability of interaction can easily be found for these elements. For neutron fields in proton therapy, the most important reactions (cross section greater than 1 mb) are the following: elastic scattering, inelastic scattering and charged particle production $^{19}F(n,\alpha)^{16}N$.

3.1.4 Bubble formation

The reason that a liquid may be in superheated state is that additional energy is needed to form a gas/liquid interface. Thus, an embryo bubble must appear with a certain minimum size. Beginning bubbles of a smaller size are unstable and are compressed by the surface tension.

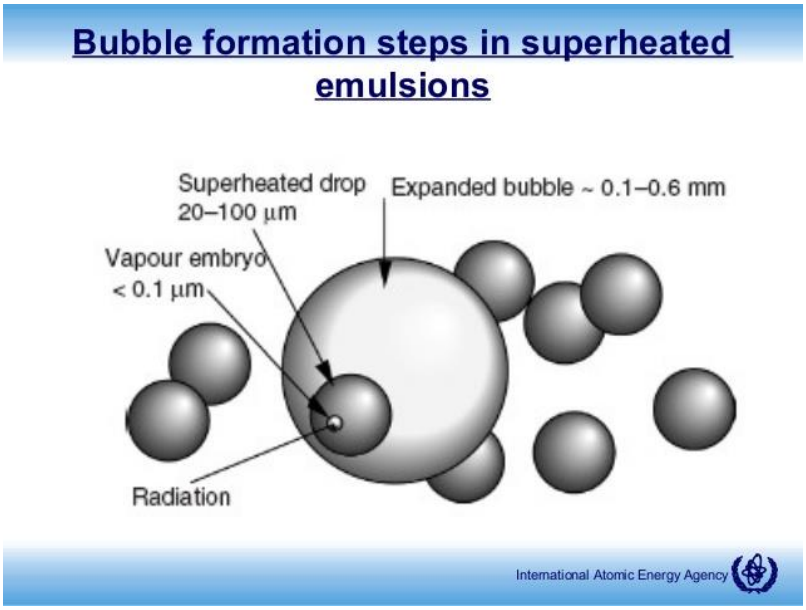

Figure 8: Bubble formation steps in superheated emulsions.

From a certain size, the critical radius, the energy gain of evaporation is greater than the energy needed to form a surface, and the evaporation continues spontaneously. A certain energy barrier linked to the critical radius must be overcome in order for nucleation to occur. With increasing temperature less energy is required for vapor nucleation.

The steps that lead to the formation of the bubbles are summarized. Some of the neutrons that reach the detector interact with it. The probability for this depends on the detector materials and the energy of the neutrons. Some of the interactions occur far from the liquid droplets, some close and some in the drops. These interactions produce secondary particles that slow down and deposit their energy into the detector. Many of these secondary particles will deposit their energy into the gel matrix and not in the detector droplets (about 20 µm diameter) and are thus lost. The particles that deposit energy into the drops create a track of microscopic bubbles. If the density of energy deposition is large enough, so if the stopping power is large enough, some of these microscopic bubbles will grow into a critical radius, after which the whole drop will evaporate. If this is not the case, the surface tensions will compress the bubbles back and there will be no trace. The surrounding gel matrix thus contributes to the extent that it can slow down and thermalize the neutrons and thus enable capture actions. For a more detailed explanation the interested reader is referred to Appendix A which also includes the efficiency of energy deposition. Of course, not all of the energy available will be transformed into the formation of a bubble, only a small portion of the deposited energy will remain in the bubble during this process.

A vaporization may occur due to impurities in the liquid, the so-called heterogeneous nucleation. This impurity forms a part of the surface so that less energy is required for

overcoming the surface forces. However, in the bubble detector there are no impurities and the overheating can be increased until homogenous nucleation occurs at some point.

Although a complete theory of radiation-induced nucleation in superheated liquid is not available, the theory of homogenous nucleation in superheated fluids by radiation was first developed by Seitz in his 'thermal spike' model [15]. In this model, the heavily charged particle deposits its energy very local as thermal energy. Along the particle path there are a series of small bubbles (spikes) that grow as the shock front moves further. This process is very complicated and involves aspects of both molecular physics and thermodynamics of fluids. Seitz's approach assumes a reversible phase transition of the superheated liquid. If the Seitz bubbles grow up and reach the critical radius, they will grow further and the whole drop will evaporate. If there is too little energy deposited at short distance then the spikes will be too small and compressed back.

3.1.5 Response

The response function can be calculated as follows:

$$R(T) = \int \Phi(E_n) V \sum N^i \sum \sigma_j^i (E_n) S_{ij}(T, E_n) dE_n.$$

Here Φ is the neutronflux, V the volume, N the number of atoms of type i in this volume, σ_j^i the cross section for the reaction of type j of the i^{th} atom and S_{ij} the efficiency factor. The latter indicates the fraction of the ions that are capable of creating a bubble, thus providing the minimum energy at a sufficiently short distance. This according to a particular model, so a certain effective length. The threshold energy of the response function is thus determined by the kind of material and the degree of overheating, as this determines the minimum energy required. The sensitivity depends on the degree of overheating (increase efficiency factor) and the amount of drops in the gel. The size of bubbles after their formation has no meaning.

Recall that the radiation weighting factor w_r depends on the energy of the neutron E_n. It is yet to be studied whether the detectors are a good measure of the equivalent dose H_T, but the response is expected to follow the w_r function more or less. The overall absorbed dose is correlated to the number of bubbles. The absorbed dose D_T in Gy can be converted to the equivalent dose in Sv using the radiation weighting factors. The equivalent dose is not measurable but is a calculated quantity. The operational quantity H*10 (ambient dose equivalent) is measurable and used for the practical evaluation of dose. The detectors are calibrated using a ^{252}Cf neutron source and exposed to a dose of 100 µSv (H*10). If desired this value can be converted to the dose equivalent H by simply multiplying with a factor. In this thesis the ambient dose equivalent H*10 will be used.

3.2 Read-out of a bubble dosimeter

There are 2 different ways to read out a bubble dosimeter, either using an active device or a passive device. The easiest passive device is that of counting vapor bubbles visually with the

naked eye, this done for the 'NeutrometerS'. For the BD-PND (discussed later on in this chapter) counting of bubbles is done optically by using a camera. Other passive devices essentially rely on the measurement of the volume of vapor formed due to nucleation. The principle is made clear by Figure 9.

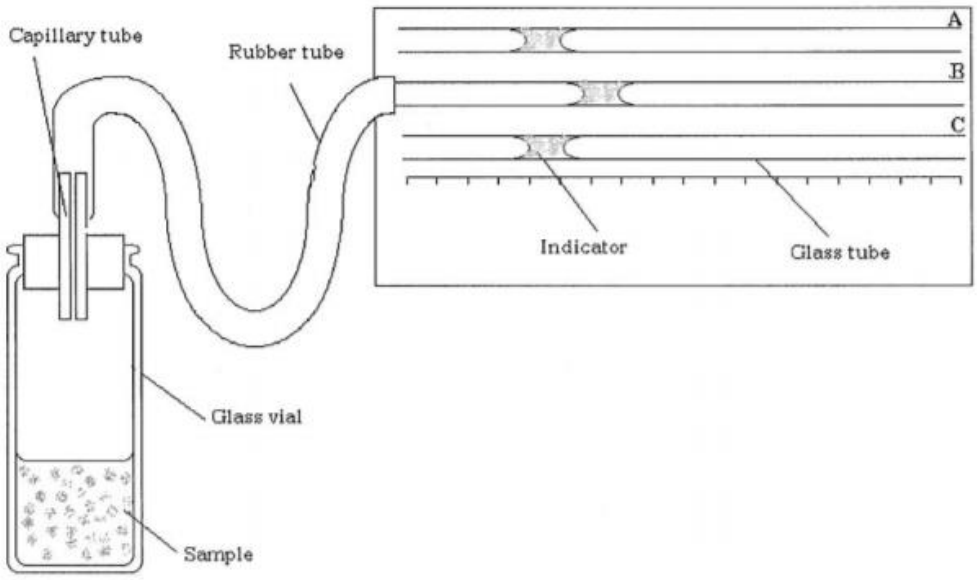

Figure 9: Schematic diagram of the passive device used to detect radiation induced vapor nucleation.

An SDD is connected to a capillary tube which in turn is in communication with a rubber tube. The gas/vapor produced by drop nucleation pushes the colored water (the indicator) along the glass tube, which is placed along a graduated scale. The displacement of the water column is directly related to the nucleated volume.

When a superheated drop in a SDD is transformed into a bubble by interaction with a neutron, a pressure pulse is generated. This acoustic pulse can be sensed by using an active device, e.g. the one developed by Apfel and Roy [16]. A piezoelectric transducer is connected to the bottom of the vial containing superheated drops and picks up the pulse which is converted into an electric signal. In this work the same working principle is used (see Chapter 5), an efficient, cheap way to read out the detector was chosen. Instead of using modified electronic circuits [17] to record, amplify and process the electric signal caused by the acoustic pulse, the data acquisition was done using a laptop and a piezoelectric microphone. Full processing and filtering of the signal is done with LabVIEW.

3.3 BTI detectors

Bubble Technology Industries (BTI) have fabricated commercial types of bubble detectors which operates as neutron dosimeters. The BD-PND (Bubble Detector – Personal Neutron Dosimeter) and BDT (Bubble Detector Thermal) will be discussed.

3.3.1 BD-PND

The BD-PND is the recommended detector for personal neutron dosimetry. Its sensitivity exceeds the ICRP-60 requirements for neutron dosimetry. It incorporates automatic compensation for sensitivity change with temperature over the operational range of 20 – 37 °C. Nuclear laboratories, utilities, and military personnel have found that the BD-PND's immediate visual response and high sensitivity, coupled with its small size, light weight and rugged construction, make it the ideal device for ALARA programs.

In these detectors the droplets are dispersed in a much more vigorous polymer. As a consequence, the bubbles that are formed remain in place and can be counted at any time after irradiation with the eye or with an automatic reading system. The detector consists of a plastic tube of 18 mm diameter and 118 mm height, sealed by a black screw cap. The tube contains about 4 cm^3 of a sturdy, transparent polymer in which the drops of the superheated liquid are spread. The drops can be seen if you hold the tube against the light, but these are much smaller than the bubbles that occur after interaction with neutrons. The weight of these bubble detectors is about 58 grams.

Figure 10: BD-PND bubble detector.

A big difference with the Apfel products is the possibility of re-use. In the initial state, a pressure greater than the vapor pressure of the detector fluid is applied to the polymer through the screw cap. This pressure causes the detector to be insensitive to radiation in this state. Before use, the pressure is removed by unscrewing the screw cap. The drops are overheated and are sensitive to radiation. If the bubbles formed are counted, the pressure can be re-applied. The bubbles are compressed again into drop form and the detector is returned to its initial state.

The BD-PND model is a temperature-compensated variant. This has been achieved by adding a compensant on top of the polymer. At increasing ambient temperature, additional pressure is exerted on the polymer by this substance. This additional pressure compensates for the higher degree of overheating at rising ambient temperature. According to the manufacturer, the BD-PND has a constant sensitivity (±20%) between 20 °C and 37 °C. The total sensitivity of the detectors can be varied by changing the number of drops. At BTI standard sensitivities are available ranging from 0.033 to 3.3 bubbles per μSv.

3.3.2 BDT

The sensitivity of the BD-PND bubble detector begins to decrease at decreasing neutron energy from about 200 keV. Recoils of neutrons with energies below 50 keV do not deposit enough energy at a short distance in the drop to transform them into a bubble. To detect thermal neutrons, substances must be introduced into the detector with high effective cross-sections for the capture of thermal neutrons. Examples are ^{35}Cl, ^{10}B or ^{6}Li, which produce a heavily charged particle when catching a neutron, which deposits enough energy at a short distance to produce bubbles.

In order to compensate the BD-PND's insensitivity to low energy neutrons, there is the BDT bubble detector. The presence of ^{6}Li in the detector gives it a high sensitivity to thermal neutrons. This is achieved by the high cross section (945b) of the $^{6}Li(n,\alpha)T$ reaction at thermal energy. Fully according to the course of the cross section of ^{6}Li, the sensitivity of the BDT decreases with 1/v for higher energies. The ^{6}Li is present as dissolved salt in the BDT polymer. Since the resulting alpha particle has only a small range (around 16 μm), only those that develop at the edge of the drop will actually be detected. The detector fluid is the same as in the BD-PNDs. In addition to the thermal detection mechanism, there is also the response for fast neutrons through the normal mechanism (the detection of recoils with sufficient energy). The sensitivity to thermal neutrons is determined by the amount of ^{6}Li and by the number of drops. The sensitivity to fast neutrons is determined by the degree of overheating and the number of drops. The BDT bubble detector is preferentially sensitive to thermalized neutrons, with an exclusion ratio of thermal-to-fast neutron response exceeding 10:1. The BDT looks the same as the BD-PND.

3.4 Summary

The superheated drop detector (SDD) consists of thousands of superheated drops dispersed in a small vial of gel which vaporize upon exposure to high LET radiation, thereby providing a directly observable indication of neutron dose. This detector possesses high sensitivity to neutrons and insensitivity to high energy photons and electrons, making it suitable for the determination of neutron dose-equivalent rates around high energy photon, electron and proton radiotherapy beams.

The principle of a bubble dosimeter is the following. A great number of very small droplets of a liquid with a low heat of vaporization are incorporated into an organic gel or polymer. For a specific temperature and pressure, the liquid droplets are superheated in a metastable state. This unstable equilibrium can be destroyed by an external energy supply.

At the interaction point between droplet and high LET particle, such as a neutron or heavy charged particle, the liquid droplet becomes vaporized as a visible gas bubble. The overall absorbed dose is correlated to the number of bubbles. A sound is emitted for each bubble being created and the bubbles are counted in real time by an electro-acoustic sensor. The dose rate corresponds to bubble frequency [18].

4 Fabrication of the SDD

In this chapter the whole process for the fabrication of the SDD will be discussed. This is a complex process in which every step must be executed with high precision and special attention for temperature and pressure. After many attempts and improvements a fabrication protocol was written in a self-explanatory structure.

4.1 Gel mixture

The SDD consists of drops of superheated liquid of low boiling point, suspended in a viscous gel. Superheated drops of R227ea as the sensitive liquid are suspended in an aquasonic gel matrix. The emulsion of halocarbon droplets are homogeneously dispersed in a compliant matrix.

The drops are in a superheated state, i.e. above their boiling point. Being metastable, the drops can be triggered to vaporize by the energy deposited through radiation interactions. This is the same principle of the classic bubble chamber, but the emulsions differ in that they are continuously sensitive to radiation since the droplets are kept in a steady superheated state.

For the gel matrix in which the halocarbon droplets are homogeneously dispersed, a mixture of glycerol and ultrasound gel was used. 100 g ultrasound gel (Anagel) is mixed with 350 g glycerol (280 ml) and 400 µl of Tween 80 (Polysorbate 80) is added as surfactant. A magnetic stirrer and a stir bar were used to get a nice homogeneous mixture (2-4 hours).

The glycerol and ultrasound gel mixture has the function of holding the droplets in the detector. The mixture should be viscous enough so that the drops won't sink, otherwise the detector is damaged because the drops are not uniformly distributed in the gel. Other types of gel can also be used as the detector medium. The surfactant acts as an emulsifier, it will make the emulsification easier and also the droplet size can be reduced with the surfactant. Another important advantage of the surfactant is that it creates a shell around the droplet (the droplet materials are of oil type in nature) and thus makes them more stable. Finally it reduces the solubility of the droplet material.

It was observed that a ultrasound gel to glycerol ratio of 1/3,5 (weight ratio) is suitable for mixing with a magnetic stirrer and it is also easier to degas. The lowest amount of glycerol for a fixed amount of pure ultrasound gel was used. For another type of gel the ratio will be different, even for this gel the amount of glycerol can be increased slightly.

4.2 Degassing of the gel

At this moment the mixture still contains air bubbles which should be removed. This is accomplished by using a vacuum pump to degas the gel. Degassing is important for the stability of the detector, if the detector is prepared without degassing it will not be stable and the gel will foam. By removing the gases from the gel, the spontaneous vaporization of

the droplets is significantly reduced. The gas pockets act as a nucleation center, i.e. it triggers the droplet vaporisation. This process will take time since the gel is quite viscous (± 5,5 hours), the gel is heated to stimulate the degassing.

An Erlenmeyer with the option to attach a vacuum tube system is used, a little amount of the gel (± 50 ml) is added to the Erlenmeyer to be degassed. When all gas pockets are removed some more gel is added, repeat this process until all the gel is added. In order to improve the degassing of the total gel a stir bar is put inside the Erlenmeyer along with the gel and the Erlenmeyer is placed on the magnetic stirrer, the gel is stirred very slowly to avoid creating extra air bubbles. To complete the degassing process the gel is heated a few times, when the rate of degassing (bubbles coming out of the gel) is slow the heating process is started by putting the Erlenmeyer on a hot plate while the vacuum pump stays on. During heating the gel isn't stirred, when there are a lot of bubbles forming on the bottom surface of the Erlenmeyer the heating is stopped and the gel is stirred slowly again. This heating cycle is repeated 2 or 3 times, when the gel seems fully degassed (no bubbles in the gel) the stirring is stopped and the vacuum pump is kept on for about half an hour.

4.3 Preparation – pressure reactor

After the gel is degassed it is poured slowly into a pressure reactor (Figure 11). The pressure reactor is required because if the gel is left open under atmospheric pressure it will again absorb gas. For this reason the pressure reactor need to be kept under vacuum.

Figure 11: Pressure reactor with aluminum container.

4.4 Fabrication of the detector – cooling and transfer of Freon

The pressure reactor is then placed in an ice bath for cooling, an expanded polystyrene (EPS or ISOMO) box and ice were used. The pressure reactor inside the ice bath is placed in the fridge to speed the cooling process and a wet towel is wrapped around the pressure reactor. It is cooled down to about 1-2 °C and a temperature probe is used to monitor the temperature. Since the active liquid, the droplet material, is of quite low boiling point (-16,4 °C) transferring at low temperature is required. At this point transfer becomes easier from a relatively high temperature source, the Freon (R227ea) container, to the pressure reactor. Also a fixed low temperature to some extent ensures a fixed amount of Freon transferring into the reactor when a fixed amount of Freon is taken into the transfer tube. If the temperature is different, a different amount of Freon will be in liquid form inside the reactor.

Once the temperature in the pressure reactor reaches about 2 °C the active liquid is transferred. The amount of Freon to be used depends on the property of the Freon as well as on the amount of gel used. For 250 ml of gel about 5-10 ml Freon is usually used. Experimentally 4,7 ml of heptafluoropropane (R227ea or HFC-227ea) was found to give the desired response (bubbles per unit dose), that is enough bubbles will be produced to be able to perform good statistics. To increase or decrease the sensitivity of the detectors the amount of Freon to be used can be decided. A transferring tube is screwed between the inlet of the pressure reactor and the R227ea container (Figure 12), some Teflon tape is put on the screw-thread of both ends to avoid gas being leaked. In order to remove the air from the tube another small vacuum pump is used before transferring the Freon. By removing the air you ensure less amount of other gas getting absorbed into the gel during stirring. Thus the detector is more stable. After the R227ea is transferred the pressure reactor is connected with the stirrer, the gel mixture and the active liquid is stirred with a fixed speed (1000 rpm) for a fixed duration of time (10 minutes). The pressure reactor is equipped with a mixer inside which comes into the gel in the aluminium container, by connecting the pressure reactor with the stirring installation the content is mixed. The stirring speed and duration can be altered to produce a detector with smaller or bigger droplets.

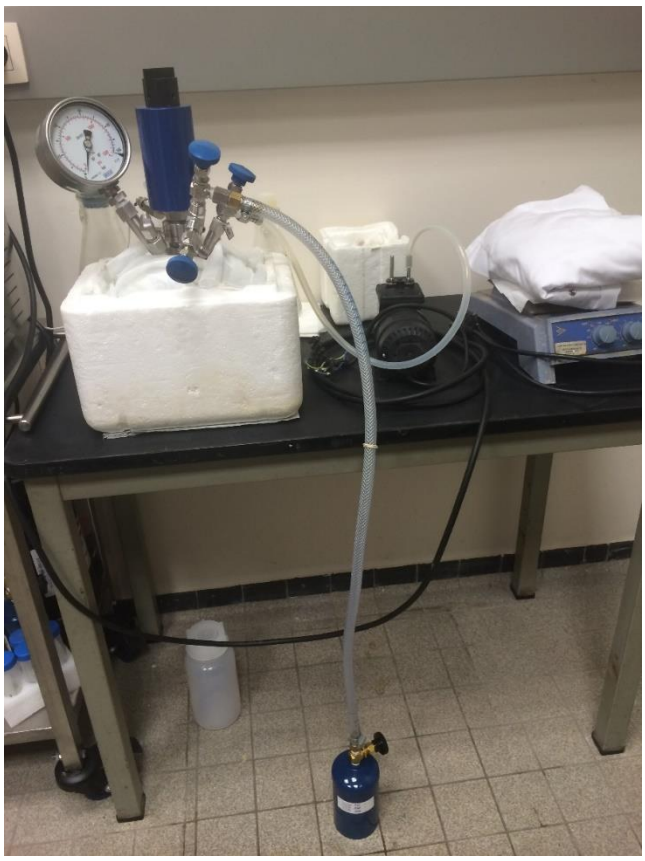

Figure 12: R227ea container connected with the pressure reactor by a tube. On the right hand side the black vacuum pump can be seen.

Another possible way to transfer the Freon was developed by using a gastight syringe, the advantage of this is that the exact volume of Freon added is known. A Pressure-Lok Serie A-2 gas syringe from VICI Precision Sampling was used (Figure 13, left-hand side).

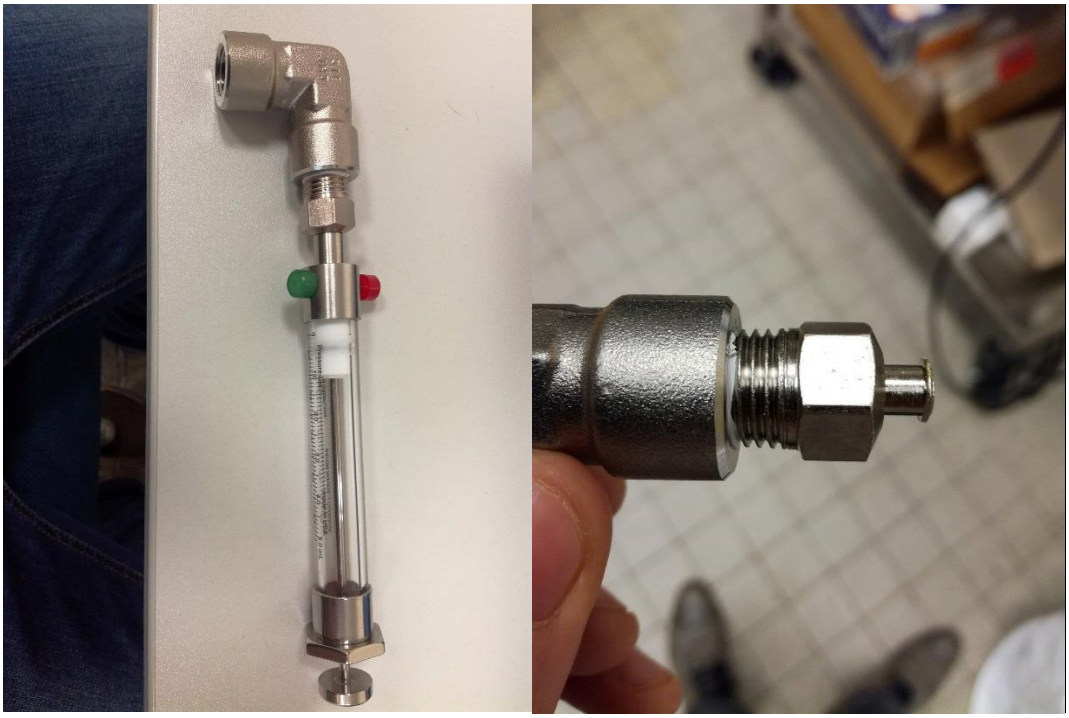

Figure 13: Gas syringe Pressure-Lok Serie A-2 from VICI Precision Sampling (left-hand side) and the elbow and coupler (right-hand side).

The gas syringe is connected to the Freon container by manner of an aluminum elbow, between the elbow and the syringe itself a coupler is placed that fits with the Luer-Lock end of the syringe. Once the Freon is taken into the syringe, the sample is locked in the gas syringe by pushing the red button until it stops against the front sleeve. This liquid and gas is now ready to be injected into the pressure reactor where it is mixed with the gel. In Figure 14 the syringe is connected to the blue Freon container.

Figure 14: Gas syringe connected to the Freon container.

4.5 Fabrication of the detector – applying pressure and final step

Once the stirring is finished the pressure reactor is connected to a compressed air tank and the pressure is increased to about 5-6 bar. Before stirring the reactor contains Freon in both liquid and gas form, the stirring process produces droplets and bubbles containing Freon. By applying pressure the bubbles are recompressed into drops. The pressure of 5-6 bar is kept on the reactor for about a night while keeping the reactor in an ice bath in the fridge. Next day the pressure is released very slowly. The pressure release should be at a slow rate and at a low temperature, otherwise the droplets will vaporize and the detector will contain a lot of bubbles. When atmospheric pressure is reached the gel is transferred to a glass bottle (very slowly using the sides to avoid creating extra bubbles), in the best case the glass bottle is kept in the fridge for 1 or 2 weeks before making the detector (final step). A small syringe is used to transfer the gel from the glass bottle to the small glass vials (the gel is pushed very slowly out of the syringe to avoid air bubble formation). The vials with the gel = the detectors are placed in the pressure reactor (remove the lid of the vial) and the pressure is increased to 5-6 bar. This should remove the bubbles from the small vials. The pressure is

kept onto the vials for about 30 minutes before slowly (1 hour back to atmospheric pressure) releasing the pressure. Figure 15 shows the final result, the SDD.

Figure 15: Self fabricated SDD.

A fully detailed self-explanatory step by step fabrication protocol with pictures can be found in Appendix B. Manufacturing the detector and the improvement of a given protocol have been a big part of this thesis, so there is large practical aspect associated with it.

5 Data acquisition and pulse shape analysis

This chapter will discuss the instruments used to register bubble nucleation events as well as the data acquisition system and pulse shape validation routine using LabVIEW.

5.1 Piezoelectric microphone

A piezoelectric microphone was used to convert the acoustic pulse associated with the process of bubble nucleation inside a liquid drop to an electrical signal. This is known as an active device.

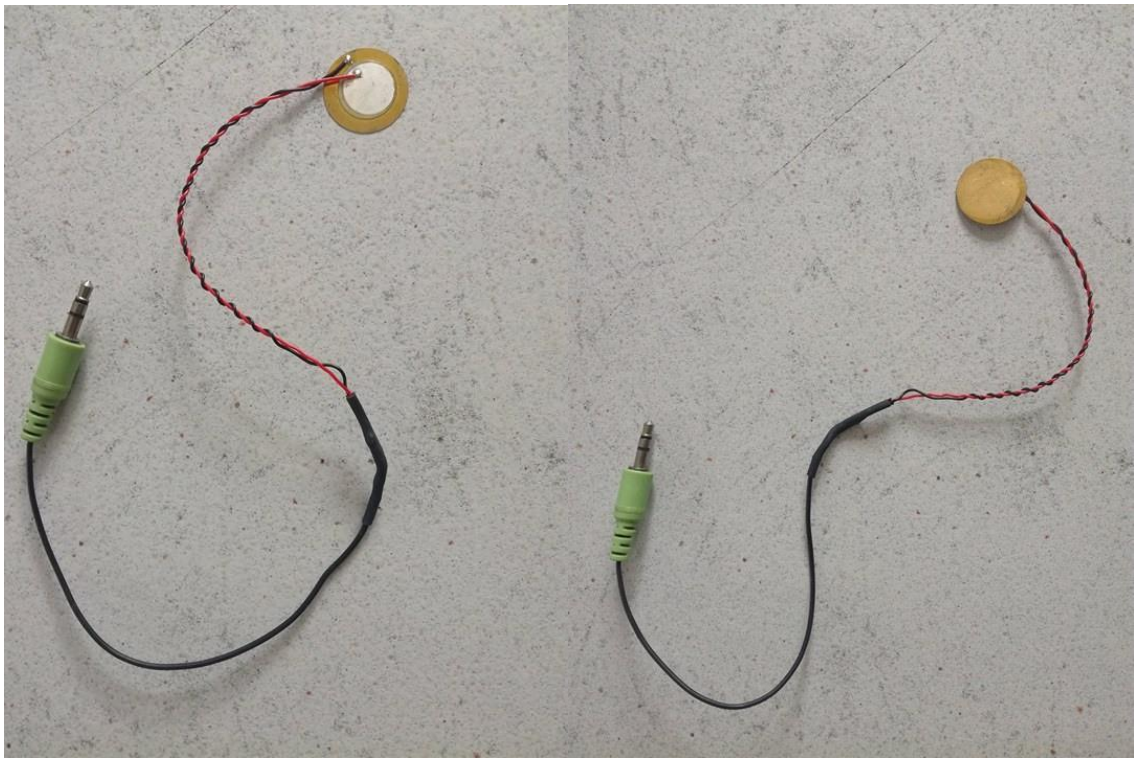

Figure 16: Piezoelectric microphone with the option to plug into the microphone port of a laptop. On the left-hand side the back of the sensor can be seen, on the right-hand the front of the detector can be seen on which the SDD stands.

The principle of operation of a piezoelectric sensor is that a force acts on two opposing faces of the sensing element. Detection of pressure variations in the form of sound is the most common sensor application, e.g. piezoelectric microphones (sound waves bend the piezoelectric material, creating a changing voltage).

The small vial of SDD rests on the piezoelectric microphone (Figure 17), so it acts as a contact microphone. It senses audio vibrations through contact with solid objects. Unlike normal air microphones, contact microphones are almost completely insensitive to air vibrations but transduce only structure-borne sound. The most commonly available contact microphone element is made of a thin piezoelectric ceramic round glued to a thin brass or alloy metal disc (Figure 16 left-hand side). This center disc is positively charged

while the brass disc is negatively charged. If the silver colored disc is cracked or scorched, the piezo will no longer function at full sensitivity.

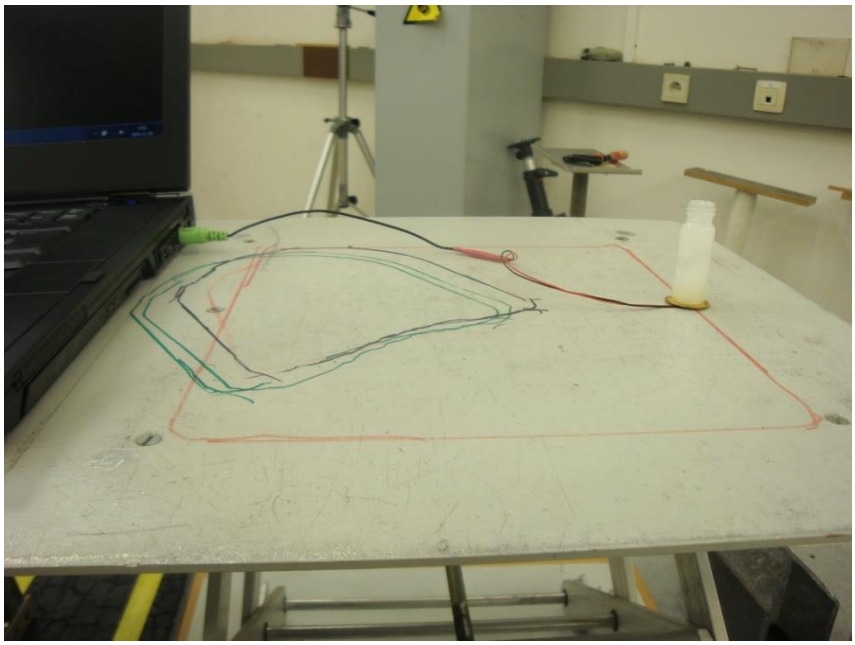

Figure 17: SDD resting on a piezoelectric microphone connected to a laptop.

The acoustic sensor contains two parallel plates in which one is movable. When acoustic signals fall on the movable plate, the distance between the plates changes and as a result its capacitance also changes. This gives rise to the corresponding electrical signal. The amplitude of the electrical signal depends on the intensity of the acoustic signal falling on it.

The detection is based on the piezoelectric effect, by which a material generates an electric potential in response to a pressure change. Any spatially separated charge will result in an electric field, and therefore an electric potential. Shown in Figure 18 is a standard dielectric in a capacitor. In a piezoelectric device, mechanical stress, instead of an externally applied voltage, causes the charge separation in the individual atoms of the material.

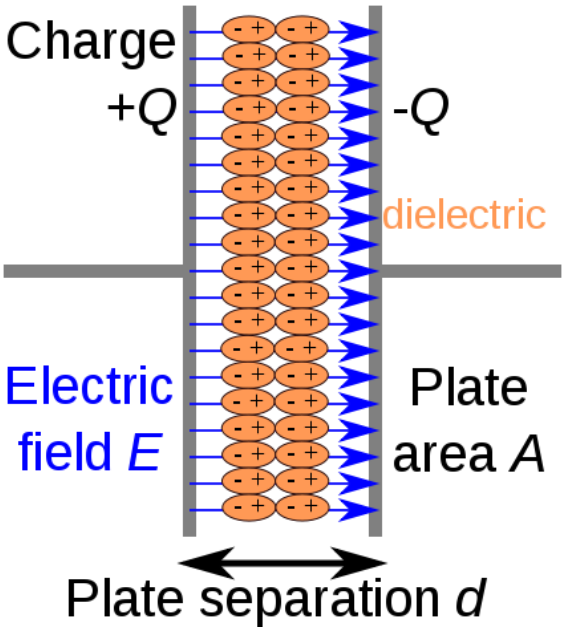

Figure 18: Charge separation in a capacitor.

To conclude, the active device senses the pressure change every time a drop nucleates by a piezoelectric transducer. When a drop vaporizes, there is a 'burst' or 'explosion' due to the release of pressure from the vapor tension of the liquid to the atmospheric pressure. This pressure pulse, associated with each drop nucleation, picked up by the piezoelectric transducer coupled at the bottom of the vial containing superheated drops, is converted into an electric signal. Between the detector and the microphone, ultrasound gel is applied to optimize the sound wave transmission.

5.2 Data acquisition

In order to monitor and register the electric signal the piezoelectric microphone is plugged into the microphone port of a laptop. A program in LabVIEW is made that records a sound via the microphone port of the laptop and displays this as a voltage in function of time.

LabVIEW (Laboratory Virtual Instrument Engineering Workbench) is a graphically-based programming language developed by National Instruments. Its graphical nature makes it ideal for test and measurement (T&M), automation, instrument control, data acquisition and data analysis applications. It has shown significant productivity improvements over conventional programming languages. Programming languages such as C and BASIC use functions and subroutines as programming elements, LabVIEW uses the VI. Simply put, a Virtual Instrument (VI) is a LabVIEW programming element. A VI consists of a front panel, block diagram and an icon that represents the program. The front panel is used to display controls and indicators for the user, while the block diagram contains the code for the VI. The icon, which is a visual representation of the VI, has connectors for program inputs and outputs. Controls can be seen as inputs, they allow a user to supply information to the VI. Indicators as outputs, they indicate, or display, the results based on the inputs given to the VI [19].

The front panel of a VI handles the function inputs and outputs and the code diagram performs the work of the VI. Multiple VIs can be used to create large-scale applications, in fact, large scale applications may have several hundred VIs. In this work the number of VIs is rather limited. A VI may be used as the user interface or as a subroutine in an application. User interface elements such as graphs are drag-and-drop easy in LabVIEW. The block diagram also contains structures and functions which perform operations on controls and supply data to indicators. Collectively controls, indicators, structures, and functions will be referred to as nodes. Nodes are connected to one another using wires, e.g., two controls and an indicator can be wired to the addition function so that the indicator displays the sum of the two controls. Because the program code is graphical, it closely fits the way engineers think, namely in block diagrams. Virtual representations of lab equipment can be dragged and dropped and wired together.

The 'Data_acquire_2.vi' program continuously displays the audio signal derived from the piezoelectric microphone by plotting the amplitude of the audio signal in volt in function of time in seconds. In another window, the saved pulses are shown by displaying the amplitude (V) in function of time (ms), the last saved pulse is displayed until a new pulse occurs. A third window shows the number of counts = pulses in function of time (s). The front panel is shown in Figure 19.

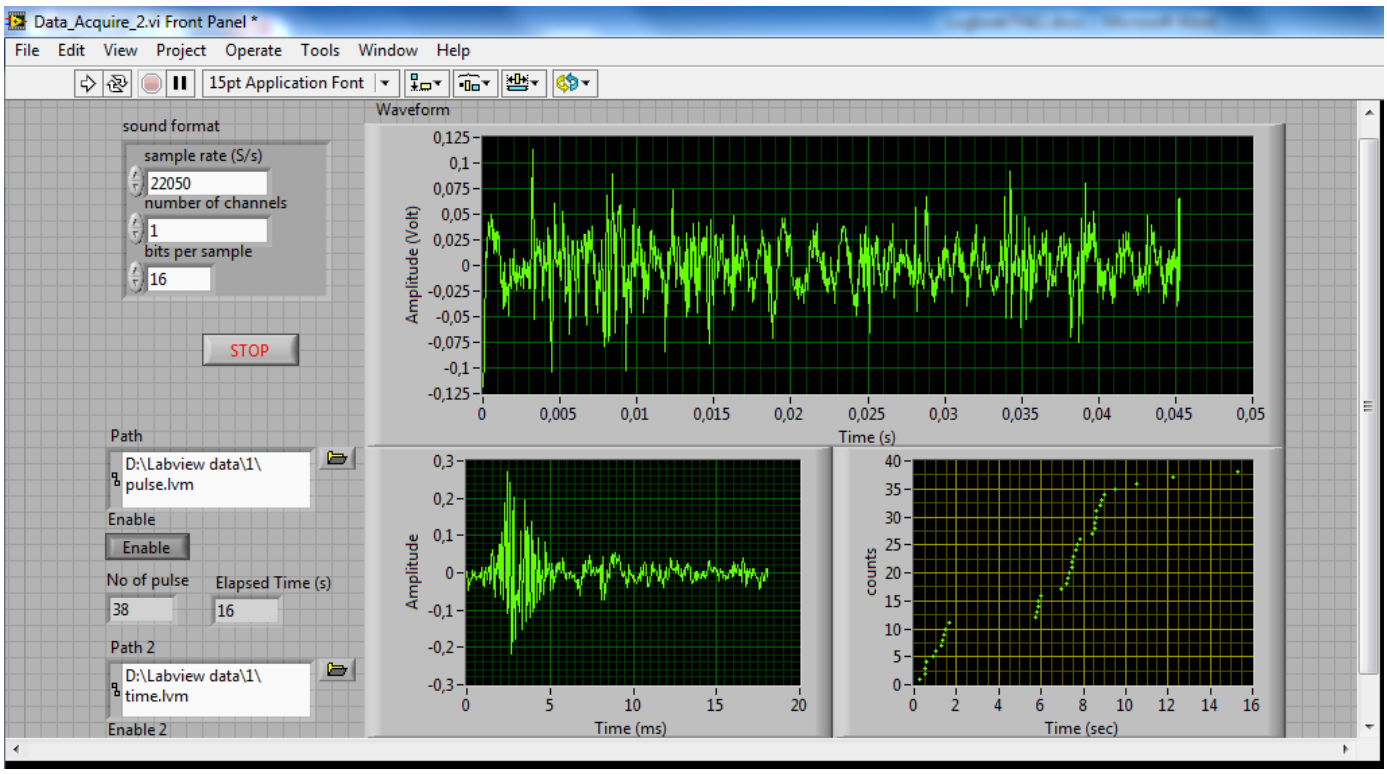

Figure 19: Front panel of Data_Acquire_2.vi which constantly displays the audio signal, the last stored pulse and the number of pulses in function of time.

In Figure 19 you can see that the background or ambient noise is displayed as well. The program uses a high pass filter (passes signals with a frequency higher than a certain cutoff frequency and attenuates signals with frequencies lower than the cutoff frequency) with a cutoff frequency of 400 Hz. A true nucleation event typically has a much higher frequency. The filter is set with an infinite impulse response (IIR filter) and has a Butterworth characteristic of the 4th order (so -80 dB/decade). The Butterworth characteristic provides a very flat amplitude response in the passband and a roll-off rate of -20 dB/decade/pole. The phase response is not linear, however, and the phase shift (thus, time delay) of signals passing through the filter varies nonlinearly with frequency. Therefore, a pulse applied to a filter with a Butterworth response will cause overshoots on the output because each frequency component of the pulse's rising and falling edges experiences a different time delay. This can be seen in Figure 20, group delay is the time delay of the amplitude envelope and is a function of frequency.

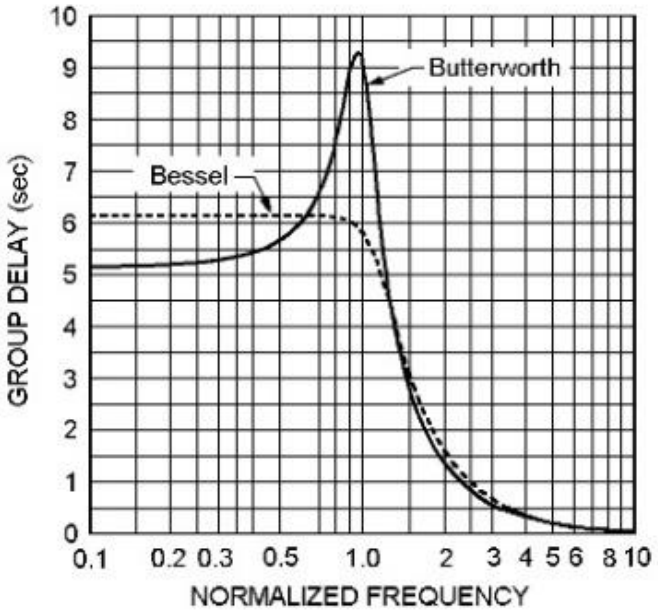

Figure 20: Group delay for the Butterworth response characteristic, where the overshoot can be seen clearly.

Filters with the Butterworth response are normally used when all frequencies in the passband must have the same gain. The Butterworth response is often referred to as a maximally flat response. This is made clear in Figure 21, with A_v the gain.

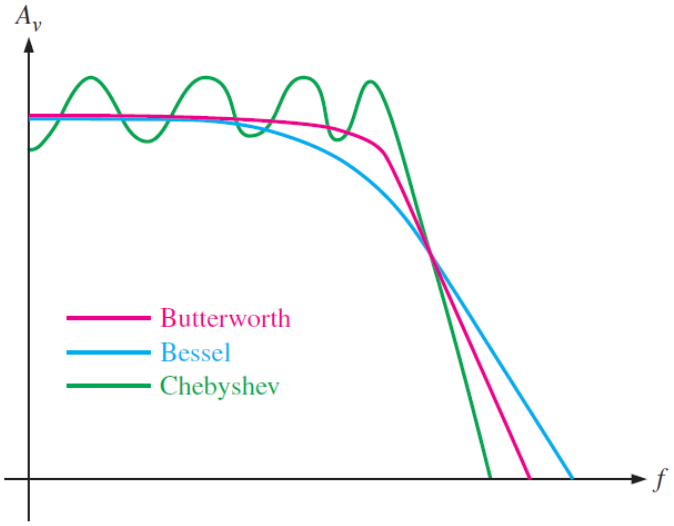

Figure 21: Comparative plots of three types of filter response characteristics.

A pulse is saved when the signal passes this filter and a certain amplitude threshold is exceeded, this amplitude threshold is set 5-10 % above the noise level.

For each saved pulses the LabVIEW Measurement format (.lvm) and the bitmap (.lvm.bmp) is stored. The LabVIEW Measurement format contains the time the pulse occurred etc. and information to be read in LabVIEW, the bitmap is used to visualize the pulse outside LabVIEW (Figure 22). The full block diagram of 'Data_Acquire_2.vi' can be found in Appendix C.

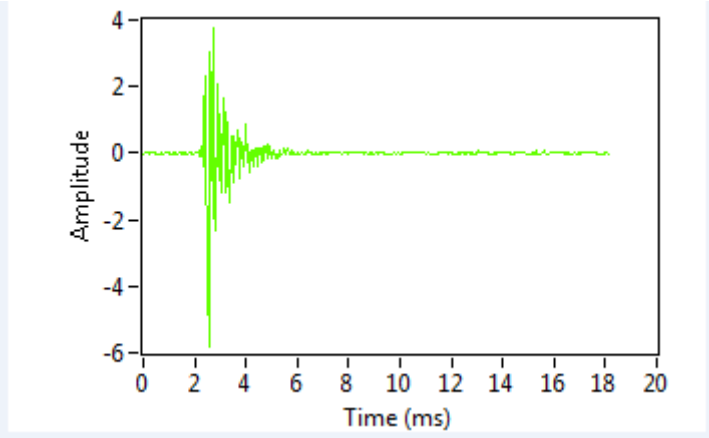

Figure 22: A pulse with .lvm.bmp extension displayed in Windows Photo Viewer.

5.3 Pulse shape validation routine

Of course, a lot of sound pulses are observed such as ambient noise, spontaneous bubbles (without a neutron collision), micro leaks and captured N_2. Therefore a manner must be sought to distinguish pulses caused by a neutron (nucleation event) from the rest. In order to distinguish nucleation event pulses from other pulses a pulse shape validation routine is made [20] with the addition of (vi) and (vii). This routine:

(i) sets an amplitude threshold;
(ii) identifies the beginning and end of each spike, based on the previous threshold;
(iii) amplitude demodulates the time evolution of the spike;
(iv) measures the decay time constant (τ) of the pulse;
(v) suppresses the pulses which exhibit τ's below and above a given window;
(vi) performs the FFT; and
(vii) suppresses the pulses which exhibit a principal frequency below and above a given window.

An interactive procedure is used to choose the amplitude threshold and can be set very low for the rejection of spurious noise. Amplitude demodulation is performed by the modulus of the Hilbert transform of the pulse waveform, $y(t) = |H\{x(t)\}|$. This results in the amplitude envelope and the maximum and the minimum of the pulse shape can now be found to set the time window used for evaluating τ. The decaying part of the envelope is then fit to an exponential, $h(t) = A\, e^{-t/\tau}$. In order to achieve this fit linear regression is used and the envelope is linearized, $\ln\big(y(t)\big) = \ln(A) - t/\tau + er(t)$ with er(t) the residual of the fit. The above is illustrated in Figure 23 and Figure 24.

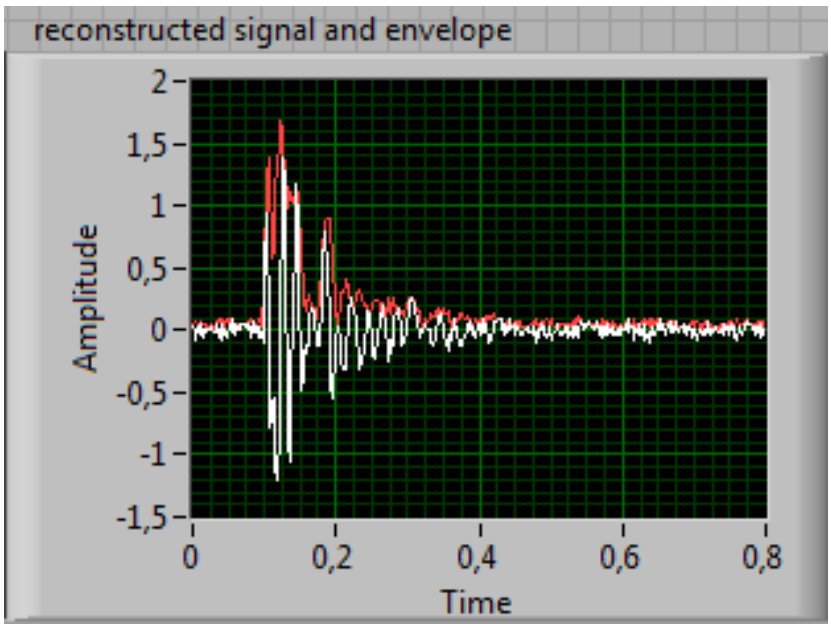

Figure 23: Typical pulse shape of a bubble nucleation event. The original signal x(t) is shown in white and in red the modulus of the Hilbert transform y(t)=Abs(H(x(t))), the amplitude envelope.

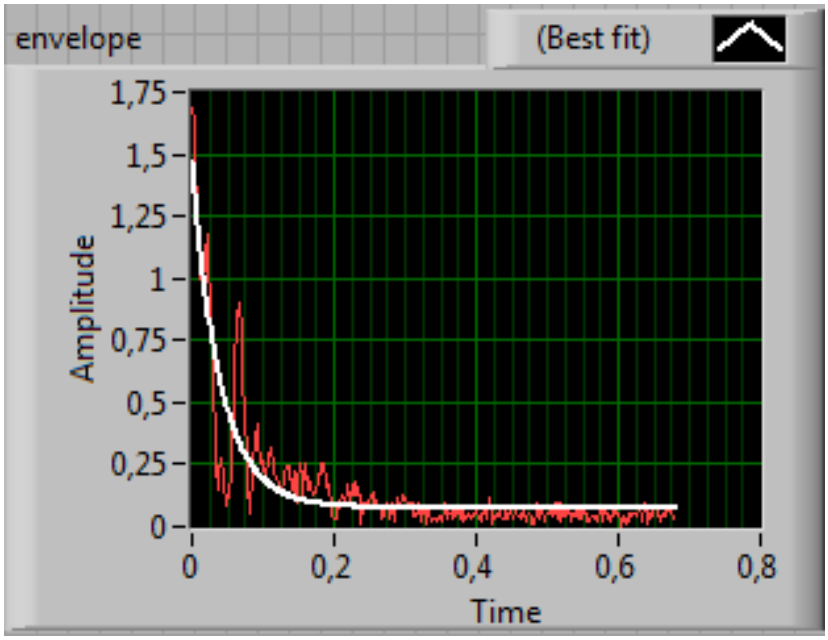

Figure 24: Best fit to an exponential function of the amplitude envelope from Figure 23, the exponential fit is shown in white and the envelope in red.

Figure 24 shows both the decay interval of the envelope, and the exponential fit.

To accomplish the above a LabVIEW program ('Hilbert transform & envelope auto.vi') is made where a previous stored pulse can be loaded, the amplitude envelope is generated, the decaying part of the envelope is fit to an exponential and the decay time constant τ is computed. Thus this program analyses how a pulse fades away.

The front panel after loading an already stored pulse is shown in Figure 25.

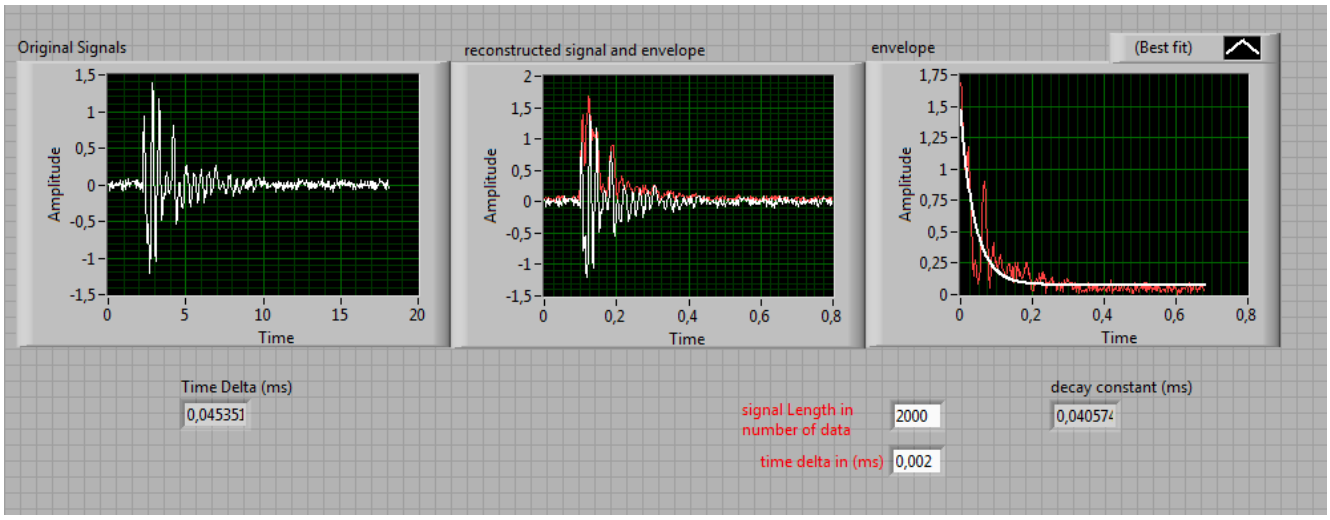

Figure 25: Front panel of 'Hilbert transform & envelope auto.vi'.

The most interesting value here is the pulse decay constant (cf. decay constant), which describes how the pulse fades away. The block diagram of 'Hilbert transform & envelope auto.vi' can be found in Appendix D. Although a lot of time was spent to develop the LabVIEW programs, these will not be discussed in detail since programming wasn't the main task. Only the general principle and the utility are discussed, because the programs were used to analyze the data.

Afterwards a way was sought to obtain the fast Fourier transform (FFT) with LabVIEW. The FFT converts the time domain to the frequency domain to display the power (dB) of the pulse in function of the frequency (Hz). 'Pulse power spectra FFT.vi' provides the necessary calculations, again a previous saved pulse can be loaded and the result is shown in Figure 26.

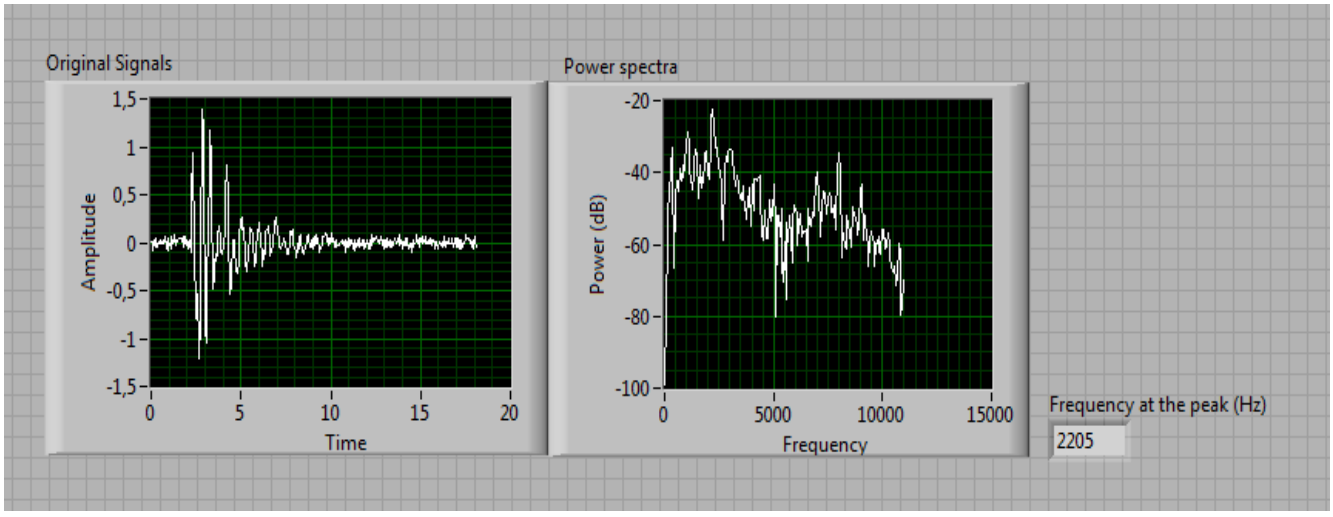

Figure 26: Typical pulse shape of a nucleation event and the fast Fourier transform of the event.

This program thus displays the original signal and the FFT. The frequency at the highest power (frequency at the peak) is displayed as well. This value will later be important to characterize a pulse caused by a neutron. The FFT is characterized by a peak, in this case at 2205 Hz, it was observed that a nucleation event has a typical window of values for this frequency. This is called the principal frequency. The block diagram is in Appendix E.

Finally, there was still the challenge to implement the 3 programs into one big program. Namely, a program that constantly measures the sound and shows it by means of Voltage in function of time, but only save a pulse if each condition is met. The pulse must have sufficient amplitude and thus exceed a certain threshold, the pulse has a particular window for the values of the frequency at the peak and the pulse has a particular window for its decay constant. This led to 'Data_acquire_2 Full.vi' whose front panel is displayed in Figure 27.

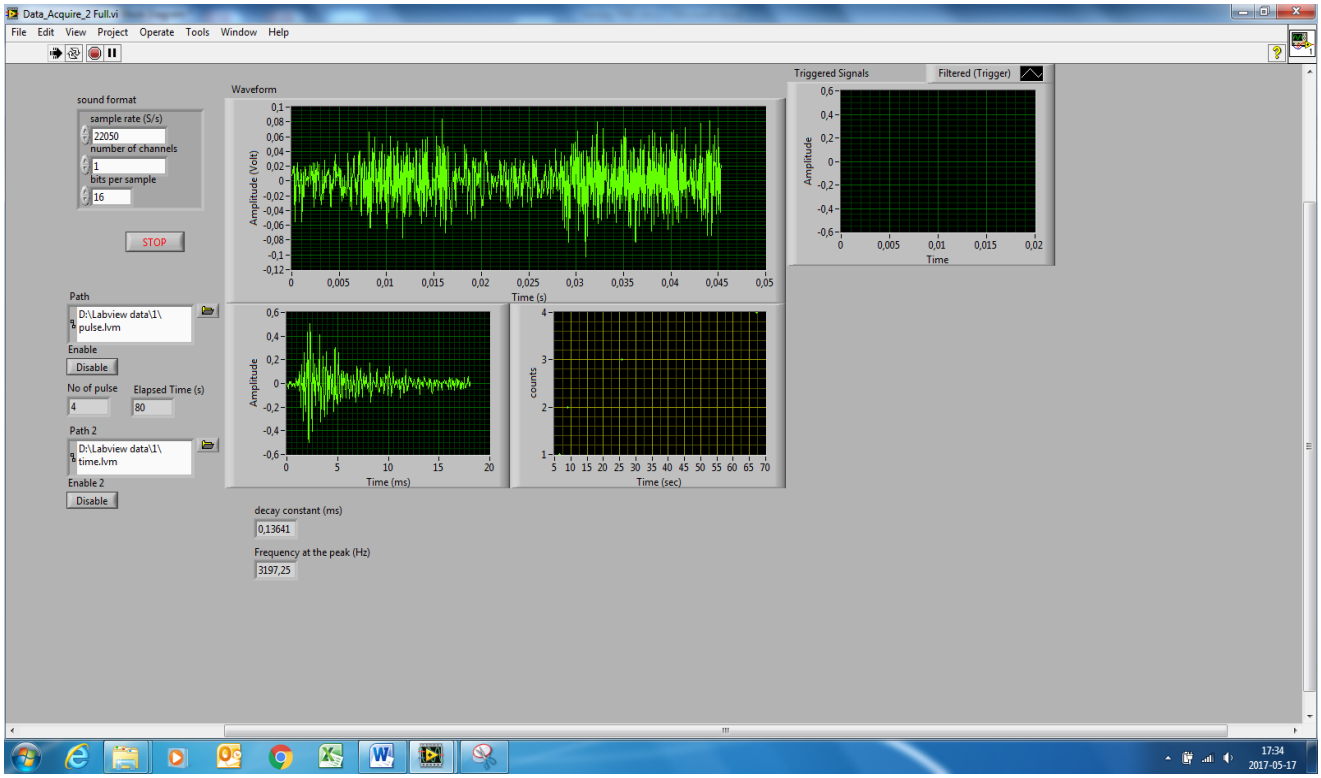

Figure 27: Front panel of Data_acquire_2 Full.vi.

The upper left shows the constant measured signal, left below only the pulses that are stored and the upper right pulses that exceed a certain threshold and where after calculations are made for the frequency and the decay constant. The latter is not visible in Figure 27 because the triggered pulse appears only briefly in the front panel and it is not possible to make a print screen at the same time.

The block diagram is shown in Appendix F, which clearly shows the 3 tests to be met before the pulse is stored. The full program for the FFT and amplitude envelope is hidden behind the FFT and Hilbert sub VI.

6 Calibration of the SDD

6.1 Calibration with ^{252}Cf

In order to use the fabricated SDDs in an unknown neutron field, the detector's sensitivity needs to be stable and read-out should be reproducible which to allow accurate calibration. That would allow to assign a certain calibration factor for each single detector in terms of bubbles/μSv. A reproducible calibration method need to be sought to express the dose response of the SDD. By irradiating the SDDs with neutrons, using a ^{252}Cf source, the response is examined. The number of bubbles created per unit dose is called the sensitivity of the detector. Californium-252 has a half-life of about 2.64 years and has two decay modes: alpha decay (96.91%) and spontaneous fission (3.09 %). In the case of spontaneous fission neutrons are emitted, the average neutron energy of the fission spectrum is 2.3 MeV and thus are fast neutrons [21].

6.1.1 Calibration building LNK KAL

This lab is a separate building on the SCK-CEN that is used to perform nuclear calibrations. In this building there are several standard arrangements with gamma, X-ray, neutron and beta sources. For calibration of neutron monitors, there are different ^{252}Cf neutron sources. The strongest source (CF3) was used for the study of the SDDs. The point-like source is in a 10 mm high and 7.8 mm diameter cylindrical capsule. This capsule is mounted on a 50 cm stainless steel rod with a polyethylene stopper at the other end. This whole is connected to a motor via a cable. In rest, the source is located in the basement of the calibration building. The motor can bring the source up to a fixed height (125 cm) in the calibration building bunker.

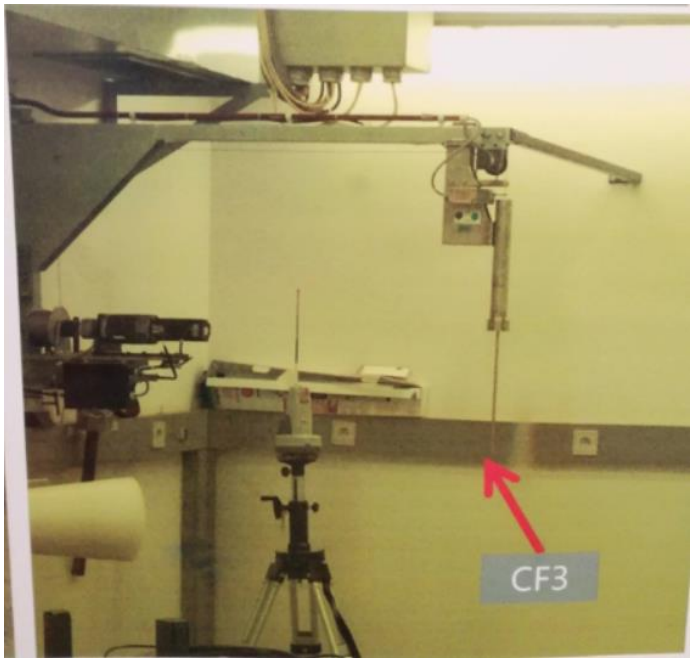

Figure 28: ^{252}Cf neutron source (CF3) at the end of a metallic rod.

The bunker is the part of the lab where the radiations with the highest dose rate occur. This bunker is 6x6 m^2 in size and is 3.5 meters high. This bunker has been air-conditioned and is always kept at 21 °C. The walls and floor are 50 cm concrete while the roof consists of 10 cm concrete.

6.1.2 Irradiation of the SDD

In Figure 29 a sketch of the hall and irradiation set-up is presented.

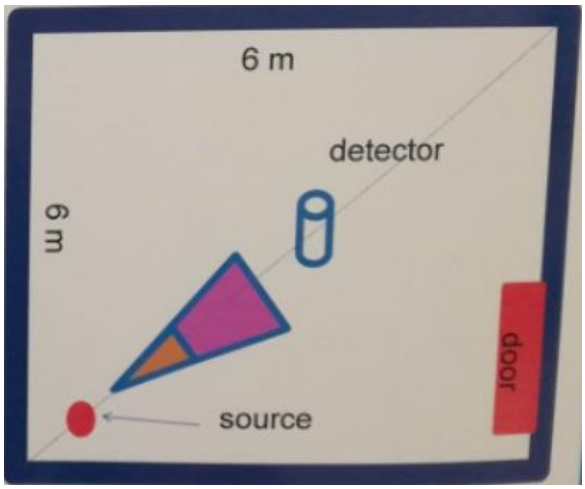

Figure 29: A sketch of the bunker and source-detector set-up.

Recall that the detector is connected to a laptop, a full calibration set-up can be seen in Figure 30.

Figure 30: Calibration set-up, including the SDD, a laptop installed with the LabVIEW program and the CF3 source.

Figure 31 is a zoomed in picture to show more clearly the ^{252}Cf source and the small vial containing the superheated droplets in a gel (SDD).

Figure 31: Neutron source at the end of the rod (left-hand side) and the SDD on the right resting on a piezoelectric microphone connected with a laptop.

The distance between the calibrated source and the detector is always 75 cm and each detector is exposed to 100 μSv (H*10), because of the decrease in activity of the source irradiations will take longer throughout the time to get 100 μSv. For example on 10/04/2017 943 seconds and on 13/07/2017 1009 seconds. Outside the bunker the time when the neutron source is active is monitored, the time when the source is in place will be noted (e.g. 13:31:14). For each registered pulse the time when the pulse occurred is saved (.lvm file). The dose rate (μSv/s) is known at LNK. By subtracting the start time (time when neutron source is in place) from the time of the saved pulse and multiplying with the dose rate, the dose at that moment is known. All saved pulses are subjected to a visual analysis, by looking at the shape, amplitude and duration of the pulse it is determined whether or not the stored pulse is a nucleation event. In this way a first filtering is done. Now, if one knows the time of the first bubble/nucleation the given dose at the first bubble is known (e.g. first bubble at 8.2 μSv). After a visual filtering a second filtering is done by looking at the decay constant and the principal frequency of the pulse, if these values differ significantly from the rest the pulse is deleted. Outliers (>3 times the standard deviation) from a certain window for decay constant and principal frequency are not considered as a true nucleation event. A LabVIEW VI is made where one can load a folder of saved pulses subjected to the visual filtering and returns the time of occurrence, decay constant and principal frequency of each pulse in the folder.

6.2 Response to thermal neutrons

6.2.1 Thermal beam at the BR1 reactor

An important aspect of neutron detectors is their response to thermal neutrons. Through interactions with matter, neutrons lose their energy until they are in equilibrium with the environment and their energy is thermal. These are in fact no mono-energetic neutrons, but they have a Maxwell distribution around a certain point, taken as standard as 0.0253 eV at room temperature.

A thermal neutron beam can only be created by slowing down fast neutrons through multiple collisions with a moderating material. This moderator has an as low as possible Z value, so that any elastic collision decreases as much as possible energy from the neutron. For the study, the thermal neutron source of the BR1 reactor on the SCK-CEN was used. The BR1 is an experimental reactor, which has been in operation since 1956. The reactor has a thermal power of 700 kW and natural uranium as fuel. These fuel rods are in a large block of graphite that serves as a moderator. A containment wall of 2.1 m concrete is located around the graphite. In the center of the reactor is a spherical cavity which is used as a neutron calibration field. However, this is not used here because the neutron flux is far too high for the envisaged applications. Therefore, one of the bundles on the side of the reactor, channel Z55, was chosen. This is an opening that leads into the reactor. In this opening is an iron collimator, so that a uniform, unidirectional neutron beam will come from the channel. This bundle consists mainly of thermal neutrons. The arrangement consists of an aluminum construction, where one detector can be brought into the bundle at the same time. A picture of the arrangement can be seen in Figure 32. A borated brick can be placed in front of the opening on the right to stop the beam.

Figure 32: Thermal beam at channel Z55 with the aluminum construction.

6.2.2 Irradiation of the SDD

During irradiations of the SDDs the reactor was working at full power, that is 700 kW. Each detector was 10 minutes in the beam. The same procedure was followed as in section 6.1.2 to process and evaluate the data. Figure 33 shows that the SDD is taped to a metal plate to stay upright with the piezoelectric transducer taped underneath the detector. While in Figure 32 the whole set-up can be seen.

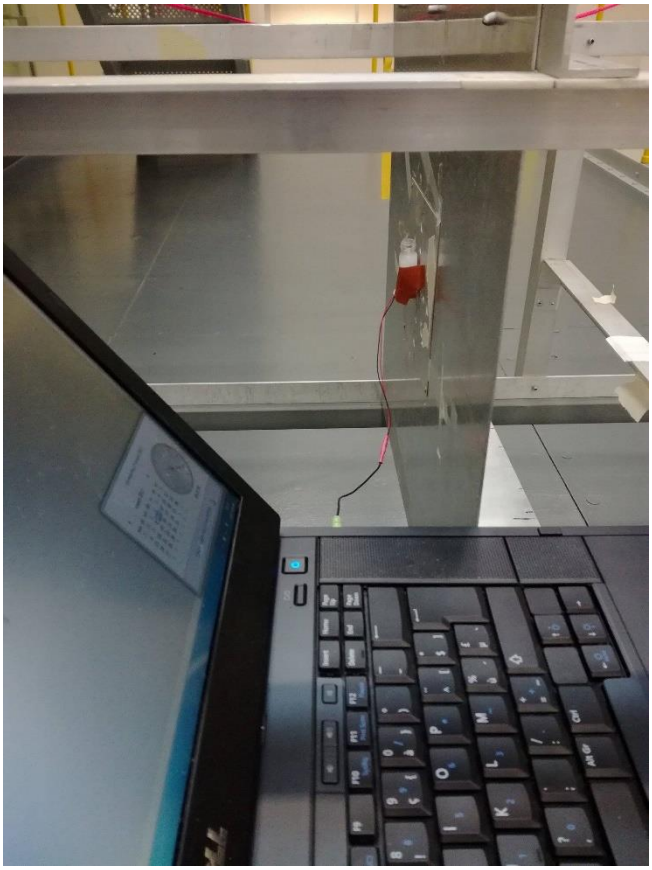

Figure 33: SDD taped to a metal plate in connection with a laptop at channel Z55B.

6.3 Calibration BDT and BD-PND

For comparison some of BTI's bubble detectors, BDT and BD-PND were calibrated as well.

6.3.1 Calibration BD-PND

The BD-PNDs were irradiated using the same ^{252}Cf source as described before. The detectors were placed together on a small rack at a distance of 75 cm from the source, this is made clear in Figure 34.

Figure 34: Irradiated BD-PNDs, the detectors were in the beam together on the small rack.

6.3.2 Calibration BDT

In order to calibrate the BDTs the thermal beam at channel Z55 was used again. Figure 35 shows the set-up. On the left-hand side the bubble detector is screwed into a holder (see Figure 36) and on the right-hand side you can see the brick placed in front of the beam.

Figure 35: Irradiation set-up for the bubble detector BDT at channel Z55.

Figure 36: Bubble detector holder with BDT in the aluminum construction at channel Z55.

The BDTs staid in the beam for 2 minutes while the reactor was operating at a power of 100 kW.

6.4 Detector's response tests and fabrication protocol improvements

This section will discuss the different tests performed and the adjustments and improvements to the fabrication protocol which were carried out on the basis of the results obtained.

6.4.1 Irradiation detectors made from old & new material

As a first test some SDDs were made from old material and new self-made material and irradiated at LNK. Five detectors were made from material already available at SCK, this gel contained an unknown amount of Freon. From the first self-made gel containing 4.7 ml of Freon, five other detectors were made. For all irradiated detectors a dose-response curve is created, this is the number of bubbles in function of the dose. The results showed that these detectors were unstable, too much spread in response between the different detectors could be noticed. For example, one detector gave 20 bubbles for 100 µSv and another only 10.

Looking at the self-made gel you could see that there was too much foam, only the lower layer of the gel was usable.

6.4.2 Detectors from adapted fabrication protocol with less Freon

It was suggested that something went wrong when transferring the gel from the pressure reactor to the glass bottle using a large syringe. After discussing with other experts the gel is now poured from the pressure reactor into the glass bottle very slowly using the sides of the glass bottle. The gel can also foam by adding too much Freon, so this time only 4.1 ml of R227EA is used. Eight new detectors were fabricated, but again the results and the gel itself showed that the detectors were unstable. The gel should not contain a lot of air bubbles and must have an even color. However the results were useful because they gave an idea of the reproducibility, the detectors were irradiated multiple times and should give a similar response.

6.4.3 Detectors from final optimized fabrication protocol including data processing and reset test

After acquiring more information about manufacturing SDDs, the fabrication process was improved. A better degassing process was developed. Before, the gel was not heated or incorrectly heated during degassing. Also, the applied pressure was maintained for longer and the pressure release happened very slowly. The full explanation can be found in Appendix B. To avoid foam even less Freon was added, only 3.5 ml. After the last tests performed the data processing software in LabVIEW was developed. A pulse shape validation routine was used to evaluate the data more objectively. After a visual analysis of the saved pulses, the pulses were subjected to a parameter analysis. As explained before, looking at the principal frequency and decay constant of the saved pulses some pulses were not considered as a true nucleation event. A new gel was manufactured, resulting in 9 new detectors. However, the irradiation results showed that these detectors weren't sensitive enough. Only a few bubbles were formed, insufficient to perform good statistics. For these SDDs a first reset test was performed, the SDD can be reset by applying 5-6 bar of pressure (placing the vial with the lid off in the pressure reactor) after being irradiated. The SDDs were irradiated multiple times throughout the time, e.g. on 27/03/2017, 30/03/2017 and 10/04/2017. Some detectors were reset between each irradiation and others weren't. The effect on the parameters that characterize a pulse with and without a reset were studied.

6.4.4 Detectors from final optimized protocol with increased sensitivity for long-term follow up and reset test

For the last tests carried out more Freon was added, 4.7 ml using the gastight syringe, to create a more sensitive detector. The SDD will form more bubbles responding to 100 μSv of dose in order to perform better statistics. Two sets of each 5 SDDs, F1-F5 and F6-F10, were irradiated.

The reset set F1-F5 was reset between each irradiation, the non-reset set F6-F10 was left in its state after irradiation. All detectors were irradiated on 28/06, 30/06, 10/07, 12/07 and 13/07/2017. The effect of time and the effect of reset on the sensitivity and on the parameters of the detectors were studied.

7 Results

Not all results will be displayed. Some results were instructive to improve the fabrication protocol and others to form an idea about reproducibility, etc. Often only a few results are shown to make a point.

7.1 Response of SDD to ^{252}Cf

For each irradiated detector a dose-response graph is drawn using the method explained before. A linear trend line through the origin is also included, showing the equation of the trend line. Some of the results of the first test are shown in Figure 37-40. SDD OU1 and OU2 were made from old material, detector 1 and 2 from new material.

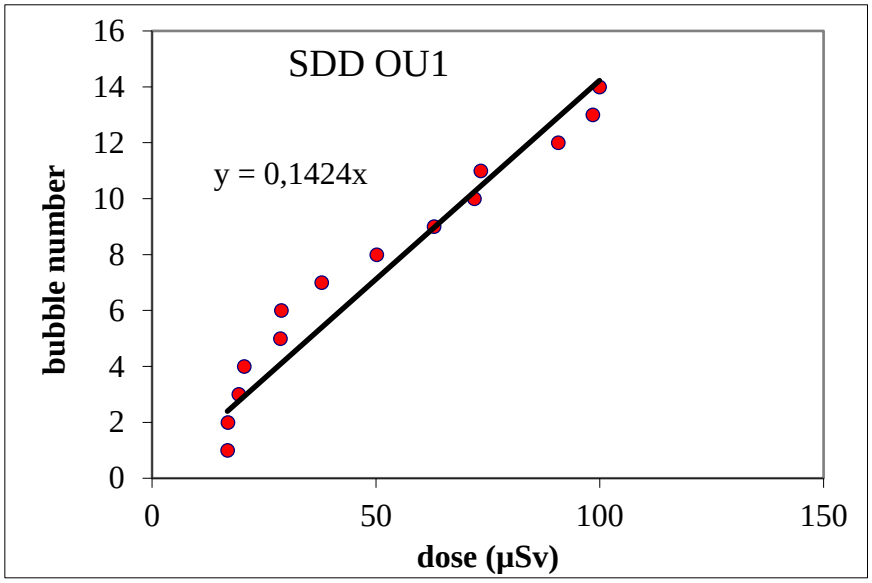

Figure 37: Dose-response graph of SDD OU1 made from old material.

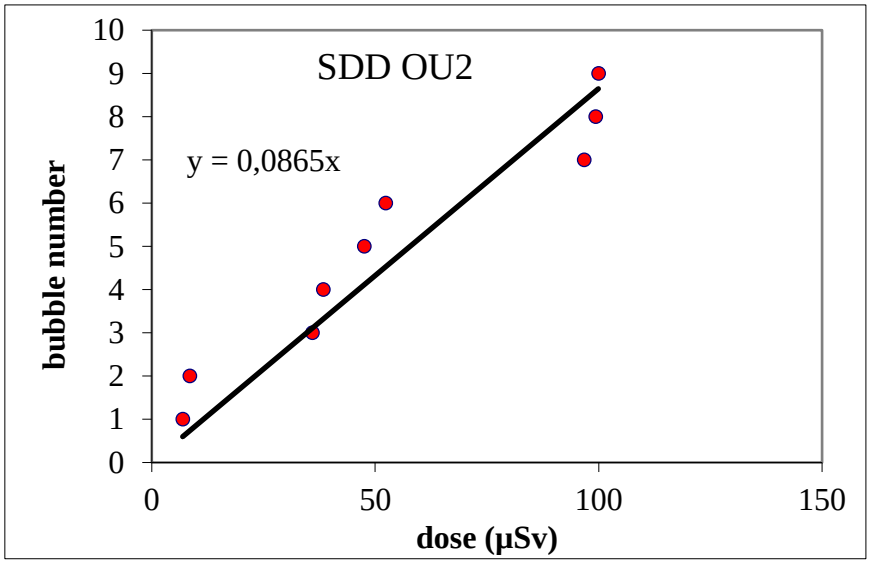

Figure 38: Dose-response graph of SDD OU2 made from old material.

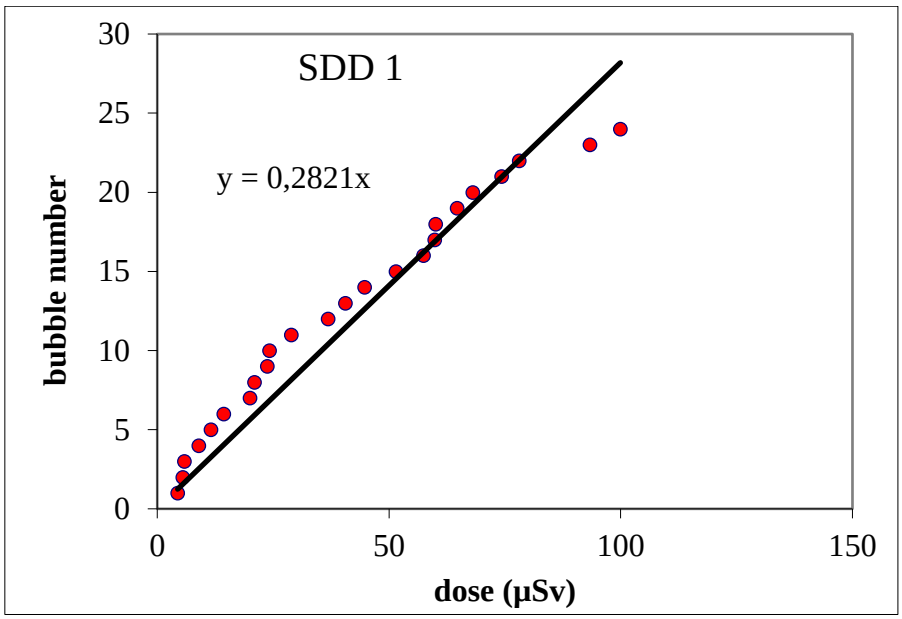

Figure 39: Dose-response graph of SDD 1 made from new material.

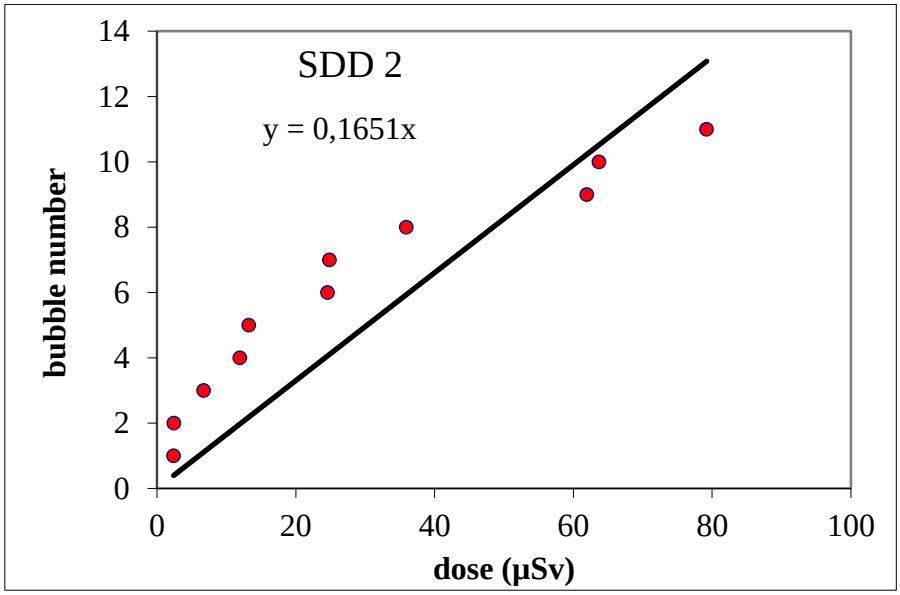

Figure 40: Dose-response graph of SDD 2 made from new material.

Figure 37 and 38 are shown to indicate that the old material isn't quite usable anymore, SDD OU1 gave 14 bubbles for 100 µSv and OU2 only 9. In Figure 39 and 40 can be seen that SDD 1 had a response of 24 nucleation events to 100 µSv of dose, while SDD 2 only gave 11 bubbles. There was too much spread in sensitivity between the detectors. These detectors were unstable and a new gel had to be made.

The new prepared gel also showed defects and the results from the irradiated detectors made from the gel demonstrated this expectation. The SDDs were irradiated on 2/03, 3/03 and 6/03/2017. Two out of five detectors were no longer useful after the first or second irradiation, others showed a similar sensitivity throughout the time. This gave an idea about the reproducibility, the extent to which the same SDD will give the same result under identical conditions.

After the mentioned improvements, the first successful gel was made. The gel contained almost no air bubbles and had an even color. The pulse shape validation routine was applied for the first time but the detectors weren't sensitive enough. Only 3-5 bubbles per 100 µSv were produced. A trend line based on 3-5 data points is not meaningful, one data point can cause a big shift in the position of the trend line. Also, in order to study the effect on the parameters (principal frequency and decay constant) more than 5 valid pulses are desired.

The same manufacturing process was retained, but more Freon was added to obtain more sensitive detectors. This resulted in SDDs F1-F10, as an example some dose-response graphs are presented in Figure 41-44.

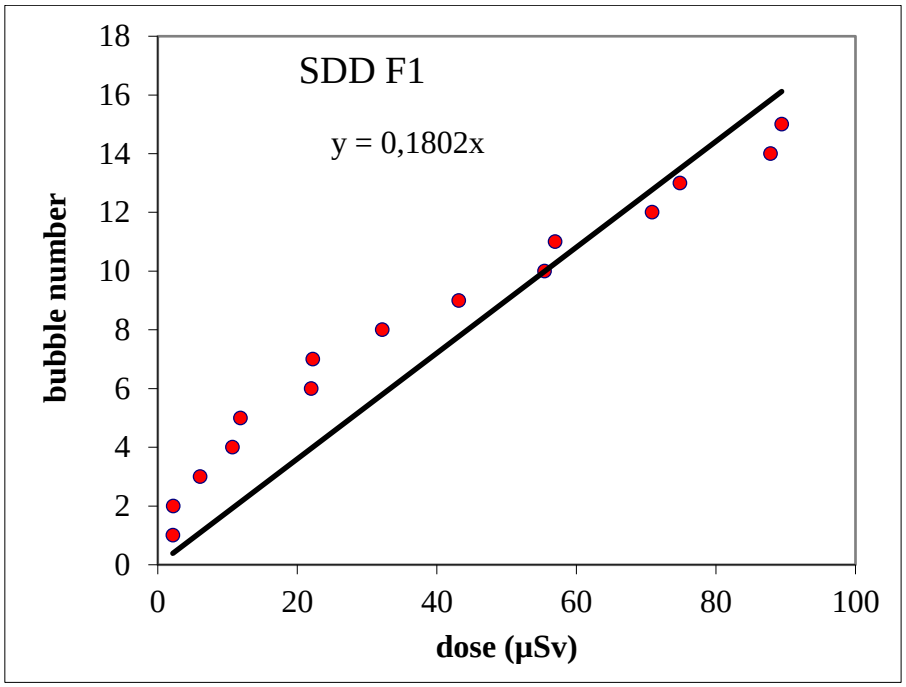

Figure 41: Dose-response graph of SDD F1 made from the final gel.

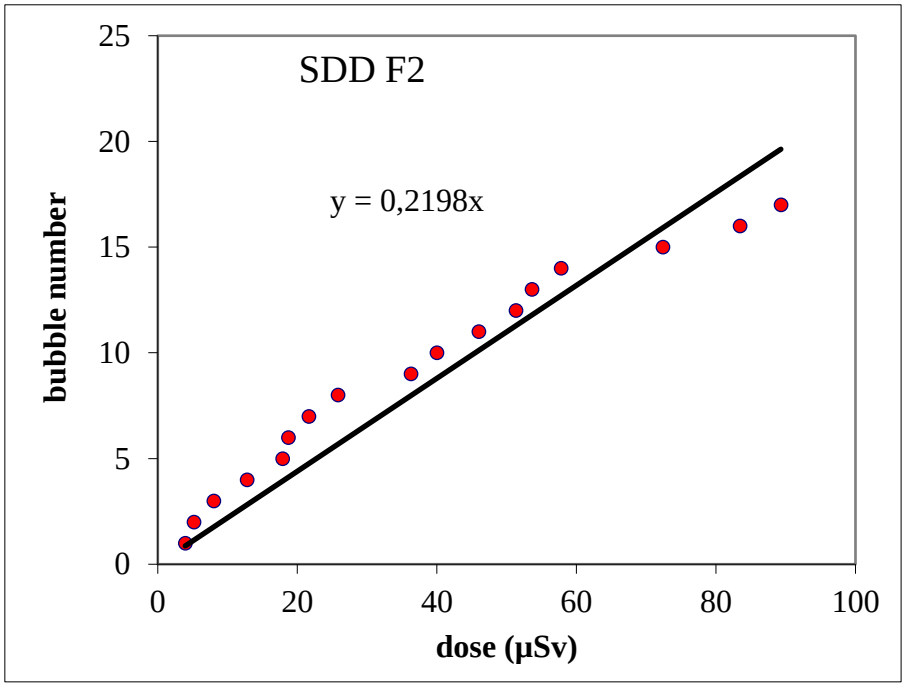

Figure 42: Dose-response graph of SDD F2 made from the final gel.

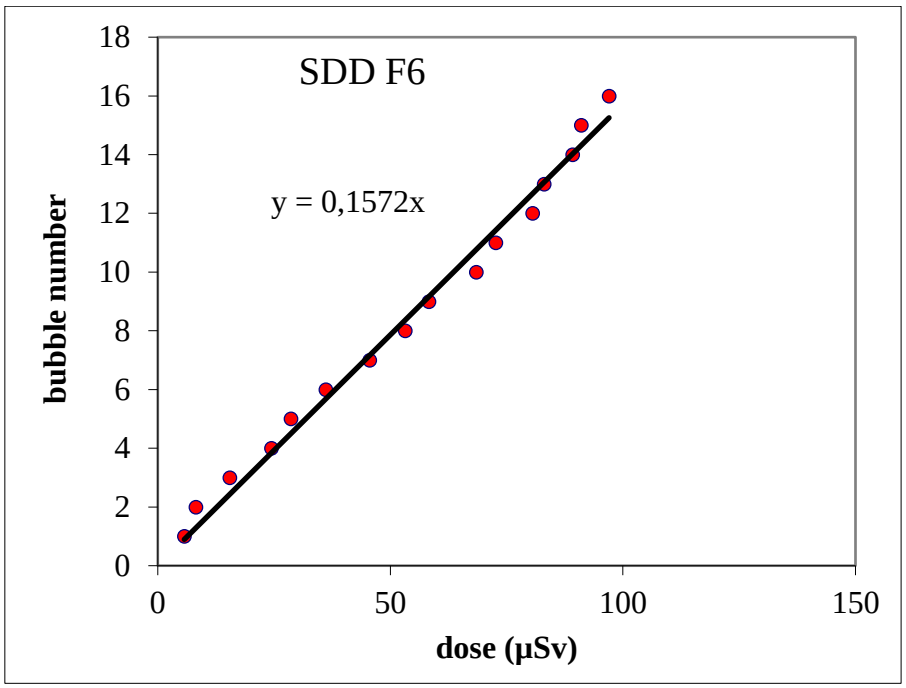

Figure 43: Dose-response graph of SDD F6 made from the final gel.

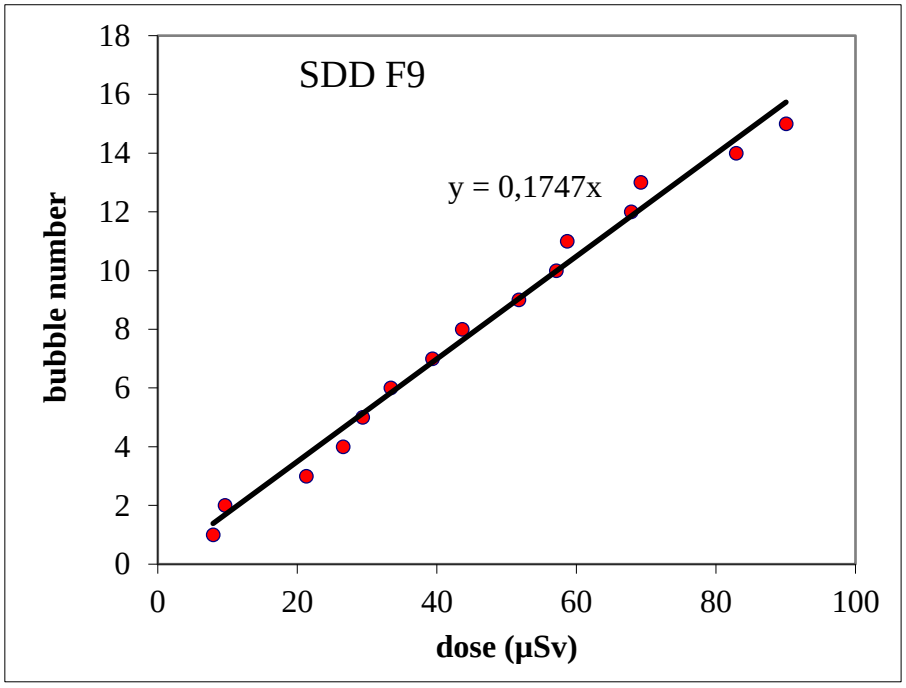

Figure 44: Dose-response graph of SDD F9 made from the final gel.

Again the pulse shape validation routine was applied and the results obtained are summarized in the table below.

Table 2: Example of parameter table for each detector.

	Irradiation 30/06				
Detector	*τ (ms)*	*f_{peak} (Hz)*	*bubbles/µSv vis.*	*bubbles/µSv par.*	*bubbles/µSv fit.*
F1	0,033 - 0,071	1925 - 2591	0,17	0,14	0,16
F2	0,036 - 0,068	1323 - 2105	0,20	0,17	0,19
F3	0,029 - 0,078	1984 - 2481	0,21	0,17	0,19
F4	0,046 - 0,061	2095 - 2977	0,16	0,13	0,13
F5	0,022 - 0,058	1544 - 2205	0,16	0,14	0,13

After each irradiation the above shown table is made for each detector. First, all stored pulses are visually evaluated, resulting in 'bubbles/µSv vis.'. Then, for each visually approved pulse, the decay constant and principal frequency is generated. Outliers are not considered as a true nucleation event. These pulses are not included in 'bubbles/µSv par.', the number of bubbles divided by 100 µSv after the parameter analysis. In Table 2 the decay constant τ in milliseconds is shown, all valid pulses after the parameter analysis of SDD F1 have a τ between 0,033 ms and 0,071 ms. The window for the frequency at the peak (=principal frequency) f_{peak} in Hertz of the valid pulses for each detector is presented as well. In the last column the slope of the linear fitted trend line (fitted from the parameter selected data) is added, 'bubbles/µSv fit.'.

The different calibration factors, bubbles/µSv vis., par. and fit., are studied. The number of bubbles after the parameter analysis is lower than after the visual analysis because some outliers are filtered out. The fitted calibration factor will be quite dependent on the spread of the bubbles as a function of the dose and lies between the values after the parameter analysis and after the visual analysis. Later on will be decided which of the three parameters is the most reproducible to serve as a calibration factor when irradiating multiple times.

The difference in sensitivity between the different detectors made from the same batch was studied. On 28/6 there was a 10% difference in sensitivity between all 10 detectors. This is a big difference since the dose should be known very accurate and therefore it was decided to calibrate the detectors individually.

7.2 Response of SDD to thermal neutrons

On 9/03/2017 detectors OU1, L1 and O5 were irradiated in the thermal beam at channel Z55 while the BR1 reactor was operating with a power of 700 kW. For this thermal power a dose rate of 6,1 µSv/s (H*10) is generated, the SDDs were 10 minutes in the beam and thus receiving 6,1 µSv/s * 600 s = 3660 µSv = 3,66 mSv. This dose is a lot higher than the 100 µSv used before because a much lower sensitivity for thermal neutrons is expected than for fast neutrons.

Table 3: Data for dose-response graph of SDD OU1.

	time recorded in time.lvm file (sec)	pulse number in time.lvm file	dose (µSv)	corrected pulse number	duration of irradiation	600	sec
detector R227_OU1	1529,904	377	707,0	1	dose rate	6,10	µSv/s
	1567,3	379	935,1	2	irradiation start	1414	sec
	1571,8	381	962,7	3	irradiation stop	2014	sec
	1669,9	386	1560,7	4			
	1849,5	387	2656,3	5	number of bubbles	6	
	1960,517	388	3333,8	6			

The necessary data to plot a dose-response chart are shown in Table 3, this is done for every detector. For SDD OU1 the irradiation started at 10:23:34, 1414 s = 23 min * 60 s/min + 34 s. The results obtained for SDD OU1, L1 and O5 are shown is Figure 45-47.

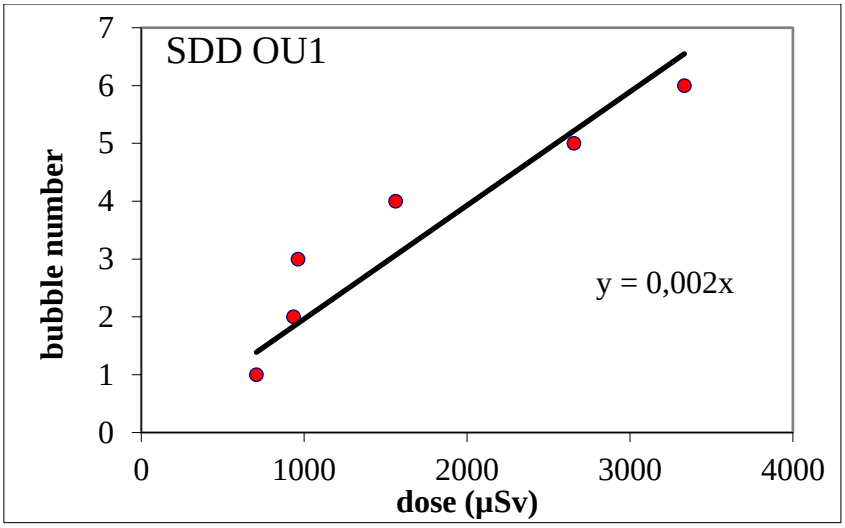

Figure 45: Dose-response graph of SDD OU1 for thermal neutrons.

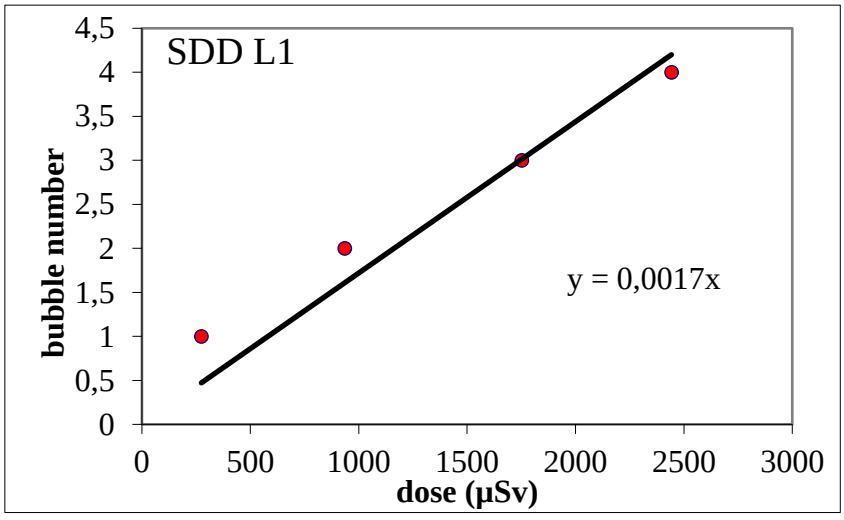

Figure 46: Dose-response graph of SDD L1 for thermal neutrons.

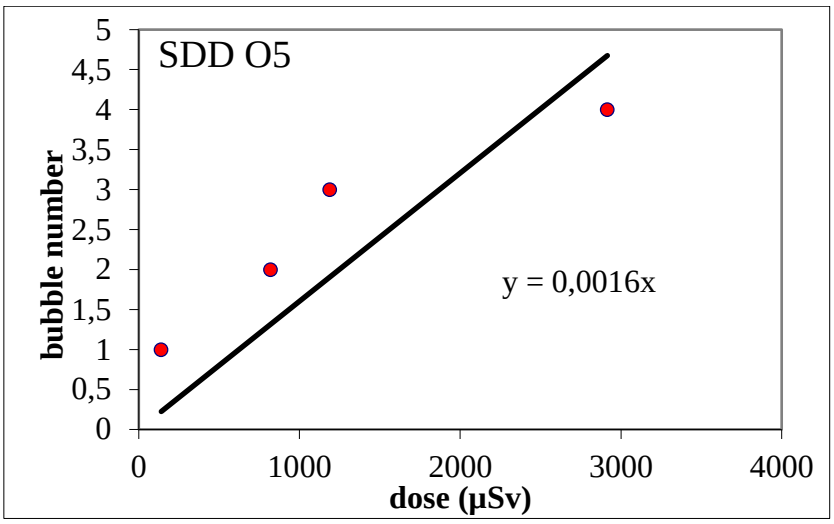

Figure 47: Dose-response graph of SDD O5 for thermal neutrons.

The made SDDs exhibit a very minor sensitivity to thermal neutrons, namely 1,09-1,64 bubbles/mSv or 0,00109-0,00164 bubbles/µSv. This is one hundred of the sensitivity to fast neutrons. However, the sensitivity to thermal neutrons cannot be fully assured because the given dose is not 100% due to thermal neutrons. In the spectrum of the beam is also a very small fraction of fast neutrons.

7.3 Effect of the amount of Freon

To study the effect of the added amount of Freon, the variation of the number of bubbles formed during the first measurement is considered.

SDD L1-L9: 3,5 ml R227EA

SDD 1-7: 4,1 ml R227EA

SDD F1-F10: 4,7 ml R227EA

Table 4: Comparison of detectors with different amounts of added Freon.

3,5 ml		**4,1 ml**		**4,7 ml**	
SDD	**# bubbles**	**SDD**	**# bubbles**	**SDD**	**# bubbles**
L1	3	1	5	F1	15
L2	4	2	7	F2	17
L8	3	4	6	F6	16
L9	3	5	6	F8	14

Table 4 shows that the sensitivity of the detectors increases with the added amount of Freon (the number of bubbles produced is due to 100 µSv). 3-4 bubbles were produced if 3,5 ml of Freon was added, almost double the number of bubbles were reached for 4,1 ml of Freon. For 4,7 ml of Freon 14-17 bubbles were produced, almost three times as much for 0,6 ml extra. These last SDDs are sensitive enough to be able to perform good statistics.

The average number of bubbles formed is plotted for the three groups in function of the added amount of Freon in Figure 48.

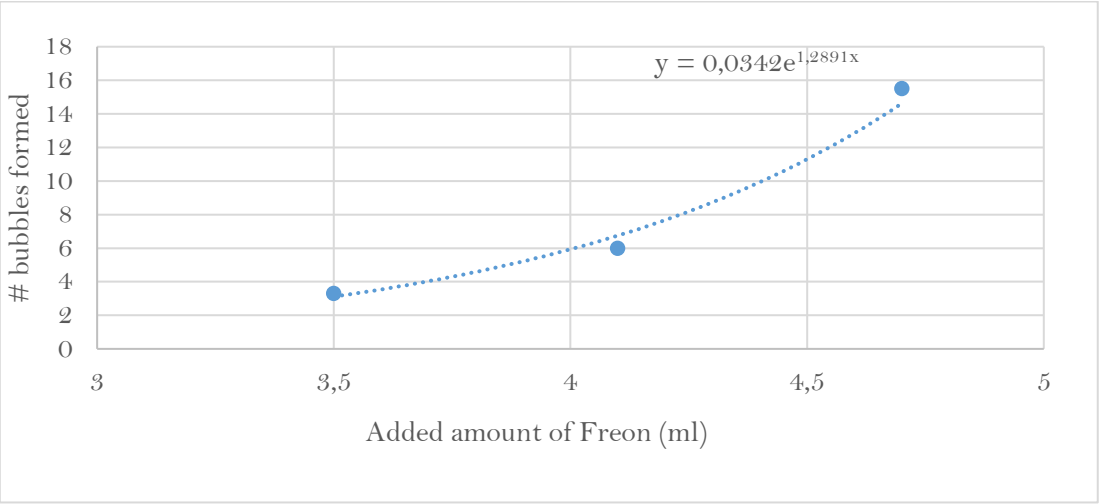

Figure 48: Number of bubbles formed in function of the added amount of Freon.

Figure 48 shows that the number of bubbles formed exponentially increases with the added amount of Freon.

7.4 Effect of time & reset

The last made detectors F1-F10 were irradiated 5 times, on 28/06, 30/06, 10/07, 12/07 and 13/07/2017, Figure 49 shows this in a timeline.

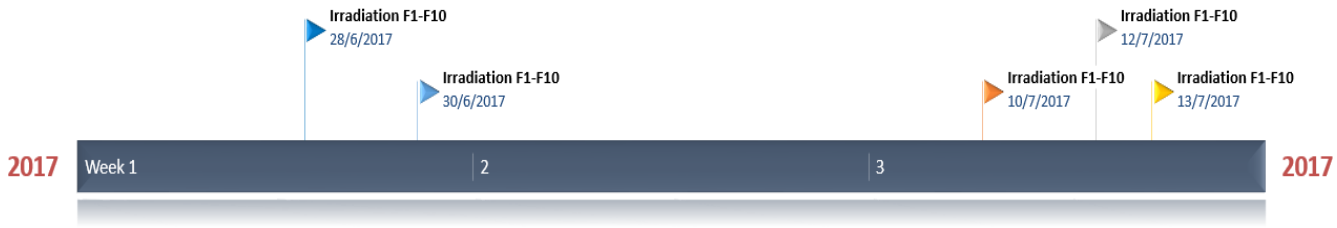

Figure 49: Timeline of final irradiations.

7.4.1 Comparison of the 3 calibration factors

The 3 different calibration factors are compared to determine which method is the most reproducible and which factor will be used afterwards to express the sensitivity of the detectors.

F1-F5: reset set

F6-F10: non-reset set

The results from the final tests are summarized in Table 5 (reset set) and Table 6 (non-reset set).

Table 5: Summary table of the final tests for the reset set F1-F5.

	Irradiation 28/06				
Detector	*τ (ms)*	*f_{peak} (Hz)*	*bubbles/μSv vis.*	*bubbles/μSv par.*	*bubbles/μSv fit.*
F1	0,024 – 0,073	1833 – 2612	0,17	0,15	0,18
F2	0,040 - 0,079	1711 - 2349	0,19	0,17	0,22
F3	0,021 - 0,085	1660 - 2730	0,20	0,17	0,19
F4	0,035 - 0,084	2237 - 2750	0,17	0,14	0,15
F5	0,027 - 0,069	1940 - 2641	0,16	0,14	0,16
	Irradiation 30/06				
Detector	*τ (ms)*	*f_{peak} (Hz)*	*bubbles/μSv vis.*	*bubbles/μSv par.*	*bubbles/μSv fit.*
F1	0,033 - 0,071	1925 - 2591	0,17	0,14	0,16
F2	0,036 - 0,068	1323 - 2105	0,20	0,17	0,19
F3	0,029 - 0,078	1984 - 2481	0,21	0,17	0,19
F4	0,046 - 0,061	2095 - 2977	0,16	0,13	0,13
F5	0,022 - 0,058	1544 - 2205	0,16	0,14	0,13
	Irradiation 10/07				
Detector	*τ (ms)*	*f_{peak} (Hz)*	*bubbles/μSv vis.*	*bubbles/μSv par.*	*bubbles/μSv fit.*
F1	0,032 - 0,053	1759 - 2705	0,16	0,15	0,15
F2	0,033 - 0,044	1592 - 2105	0,18	0,16	0,16
F3	0,041 - 0,076	1540 - 2540	0,18	0,15	0,16
F4	0,021 - 0,067	2411 - 2838	0,17	0,14	0,16
F5	0,042 - 0,071	2050 - 2790	0,14	0,13	0,14
	Irradiation 12/07				
Detector	*τ (ms)*	*f_{peak} (Hz)*	*bubbles/μSv vis.*	*bubbles/μSv par.*	*bubbles/μSv fit.*
F1	0,026 - 0,071	2094 - 2757	0,17	0,15	0,15
F2	0,054 - 0,094	1980 - 2535	0,19	0,16	0,16
F3	0,036 - 0,086	1874 - 2480	0,16	0,15	0,15
F4	0,031 - 0,099	2315 - 3032	0,18	0,14	0,15
F5	0,041 - 0,11	2426 - 2977	0,17	0,13	0,12
	Irradiation 13/07				
Detector	*τ (ms)*	*f_{peak} (Hz)*	*bubbles/μSv vis.*	*bubbles/μSv par.*	*bubbles/μSv fit.*
F1	0,035 – 0,084	1914 - 2544	0,17	0,14	0,14
F2	0,049 – 0,073	1674 - 2512	0,18	0,15	0,15
F3	0,033 – 0,087	1792 - 2845	0,18	0,15	0,14
F4	0,029 – 0,075	2150 - 2831	0,15	0,13	0,13
F5	0,034 – 0,081	1804 - 2777	0,15	0,12	0,11

Table 6: Summary table of the final tests for the non-reset set F6-F10.

	Irradiation 28/06				
Detector	*τ (ms)*	*f_{peak} (Hz)*	*bubbles/µSv vis.*	*bubbles/µSv par.*	*bubbles/µSv fit.*
F6	0,045 - 0,068	2112 - 2734	0,18	0,16	0,16
F7	0,036 - 0,067	1851 - 2682	0,17	0,13	0,11
F8	0,044 - 0,083	1783 - 2444	0,17	0,14	0,12
F9	0,046 - 0,082	2147 - 2690	0,17	0,15	0,17
F10	0,055 - 0,076	1540 - 2289	0,19	0,18	0,17
	Irradiation 30/06				
Detector	*τ (ms)*	*f_{peak} (Hz)*	*bubbles/µSv vis.*	*bubbles/µSv par.*	*bubbles/µSv fit.*
F6	0,024 - 0,079	3725 - 4235	0,16	0,14	0,14
F7	0,033 - 0,088	5122 - 5674	0,15	0,12	0,14
F8	0,053 - 0,093	4037 - 4920	0,16	0,14	0,14
F9	0,040 - 0,068	4750 - 5278	0,15	0,14	0,13
F10	0,035 - 0,067	3569 - 3866	0,17	0,16	0,17
	Irradiation 10/07				
Detector	*τ (ms)*	*f_{peak} (Hz)*	*bubbles/µSv vis.*	*bubbles/µSv par.*	*bubbles/µSv fit.*
F6	0,035 - 0,069	3197 - 4796	0,18	0,16	0,17
F7	0,023 - 0,075	7993	0,16	0,12	0,12
F8	0,030 - 0,055	5110 - 6259	0,15	0,12	0,13
F9	0,043 - 0,067	4411 - 4987	0,17	0,13	0,14
F10	0,028 - 0,059	6740 - 7889	0,17	0,15	0,15
	Irradiation 12/07				
Detector	*τ (ms)*	*f_{peak} (Hz)*	*bubbles/µSv vis.*	*bubbles/µSv par.*	*bubbles/µSv fit.*
F6	0,027 - 0,083	3363 - 4346	0,16	0,14	0,14
F7	0,013 - 0,064	3194 - 4876	0,17	0,13	0,14
F8	0,039 - 0,091	3219 - 4274	0,14	0,13	0,13
F9	0,014 - 0,098	3797 - 5337	0,18	0,14	0,14
F10	0,019 - 0,072	3915 - 5732	0,16	0,16	0,18
	Irradiation 13/07				
Detector	*τ (ms)*	*f_{peak} (Hz)*	*bubbles/µSv vis.*	*bubbles/µSv par.*	*bubbles/µSv fit.*
F6	0,044 - 0,079	3833 - 4614	0,16	0,12	0,12
F7	0,032 - 0,081	3711 - 4359	0,18	0,15	0,16
F8	0,021 - 0,076	4650 - 4730	0,17	0,15	0,15
F9	0,025 - 0,089	5252 - 5827	0,16	0,12	0,12
F10	0,037 - 0,069	4940 - 5541	0,16	0,15	0,17

The parameter analysis shows more constant results, that is less variation over time, than the visual analysis and linear fit. This is evident among other things when considering the deviation from the average sensitivity per detector. In Table 7 the deviation from the average value for each detector is calculated, e.g. for F1 on 28/06 the deviation from the average number of bubbles/µSv after a visual check of the stored pulses (= deviation from average (vis)) = 0,17 / average (0,17; 0,17; 0,16; 0,17; 0,17) = 1,01 or 1 %.

Table 7: Deviation from average bubbles/μSv after the visual analysis (vis), parameter analysis (par) and slope of fitted trend line.

	deviation from average		
	Irradiation 28/06		
Detector	*deviation from average (vis)*	*deviation from average (par)*	*deviation from average (fit)*
F1	1%	3%	16%
F2	1%	3%	26%
F3	8%	8%	18%
F4	2%	3%	5%
F5	3%	6%	18%
Average	3%	4,60%	16,60%
Average abs. deviation	3,00%	4,60%	16,60%
	Irradiation 30/06		
Detector	*deviation from average (vis)*	*deviation from average (par)*	*deviation from average (fit)*
F1	1%	-4%	6%
F2	6%	5%	9%
F3	13%	8%	14%
F4	-4%	-4%	-9%
F5	3%	6%	-1%
Average	3,80%	2,20%	3,80%
Average abs. deviation	5,40%	5,40%	7,80%
	Irradiation 10/07		
Detector	*deviation from average (vis)*	*deviation from average (par)*	*deviation from average (fit)*
F1	-5%	3%	-6%
F2	-4%	-1%	-10%
F3	-3%	-5%	-5%
F4	2%	3%	-13%
F5	-10%	-2%	3%
Average	-4%	-0,40%	-6,20%
Average abs. deviation	4,80%	2,80%	7,40%
	Irradiation 12/07		
Detector	*deviation from average (vis)*	*deviation from average (par)*	*deviation from average (fit)*
F1	1%	3%	-5%
F2	1%	-1%	-11%
F3	-14%	-5%	-11%
F4	8%	3%	2%
F5	9%	-2%	-8%
Average	1%	-0,40%	-6,60%
Average abs. deviation	6,60%	2,80%	7,40%
	Irradiation 13/07		
Detector	*deviation from average (vis)*	*deviation from average (par)*	*deviation from average (fit)*
F1	1%	-4%	-12%
F2	-4%	-7%	-14%
F3	-3%	-5%	-16%
F4	-10%	-4%	-11%
F5	-4%	-9%	-14%
Average	-4%	-5,80%	-13,40%
Average abs. deviation	4,40%	5,80%	13,40%
Total abs. deviation	**4,84%**	**4,28%**	**10,52%**

Deviations from the average number of bubbles/µSv of 10 % and more (below or above the average) are marked in red. This is only the case if the visual analysis is used to describe the sensitivity of the detector or if the slope of the fitted trend line is used. The most constant sensitivity and results are obtained when the parameter analysis is used. The deviations from the average number of bubbles/µSv after the parameter analysis are all below 10 %.

The average absolute deviation is also included in Table 7 to consider the average variation. The absolute values of the deviations is taken and the average of this is calculated. The parameter analysis has the lowest average absolute deviation, except on 28/06 and 13/07 the visual analysis has a lower value. The total average absolute deviation throughout the time is shown at the bottom of Table 7. The parameter analysis has the lowest value of 4,28 % and thus the lowest average variation over time. The visual analysis does not have a significantly higher value, but this can be explained by repeatedly looking at thousands of pulses, some pulses were not visually accepted which might be accepted for another viewer.

Also the average of the deviations from the average sensitivity is included in Table 7 to determine whether there is a systematic underestimation or overestimation. For all 3 calibration factors there is an overestimation in the beginning (on 28/6 and 30/6). Subsequently, this evolves into a systematic underestimation, for all 3 calibration factors the value is below average sensitivity over time. This could be due to the sensitivity decreasing throughout the time, making an overestimation at the beginning and then an underestimation over the average. This will be discussed further later in the thesis.

From now on the parameter analysis will be used to describe the sensitivity of the SDDs.

7.4.2 Deviation from average sensitivity for reset vs. non-reset set throughout time

The comparison between the reset set (F1-F5) and the non-reset set (F6-F10) is made considering the deviation from the average sensitivity throughout the time in Table 8.

Table 8: Deviation from the average sensitivity throughout the time for reset vs. non-reset set.

Reset		**Non-reset**	
	Irradiation 28/06		
Detector	*deviation from average (par)*	*Detector*	*deviation from average (par)*
F1	+3 %	F6	+11 %
F2	+3 %	F7	+4 %
F3	+8 %	F8	+3 %
F4	+3 %	F9	+10 %
F5	+6 %	F10	+13 %
Average	+4,6 %	Average	+8,2 %
Average abs. deviation	4,6 %	Average abs. deviation	8,2 %
	Irradiation 30/06		
Detector	*deviation from average (par)*	*Detector*	*deviation from average (par)*
F1	-4 %	F6	-3 %
F2	+5 %	F7	-8 %
F3	+8 %	F8	+3 %

F4	-4 %	F9	+3 %
F5	+6 %	F10	+0 %
Average	+2,2 %	Average	-1%
Average abs. deviation	5,4 %	Average abs. deviation	3,4 %
	Irradiation 10/07		
Detector	*deviation from average (par)*	*Detector*	*deviation from average (par)*
F1	+3 %	F6	+11 %
F2	-1 %	F7	-8 %
F3	-5 %	F8	-12 %
F4	+3 %	F9	-4 %
F5	-2 %	F10	-6 %
Average	-0,4 %	Average	-3,8 %
Average abs. deviation	2,8 %	Average abs. deviation	8,2 %
	Irradiation 12/07		
Detector	*deviation from average (par)*	*Detector*	*deviation from average (par)*
F1	+3 %	F6	-3 %
F2	-1 %	F7	+0 %
F3	-5 %	F8	-4 %
F4	+3 %	F9	+3 %
F5	+2 %	F10	+0 %
Average	+0,4 %	Average	-1 %
Average abs. deviation	2,8 %	Average abs. deviation	2,0 %
	Irradiation 13/07		
Detector	*deviation from average (par)*	*Detector*	*deviation from average (par)*
F1	-4 %	F6	-17 %
F2	-7 %	F7	+15 %
F3	-5 %	F8	+10 %
F4	-4 %	F9	-12 %
F5	-9 %	F10	-6 %
Average	-5,8 %	Average	-2 %
Average abs. deviation	5,8 %	Average abs. deviation	10,0 %
Total abs. deviation	**4,28 %**	**Total**	**6,36 %**

Again deviations of 10 % and more are marked in red, this is only the case for the non-reset set. The maximum deviation from the average sensitivity is 9 % if the SDDs are reset between each irradiation, for the non-reset set this is 17 %. Also for the non-reset SDDs there are more fluctuations in deviation from the average sensitivity throughout the time. Again the average absolute deviation (marked in blue) is calculated, for the reset set the values lie between 2,8 % and 5,8 %. However, for the non-reset set the values range from 2,0 % to 10 %. The total average absolute deviation for the reset SDDs is 4,28 %, while this is 6,36 % for the non-reset SDDs. This means that the reset set has a more constant response across time, by applying a reset the results vary less over time.

Again if the average of the deviations is considered there is an overestimation at the beginning and an underestimation relative to the average over time, this for both the reset set and the non-reset set. The presumption that the sensitivity decreases throughout the time is gaining weight.

7.4.3 Sensitivity of reset vs. non reset set throughout time

The number of bubbles formed per µSv throughout the time is studied, again SDD F1-F5 are compared with SDD F6-F10. This is made clear in Figure 50 and Figure 51.

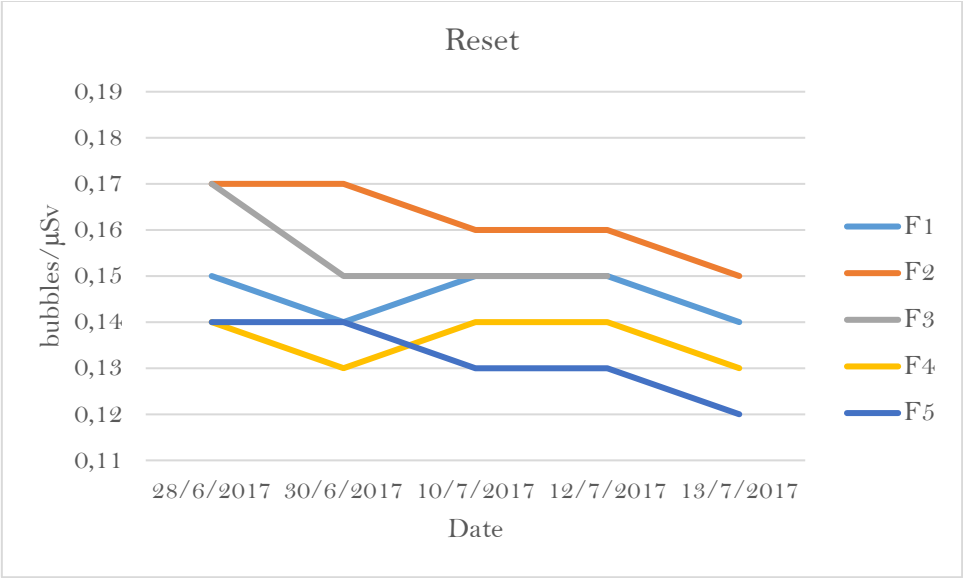

Figure 50: Sensitivity of the reset set throughout the time.

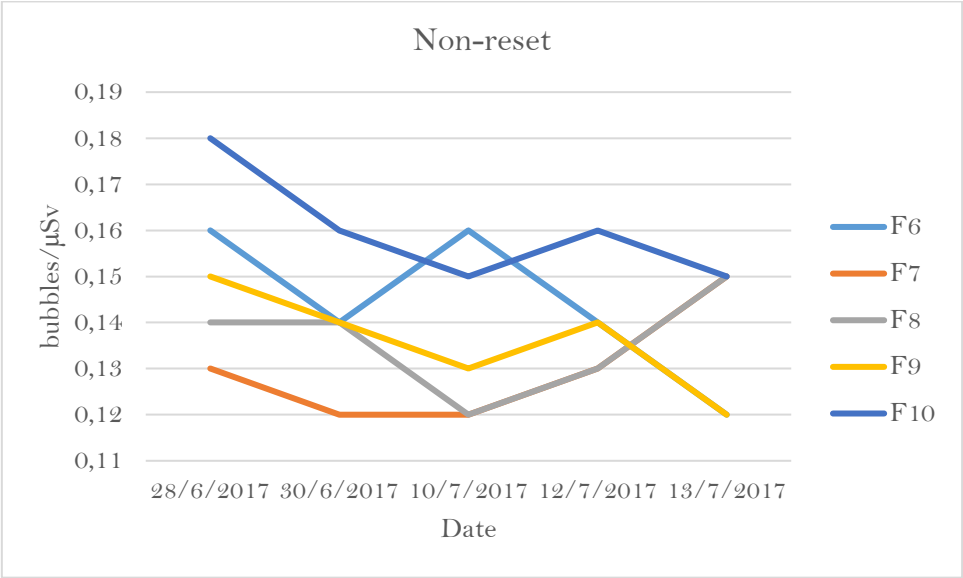

Figure 51: Sensitivity of the non-reset set throughout the time.

The lines in Figure 51 have erratic fluctuations as for the lines in Figure 50 show a more constant progression. This suggests that it is better to reset the SDDs between each irradiation, in order to have a more constant response. For the reset set a slight decrease in sensitivity across time is visible. This also the case for the non-reset set except for F7 & F8.

Both the reset and the non-reset set have an average decrease in sensitivity of 0,014 bubbles/µSv between 28/6 and 13/7. This also explains why there are more negative values for the deviation from the average sensitivity on 13/7.

7.4.4 Change of peak frequency over time

The maximum frequency at the peak of the FFTs of the parameter selected pulses, $f_{peak, max}$, are studied over time (third column of Table 5 and 6). The percentage change relative to the starting value on 28/06, $\Delta\%\ f_{peak, max}$, is calculated for the reset and non-reset set in Table 9.

Table 9: Percentage change relative to the starting value on 28/06, $\Delta\%\ f_{peak, max}$, for each detector across time.

Reset		**Non-reset**	
	Irradiation 30/06		
Detector	$\Delta\%\ f_{peak, max}$	*Detector*	$\Delta\%\ f_{peak, max}$
F1	-0,80	F6	54,90
F2	-10,39	F7	111,56
F3	-9,12	F8	101,31
F4	8,25	F9	96,21
F5	-16,51	F10	68,89
	Irradiation 10/07		
Detector	$\Delta\%\ f_{peak, max}$	*Detector*	$\Delta\%\ f_{peak, max}$
F1	3,56	F6	75,42
F2	-10,39	F7	198,02
F3	-6,96	F8	156,10
F4	3,20	F9	85,39
F5	5,64	F10	244,65
	Irradiation 12/07		
Detector	$\Delta\%\ f_{peak, max}$	*Detector*	$\Delta\%\ f_{peak, max}$
F1	5,55	F6	58,96
F2	7,92	F7	81,80
F3	-9,16	F8	74,88
F4	10,25	F9	98,40
F5	12,72	F10	150,42
	Irradiation 13/07		
Detector	$\Delta\%\ f_{peak, max}$	*Detector*	$\Delta\%\ f_{peak, max}$
F1	-2,60	F6	68,76
F2	6,94	F7	62,53
F3	4,21	F8	93,54
F4	2,95	F9	116,62
F5	5,15	F10	142,07

It is noticed that the maximum peak frequency of the valid pulses does not change dramatically if the SDDs are reset, the maximum change relative to the starting value is 16,51 %. On the other hand if the SDDs are not reset between each irradiation, big increases in maximum peak frequency can be seen varying from 54,90 % to 244,65 %. There could be expected that there is a certain constant rise in maximum frequency if the detector is not reset and that this remains approximately the same over time. However, this is not the case and is made clear in Figure 52.

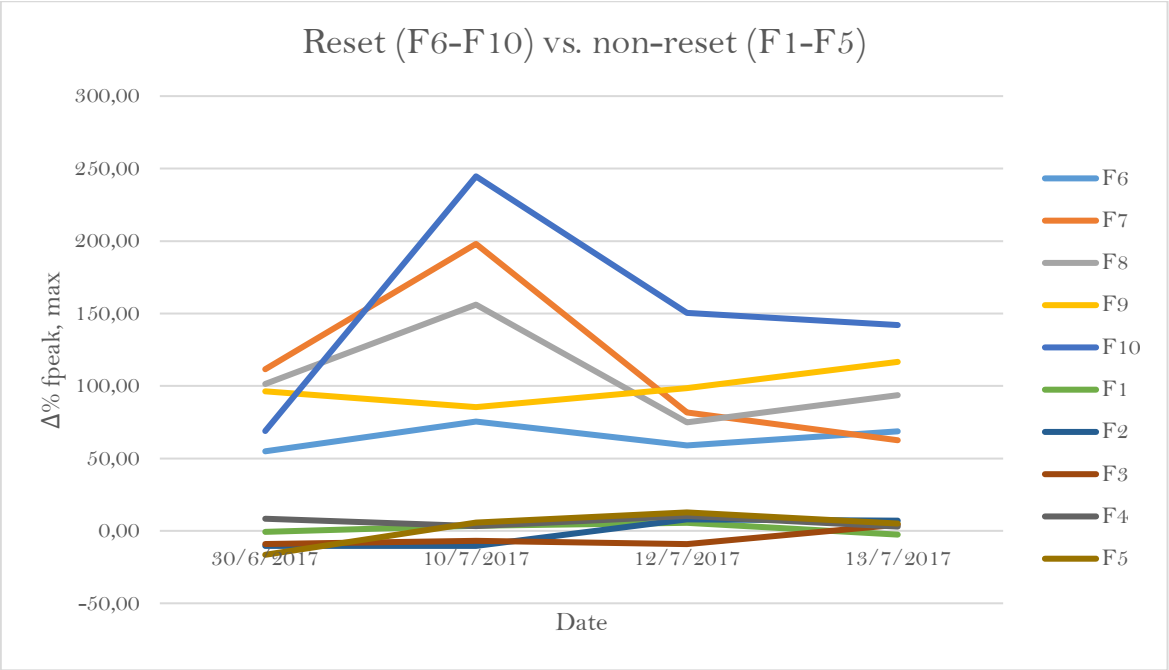

Figure 52: Percentage change in maximum peak frequency, Δ% $f_{peak,\,max}$, over time for all SDDs.

For SDD F1-F5 (reset set), in the bottom part of the graph, there is almost no percentage change in maximum peak frequency and remains approximately constant over time. SDD F6-F10 (non-reset set), in the upper part of the graph, show large fluctuations over time in percentage change. A reset is recommended in order to perform a parameter analysis to determine whether a pulse is a true nucleation event or not. The reset set exhibits a more constant response in maximum peak frequency of the valid pulses and thus a better reproducibility.

7.4.5 Deviation from first reading

To determine if the first measurement/reading can serve as a reference for a later measurement, the deviation of the detector's response relative to the first reading is calculated. The data are summarized in Table 10.

Table 10: Deviation from the first reading throughout the time for reset vs. non-reset set.

Reset		**Non-reset**	
Irradiation 30/06			
Detector	*Deviation from first reading*	*Detector*	*Deviation from first reading*
F1	-7%	F6	-12%
F2	0%	F7	-8%
F3	0%	F8	0%
F4	-7%	F9	-7%
F5	0%	F10	-11%
Average abs.	3%	**Average abs.**	8%
Coeff. of variation	4%	**Coeff. of variation**	5%

Irradiation 10/07			
Detector	*Deviation from first reading*	*Detector*	*Deviation from first reading*
F1	0%	F6	0%
F2	-6%	F7	-8%
F3	-12%	F8	-14%
F4	0%	F9	-13%
F5	-7%	F10	-17%
Average abs.	5%	**Average abs.**	10%
Coeff. of variation	5%	**Coeff. of variation**	7%
Irradiation 12/07			
Detector	*Deviation from first reading*	*Detector*	*Deviation from first reading*
F1	0%	F6	-12%
F2	-6%	F7	0%
F3	-12%	F8	-7%
F4	0%	F9	-7%
F5	-7%	F10	-11%
Average abs.	5%	**Average abs.**	7%
Coeff. of variation	5%	**Coeff. of variation**	5%
Irradiation 13/07			
Detector	*Deviation from first reading*	*Detector*	*Deviation from first reading*
F1	-7%	F6	-25%
F2	-12%	F7	15%
F3	-12%	F8	7%
F4	-7%	F9	-20%
F5	-14%	F10	-17%
Average abs.	10%	**Average abs.**	17%
Coeff. of variation	4%	**Coeff. of variation**	19%

Table 10 clarifies that the first reading of sensitivity (= calibration factor) can be used as a guideline for later measurements. An absolute average deviation from the first reading of 10 % or less is reached for both the reset and the non-reset set. Except for the non-reset SDDs on 13/07 this is 17 % and this is too much. Which again indicates that it is always better to reset an SDD after irradiation. The data of the non-reset set are more spread than the data of the reset set. The coefficient of variation (= standard deviation / average) depicts the dispersion of data. For the reset set the coefficient of variation stays below 5 %, while for the non-reset set a coefficient of variation of 7 % and 19 % can be noticed. However, it is recommended to calibrate each detector individually, for example SDD F5 exhibited a deviation from the first reading of 14 % on 13/07, this deviation is too high if the dose in an area needs to be determined very accurately. Some SDDs of the non-reset set showed a deviation from the first reading of 20 % or more. This shows again that a reset is recommended and will result in more consistent results.

7.4.6 Linearity

Additionally, the linearity of the dose-response graphs of SDDs F1-F10 is examined. It is expected and desirable that the number of bubbles formed will be directly proportional and increases linearly with increased dose. For each detector after each irradiation a similar table as Table 11 is made.

Table 11: Example of data for dose-response graph construction and linearity study of a SDD.

detector R227_F6	time recorded in time.lvm file (sec)	pulse number in time.lvm file	dose (µSv)	corrected pulse number	duration of irradiation	998	sec	assuming fit is correct	linearity index	CF	linearity index
	2976,746	5	5,7	1	dose rate	0,10	µSv/s	0,89	1,119	0,91	1,099
	3001,6	18	8,2	2	irradiation start	2920	sec	1,28	1,557	1,31	1,530
	3074,2	26	15,5	3	irradiation stop	3918	sec	2,43	1,235	2,47	1,213
	3163,98	47	24,4	4				3,84	1,041	3,91	1,023
	3205,834	59	28,6	5	number of bubbles	16		4,50	1,111	4,58	1,091
	3280,1	112	36,1	6				5,67	1,058	5,77	1,039
	3374,2	172	45,5	7				7,15	0,978	7,28	0,961
	3450,7	230	53,2	8				8,36	0,957	8,51	0,940
	3501,5	247	58,3	9				9,16	0,983	9,32	0,965
	3603,45	299	68,5	10				10,77	0,929	10,96	0,913
	3645,12	305	72,7	11				11,42	0,963	11,63	0,946
	3723,965	312	80,6	12				12,66	0,948	12,89	0,931
	3748,55	389	83,0	13				13,05	0,996	13,28	0,979
	3809,99	401	89,2	14				14,02	0,999	14,27	0,981
	3828,735	407	91,1	15				14,31	1,048	14,57	1,030
	3888,224	443	97,0	16				15,25	1,049	15,52	1,031
								av	1,061		1,042
								cov	14%		14%

In Table 11 the linear fitted trend line of SDD F6 has the equation: y = 0,1572 * x, the column 'assuming fit is correct' calculates the number of bubbles that would be produced for a certain given dose if the sensitivity of the detector is 0,1572 bubbles/µSv (e.g. 5,7 µSv * 0,1572 bubbles/µSv = 0,89 bubbles). The column 'CF' (calibration factor) assumes that the sensitivity of the SDD is 0,16 bubbles/µSv, because 16 parameter selected bubbles were formed for 100 µSv. The same calculation as for 'assuming fit is correct' is performed, e.g. 5,7 µSv * 0,16 bubbles/µSv = 0,91 bubbles. The linearity index determines whether the corrected pulse numbers are an overestimation or underestimation according to the fit respectively according to the calibration factor (e.g. 1 / 0,89 = 1,119). Also the average linearity index is calculated and the coefficient of variation.

To study whether a reset achieves better linearity, the average linearity index for the reset and non-reset set is plotted throughout the time. Figure 53 and 54 show the average linearity index according to the fit of the SDDs over time.

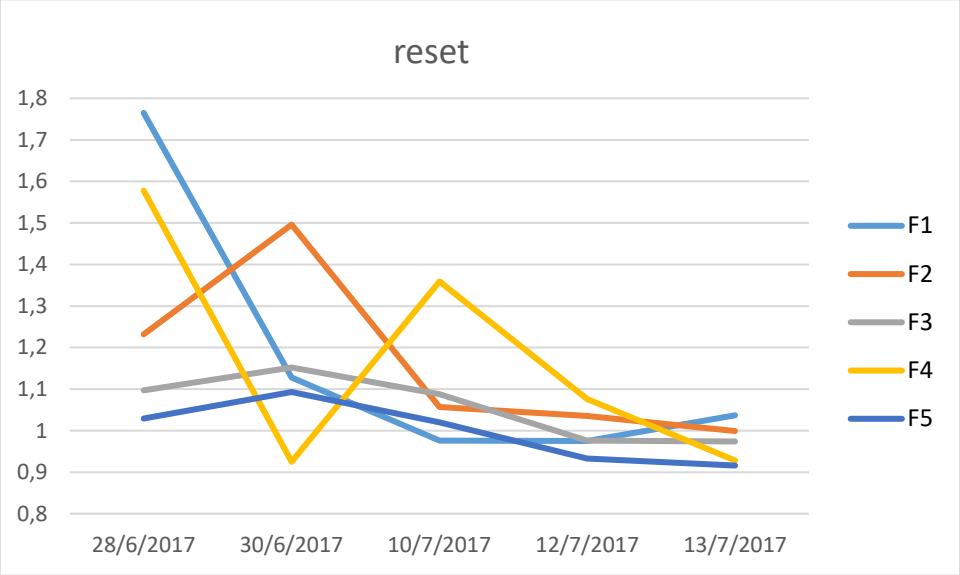

Figure 53: Average linearity index according to the fit for the reset set over time.

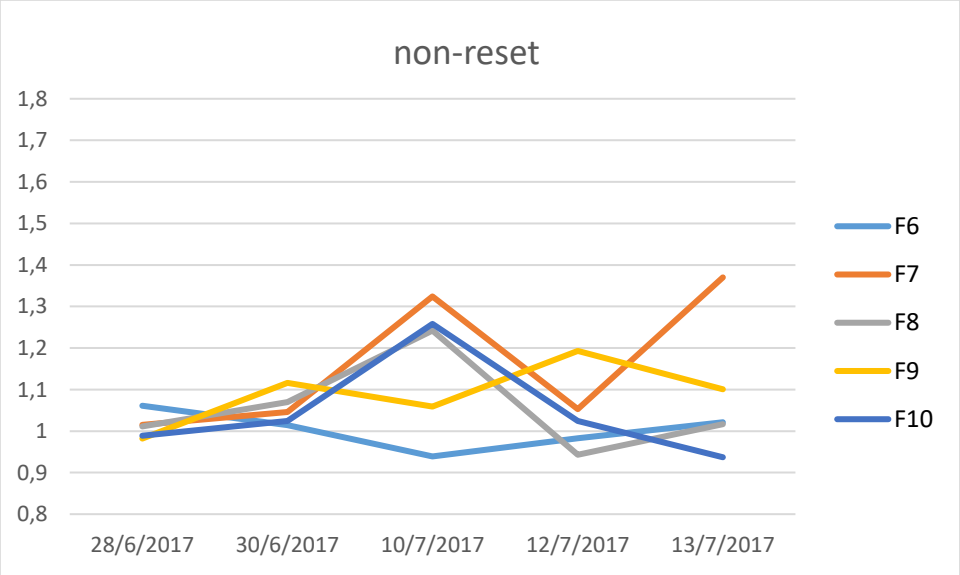

Figure 54: Average linearity index according to the fit for the non-reset set over time.

For the reset set the average linearity indices of the different SDDs start with relatively large differences on 28/06, but evolve to 1 over time, the lines in Figure 53 come closer to each other. On the other hand, the non-reset set starts with a much better linearity than the reset set, however the lines in Figure 54 are further spread over time. The average linearity index according to the fit increases over time for the non-reset set. Although, in order to make a better comparison, the reset and non-reset set should start with similar linearity.

Figure 55 and 56 finally show the average linearity index according to the calibration factor of the SDDs over time.

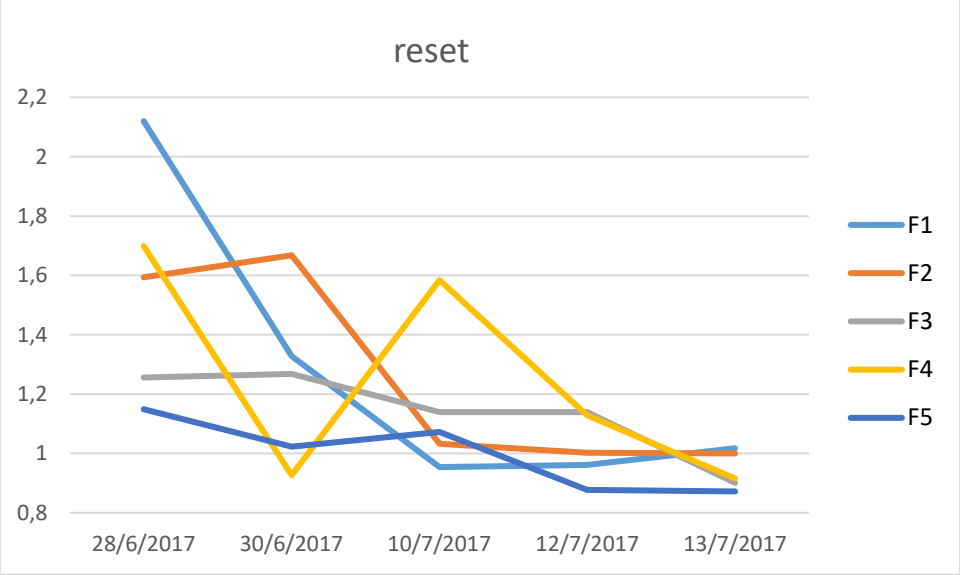

Figure 55: Average linearity index according to the calibration factor for the reset set over time.

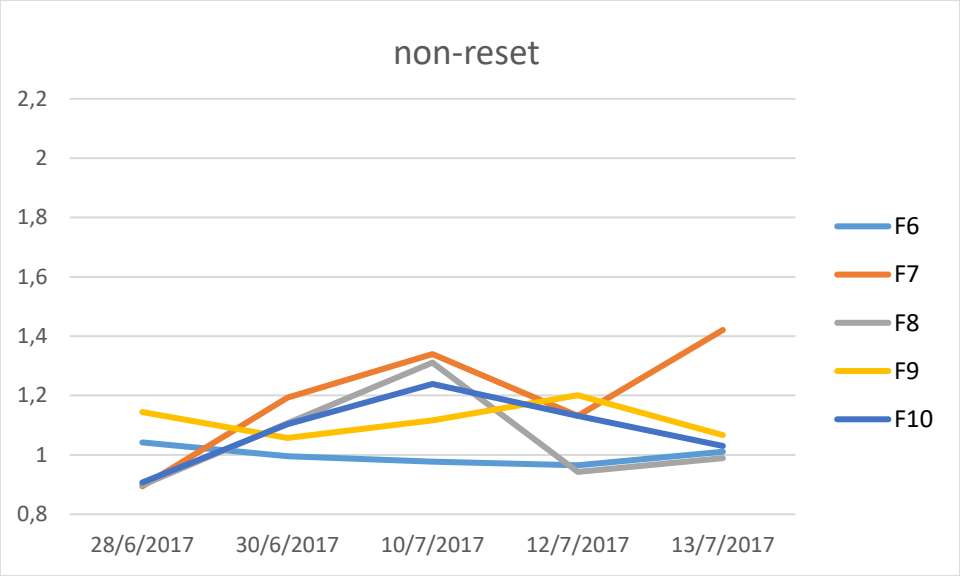

Figure 56: Average linearity index according to the calibration factor for the non-reset set over time.

Again the reset set starts with a much worse linearity than the non-reset set and the lines in Figure 55 get more together over time, approaching 1. The average linearity index according to the calibration factor of the non-reset SDDs also approach 1 over time, except for F7. The above shows that for better linearity, it is probably also better to apply a reset. However, as mentioned before, it is difficult to arrive at a conclusion from these data because the detector's linearities were quite different between the 2 sets to start with.

8 Conclusion

To conclude, the SDDs must be manufactured by strictly following a dedicated protocol. An existing fabrication protocol has been improved and optimized to finally bring about a fully detailed self-explanatory step by step fabrication protocol with pictures.

After several attempts to fabricate the detector, it was found that the sensitivity of the detectors increases by increasing the amount of Freon added. The number of bubbles generated increases exponentially with the amount of R227EA added. However, these detectors are limited in sensitivity because of the limited volume. Only a small vial containing gel is used as an SDD, but are chosen over the BTI detectors that are more sensitive because the small volume is just required to implement the detectors in a phantom. The commercial BTI detectors take a lot of space, are very expensive and have limited life time.

It was noted that detectors made from the same batch showed 10 % difference in response (sensitivity). Therefore, the detectors must be calibrated individually. Three different calibration factors: bubbles/µSv visual, bubbles/µSv parameter and bubbles/µSv fit were studied throughout the time. During this master's thesis, a LabVIEW program was optimized in order to try to objectively evaluate stored pulses instead of subjectively (= visual analysis). Any pulse caused by a neutron can be characterized by different parameters. The values of these parameters are within a particular window when it comes to a true nucleation event. The results showed that each SDD has specific values for these parameters. Using this parameter analysis, the least varying results were obtained throughout the time. The sensitivity of the SDD will be expressed as bubbles/µSv parameter.

Two sets of SDDs were monitored throughout the time. One set was reset between each irradiation. A reset means placing the small vial (without cap) in the pressure reactor and applying 5-6 bar pressure, after which the pressure is slowly reduced. This ensures that bubbles remaining in the detector after irradiation mostly disappear. The other set, the non-reset set, was left in its state after irradiation. By applying a reset a better reproducibility is achieved and thus is recommended. In this way, a more constant sensitivity as well as more similar detector's specific parameters over time are accomplished.

In order to further calibrate this detector, the energy response when irradiated by a Van de Graaff accelerator and in a proton therapy center should still be verified. The effect of temperature on the SDD and other climatic conditions is yet to be tested. Finally, the sensitivity of the detector to gamma rays should still be investigated.

References

[1] K. Oeffinger, A. Mertens and C. Sklar, "Chronic Health Conditions in Adult Survivors of Childhood Cancer", *Oncology Times*, vol. 29, no. 1, p. 26, 2007.

[2] W. Newhauser and M. Durante, "Assessing the risk of second malignancies after modern radiotherapy", *Nature Reviews Cancer*, vol. 11, no. 6, pp. 438-448, 2011.

[3] W. Newhauser and R. Zhang, "The physics of proton therapy", *Physics in Medicine and Biology*, vol. 60, no. 8, pp. R155-R209, 2015.

[4] C. Yamauchi-Kawara, K. Fujii, T. Aoyama, M. Yamauchi and S. Koyama, "Radiation dose evaluation in multidetector-row CT imaging for acute stroke with an anthropomorphic phantom", *The British Journal of Radiology*, vol. 83, no. 996, pp. 1029-1041, 2010.

[5] I. Seth, J. L. Schwartz, R. D. Stewart, R. Emery, M. C. Joiner, and J. D. Tucker, "Neutron exposures in human cells: Bystander effect and relative biological effectiveness", *PLoS One*, vol. 9, no. 6, 2014.

[6] R. Vetter, "ICRP Publication 103, The Recommendations of the International Commission on Radiological Protection", *Health Physics*, vol. 95, no. 4, pp. 445-446, 2008.

[7] R. Apfel and S. Roy, "Superheated Drop Detector: A Possible Alternative for Neutron Dosimetry", *Radiation Protection Dosimetry*, vol. 10, no. 1-4, pp. 327-330, 1985.

[8] G. Knoll, *Radiation detection and measurement.* New York: Wiley, 1979.

[9] D. Hankins and J. Westermark, "Preliminary Study on the Use of the Track Size Distribution on Electrochemically Etched CR-39 Foils to Infer Neutron Spectra", *Radiation Protection Dosimetry*, vol. 20, no. 1-2, pp. 109-112, 1987.

[10] E. Piesch, "Progress in albedo neutron dosimetry", *Nuclear Instruments and Methods*, vol. 145, no. 3, pp. 613-619, 1977.

[11] D. Glaser, "Some Effects of Ionizing Radiation on the Formation of Bubbles in Liquids", *Physical Review*, vol. 87, no. 4, pp. 665-665, 1952.

[12] S. C. Roy, "Superheated liquid and its place in radiation physics", *Radiat. Phys. Chem.*, vol. 61, no. 3–6, pp. 271–281, 2001.

[13] F. D'Errico, "Radiation dosimetry and spectrometry with superheated emulsions", *Nucl. Instruments Methods Phys. Res. Sect. B Beam Interact. with Mater. Atoms*, vol. 184, no. 1–2, pp. 229–254, 2001.

[14] R. Sarkar, B. K. Chatterjee, B. Roy, and S. C. Roy, "Radiation detection by using superheated droplets", *Radiat. Phys. Chem.*, vol. 75, no. 12, pp. 2186–2194, 2006.

[15] F. Seitz, "On the Theory of the Bubble Chamber", *Physics of Fluids*, vol. 1, no. 1, p. 2, 1958.

[16] R. Apfel and S. Roy, "Instrument to detect vapor nucleation of superheated drops", *Review of Scientific Instruments*, vol. 54, no. 10, pp. 1397-1400, 1983.

[17] M. Felizardo, R. Martins, A. Ramos, T. Morlat, T. Girard, F. Giuliani, D. Limagne, G. Waysand and J. Marques, "Improved acoustic instrumentation of the SIMPLE detector", *Nuclear Instruments and Methods in Physics Research Section A: Accelerators, Spectrometers, Detectors and Associated Equipment*, vol. 585, no. 1-2, pp. 61-68, 2008.

[18] G. Shani, *Radiation dosimetry*. Boca Raton, Fla.: CRC Press, 2001.

[19] R. Bitter, T. Mohiuddin and M. Nawrocki, *LabView advanced programming techniques*. Boca Raton: CRC Press/Taylor & Francis Group, 2007.

[20] M. Felizardo, R. Martins, A. Ramos, T. Morlat, T. Girard, F. Giuliani and J. Marques, "New acoustic instrumentation for the SIMPLE superheated droplet detector", *Nuclear Instruments and Methods in Physics Research Section A: Accelerators, Spectrometers, Detectors and Associated Equipment*, vol. 589, no. 1, pp. 72-84, 2008.

[21] A. Boulogne and A. Evans, "Californium-252 neutron sources for medical applications", *The International Journal of Applied Radiation and Isotopes*, vol. 20, no. 6, pp. 453-461, 1969.

[22] S. Roy, "Superheated liquid and its place in radiation physics", *Radiation Physics and Chemistry*, vol. 61, no. 3-6, pp. 271-281, 2001.

[23] M. Harper and M. Nelson (INVITED), "Experimental Verification of a Superheated Liquid Droplet (Bubble) Neutron Detector Theoretical Model", *Radiation Protection Dosimetry*, vol. 47, no. 1-4, pp. 535-542, 1993.

[24] R. Apfel, "The superheated drop detector", *Nuclear Instruments and Methods*, vol. 162, no. 1-3, pp. 603-608, 1979.

[25] Y. Sun, B. Chu and R. Apfel, "Radiation-induced cavitation process in a metastable superheated liquid I. Initial and pre-bubble formation stages", *Journal of Computational Physics*, vol. 103, no. 1, pp. 116-125, 1992.

Appendices

Appendix A: Bubble formation & efficiency of energy deposition

The radius of the critical bubble is achieved when the external pressure and the pressure through the surface forces are balanced by the internal gas pressure, or in the formula form:

$$r_c = 2\gamma(T)/\Delta P. \quad \text{I}$$

With r_c the critical radius, $\gamma(T)$ is the surface tension of the liquid at temperature T, ΔP is the difference between the equilibrium vapour pressure (P_v) and the externally applied pressure (P_0) which is atmospheric pressure in this case [22].

Using classical thermodynamics, one can calculate the minimum work (W) required in creating a spherical bubble of radius r, given by

$$W = 4\pi r^2\gamma(T) - \frac{4}{3}\pi r^3\Delta P. \quad \text{II}$$

This minimum work to create a bubble increases with the size of the bubble, reaching a maximum and then decreasing. The maximum constitutes an energy barrier which must be overcome in order for nucleation to occur. The radius of the bubble corresponding to this maximum is called the critical radius r_c.

Substituting equation I into equation II, the minimum reversible work needed to form the critical size bubble is given by

$$W = (16\pi/3)[\gamma^3(T)/(\Delta P)^2]. \quad \text{III}$$

This important equation implies that as the temperature increases, W decreases thus requiring less energy for vapor nucleation.

An expression for the minimum energy needed to form a critical bubble is:

$$E_{min} = 4\pi {r_c}^2\gamma(T) - \frac{4}{3}\pi {r_c}^3\Delta P + \frac{4}{3}\pi {r_c}^3\rho_v h_{fg} + W_k + W_j + W_{visc} + W_h\,. \quad \text{IV}$$

Here ρ_v is the density of the gas and h_{fg} the heat of evaporation. The first two terms are the minimum reversible labor required for bubble formation (Gibbs free energy), the third term is the evaporation energy. The last four terms indicate the kinetic energy exerted by the bubble on the liquid wall, the acoustic energy lost by the generation of sound waves, the energy lost by the viscous forces during the growth of the bubble and the thermal energy lost while growing the bubble to its critical size. When we only keep the reversible terms and neglect the rest we get the minimum energy needed to form a bubble (after substitution of r_c):

$$E_{min} = (16\pi/3)[\gamma^3(T)/(\Delta P)^2][1 + \frac{2P_v}{\Delta P}(1 + \frac{h_{fg}}{R^*T})]. \quad \text{V}$$

Here, R^* is the gas constant. It is clear that as ΔP increases, the necessary energy decreases. The minimum energy also depends on the type of detector material.

For a given neutron energy, different nuclei of the liquid will receive different amounts of energy, depending on their atomic weight. The ion with the highest value of linear energy transfer (LET) or (dE/dx) in the liquid will play the major role in vapour nucleation. The

energy deposited by the charged particle within a distance L along the radiation particle track, must be larger than W required for bubble formation and is given by

$$W = L(dE/dx) = ar_c\ (dE/dx). \qquad \text{VI}$$

The length L is associated with the critical bubble radius r_c by a numerical constant a.

From equation V, the amount of energy required to form a bubble is known. The stopping power tells us how much energy a charged particle deposits along its way. The question now is: about what effective length L the deposited energy is included to form one bubble. In general, this length is related to the critical radius of the bubble L = a r_c. Values for a were calculated and postulated between the geometrically intuitive 2 to 13. This is because the pressure and temperature during formation are not well known. It is therefore difficult to estimate the viscosity and surface tension. More recently, it was assumed that L would be rather proportional to r_0, with r_0 the critical volume in its liquid phase [23]. In any case, if L is supposed to be known, the energy available for bubbling can be calculated.

Of course, not all of the energy available will be transformed into the formation of a bubble. The reason for this is that the reversible model as described here does not fully reflect reality. The actual phenomenon begins with the formation of a shockfront by heating a small area to temperatures and pressures far beyond their critical values. If this high temperature and pressure area is sufficiently exhausted, the formation of a vapor and liquid interface will occur on a particular radius. This vapor drop grows and reaches the radius of the critical bubble if the interaction was sufficiently energetic. The bubble will then grow but only a small portion of the deposited energy will remain in the bubble during this process. By changing the pressure at which bubbles originated, Apfel could calculate what energy was needed for bubble formation [24]. Assuming that a = 2, he could compare this energy to those that were effectively available by the recoil ions. He only found a return of 3 to 5% for the energy conversion in bubbles. By considering that the energy deposited along that part of the ion's range corresponding to twice the critical radius contributes significantly to bubble formation, Apfel found that W corresponds to only 3–5% of the energy deposited by the ions in the critical diameter $2r_c(dE/dx) = E_c$.

The complete history of bubble formation through radiation interaction has been solved using calculation models [25]. Assuming that the energy deposition occurs uniformly and directly on a straight line, a system of nonlinear partial differential equations is obtained from fluid dynamics. If one resolves this one finds a calculated critical radius of about 2/5 of the value according to the Seitz model. Such calculations are clearly just an approximation of reality, but can still help to get a better insight into this complex phenomenon.

Appendix B: SDD fabrication protocol

Overview:

Day 1: Prepare the mixture and stir (this step can be done in advance), degas the gel, cool the gel and apply pressure.

Day 2: Release the pressure very slowly.

Day 3: Transfer the gel to glass bottle and leave in fridge.

1) **Prepare the gel by mixing glycerol and ultrasound gel and add surfactant (± 3 hours).**

   - The gel matrix used for the fabrication of the superheated droplet detector (SDD) consists of glycerol and an ultrasound gel.

     In a 1 liter measuring cup add:
     -US gel (Anagel) – 100 g
     -Glycerol – 350 g glycerol (corresponding to 280ml)
     -Tween 80 – 400µl

1 liter measuring cup

   - Mix manually with a spatula, add the stir bar and then put on the magnetic stirrer for mixing by switching on the stirring (level 3-4). This should take 2-4 hours to get a nice homogeneous mixture. Now the mixture still contains air bubbles which should be removed. If you leave it there put some tissue paper over it with a plastic stretcher.

Stir bar

   - **Note:** It was observed that a gel to glycerol ratio of 1:3.5 (weight ratio) is suitable for mixing with a magnetic stirrer and it is also easier to degas.

2) **Degas the gel (very important procedure ± 5.5 hours).**

   - The glycerol and ultrasound gel is first mixed homogeneously and then it is degassed using a vacuum pump.

- Use the Erlenmeyer with the option to attach the vacuum tube system and plastic stopper. Also take the tube for degassing as well as a spatula and some tissue. Procedure is done in the LRM (Edmond Dupuis's Lab) which needs to be organized with the people working there.

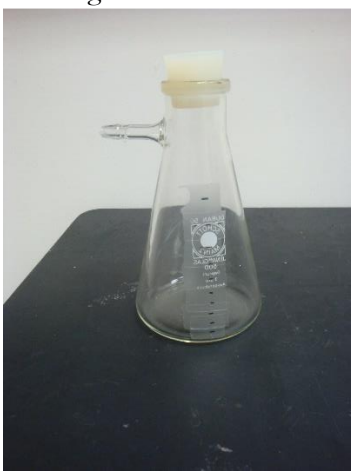

Erlenmeyer with the option to attach the vacuum tube system and plastic stopper

- First add a little amount of the gel (± 50 ml) from the measuring cup to the Erlenmeyer and add the tube from the Erlenmeyer to the vacuum system (near valve 1).

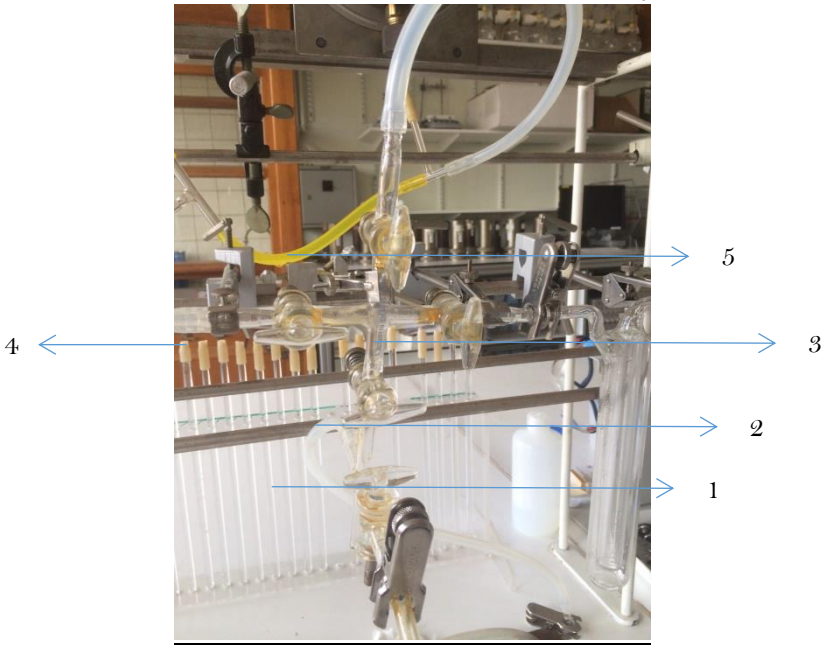

Vacuum system at LRM

- Close all the valves (1-5) and switch on the vacuum pump (red button underneath the table right).

- Valve 3 stays closed during the procedure.

- Open valve 2, 4 and 5 to decrease the pressure. The barometer will show maximal under pressure which is necessary for the degassing.

- Valve 1 stays closed to create a vacuum in the tubes first.

- Slowly open valve 1 to remove the air from the Erlenmeyer. Bubbles will start forming which you can remove by slightly shaking the Erlenmeyer (in doing that do also hold the tube in the other hand).

- When nothing is moving anymore, close valve 1.

- First remove the tube from the Erlenmeyer and then the stopper to add some more gel to the Erlenmeyer.

- Add some more (±50 ml) and start same procedure again.

- Add a stir bar inside the Erlenmeyer along with the gel and put the Erlenmeyer on the magnetic stirrer. The rotation speed should be as low as possible (± level 2).

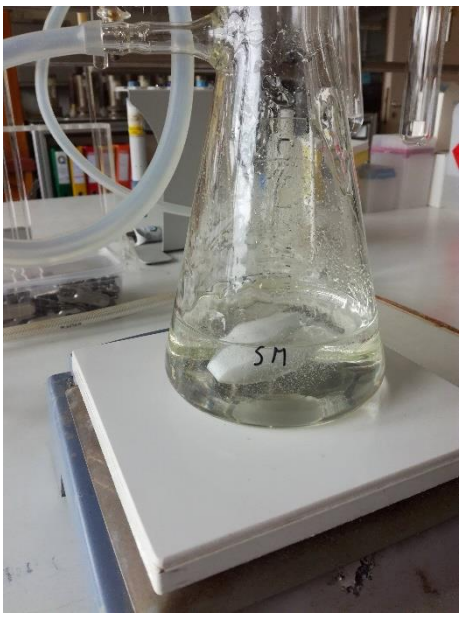

Erlenmeyer with gel and stir bar on the magnetic stirrer

- The last time some gel will stick to the wall. Make sure that nothing is left on the inner side of the Erlenmeyer because it will cause the stopper to be sucked inside the Erlenmeyer. So do clean left-overs in the Erlenmeyer with some tissue.

- When the rate of degassing (bubbles coming out of the gel) is slow start the heating process by putting the Erlenmeyer on a hot plate, the vacuum pump stays on. During heating you may stop the stirring magnet. Don't heat too much. When you see a lot of bubbles are forming from the bottom surface of the Erlenmeyer, stop heating and start the magnetic stirrer. The rotation speed should be as low as possible. You need to repeat this heating cycle 2-3 times. When you think that the gel is degassed, stop stirring and keep the degassing on for about half an hour.

! Care should be taken during heating such that it does not start boiling of the gel. A cloudy or yellowish gel indicates a degraded gel due to the overheating.

- Close valves 1 and 2. Switch off the pump and open valve 3 to get room pressure back in the system.

3) Put the gel into the pressure chamber.

- Once the degassing is completed, the gel is immediately transferred into the pressure reactor.

- To open the pressure chamber, unscrew all the bolts and open the clicking system of the reinforcing aluminium.

Bolts and clicking system

- Fill the big aluminium container with 250 ml of the gel (use the meter to point out how much needs to be added). The container is 11.7 cm deep and has a diameter of 7.5 cm. Fill it up to 5.7 cm from the bottom (6cm from the top will be empty). This corresponds to 250 ml gel.

Pressure chamber with aluminium container

- Clean the sides.

- Close the pressure chamber. Make sure the clicking systems are on the sides so that the pressure chamber fits in the mixing installation. There are small holes on the sides of the pressure chamber that indicate how to put it into the mixer. Screw the bolts tightly with spanner and tighten firmly.

Holes on the sides of the aluminium container *Bulges on stirring installation to fit with holes*

4) **Vacuum the pressure chamber.**

- In order to remove the air from the container go back to the LRM lab.
- Connect the tube (as in the picture) and open valves (all except valve 1 and 3).
- Turn on the vacuum pump and open valve 1.
- Then open the blue valve on the aluminium container. The pressure on the device should decrease slightly. Leave it for 15 min.
- After 15 min close the valve of the pressure chamber. Then close valve 1 and 2. Switch off the pump and open valve 3.

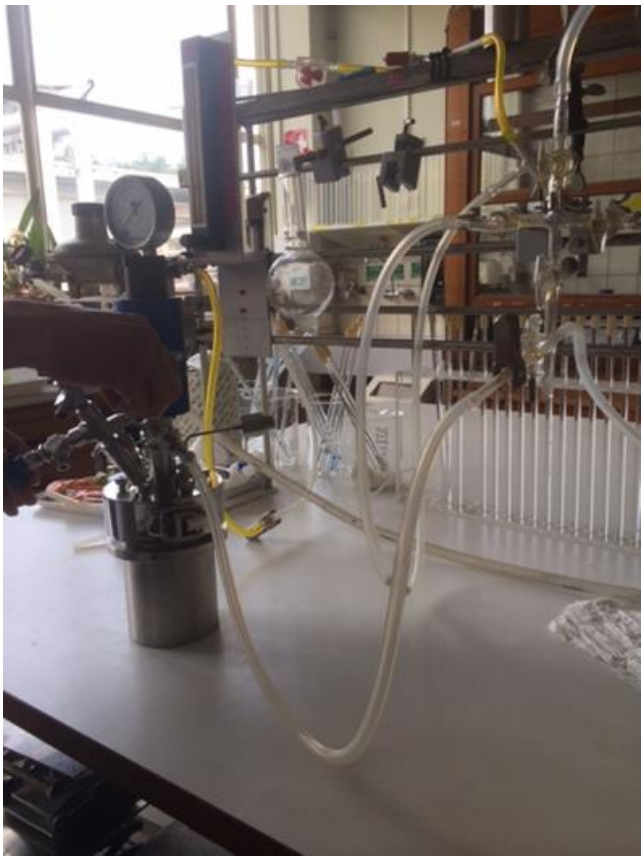

Pressure chamber connected to vacuum system

5) Cool the pressure chamber (±1.5 hours) and transfer the Freon (±0.5 hour).

- The pressure reactor is then placed in an ice bath for cooling. You can use an EPS/ISOMO tank (Expanded Polystyrene) and ice.

- Cool down to about 1-2 °C, use the temperature probe to monitor the temperature.

- Put the pressure reactor inside of the ice bath in the fridge to speed the cooling process and wrap a wet towel around the pressure reactor.

- Once the temperature in the pressure reactor reaches about 2°C, the active liquid (Freon) is transferred. The amount of Freon to be used depends on the property of the Freon and also depends on the amount of gel used. For 250 ml gel about 5-10 ml Freon is usually used.

- For neutron detectors this is 2H-heptafluoropropane (FC-227EA) or 1,1,1,2-tetrafluoroethane (R-134A). Use the FC-227EA (= R227).

- Use the part with 2 inlets and 2 valves (DIP TUBE) of the pressure reactor and connect one end of a tube with the top inlet and the other end with the R227 container.

On the left hand you can see the part with 2 inlets and 2 valves (DIP TUBE)

- Put some Teflon tape on the screw-thread of the inlet and on the screw-thread of the end of the R227 container. Don't screw the tube too tightly, just use your hands.

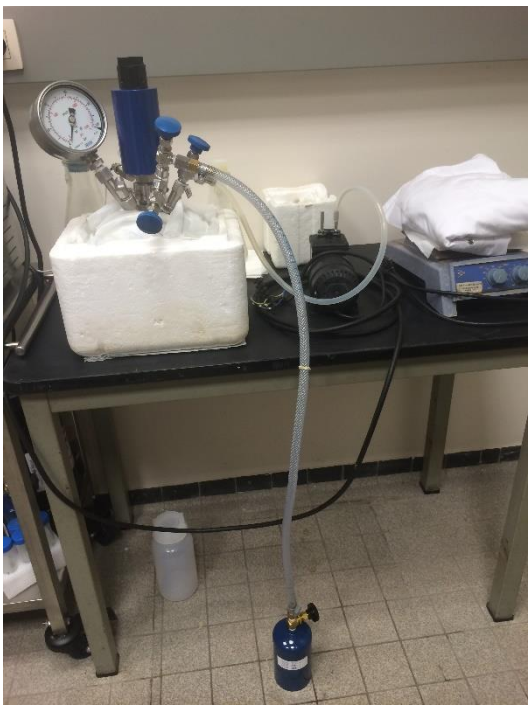

R227 container connected with the pressure reactor by a tube. On the right hand side you can see the black vacuum pump

- In order to remove the air from the tube connect the part of the pressure reactor with 1 valve and 1 inlet (VENT) to the black vacuum pump. Open all valves except the valve of the product. Let the pump work for about 3 minutes. Then close all valves and switch off the pump.

Black vacuum pump

- Now open the valve of the product (R227) and let the liquid come to 5 (which corresponds to a volume about 4.1 ml) or 6 (which is about 600 µl more than 5), 1 cm corresponds to 600 µl. To increase or decrease the sensitivity of the detector (bubbles per unit dose) the amount of Freon to be used can be decided. Close the valve of the product. The liquid should be at level 5 or 6.

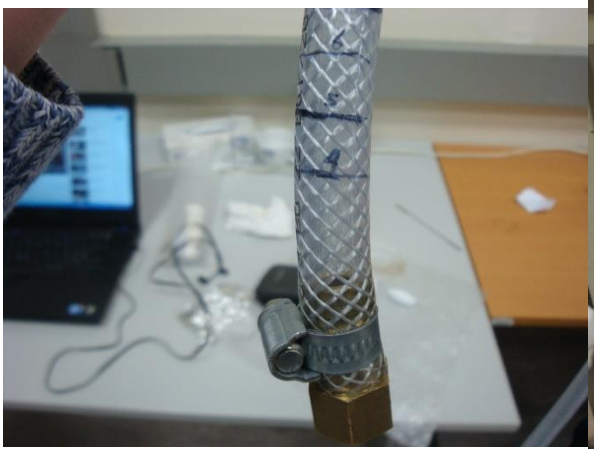

Tube with markings 4, 5 and 6

Tube connected to R227 container

- Let the liquid flow towards the pressure reactor. When the liquid is correct you move it slowly inside the pressure reactor by very slowly opening the valve. Pressure will increase slowly. Then fully open the valve to remove all the liquid, the pressure should be at 2 bar (for R-227) and the liquid should completely be removed. Close the valve tightly and remove the tube (may smell and you need to put some tissue at the end of the tube so that no dust can come inside the tube).

- The pressure reactor is then connected with the stirrer and stirred with a fixed speed (1000 rpm) for a fixed duration of time (10 minutes). 1000 rpm corresponds to 70%. The temperature will increase (5 min < 7 °C and 10min < 9 °C). If it heats up too fast then stop and put the reactor in an ice bath after removing it from the stirring set-up and start a bit later.

Stirring installation with temperature probe

- The stirring speed and duration can be altered to produce a detector with smaller or bigger droplets.

6) Apply pressure and make the detector.

- After stirring the pressure reactor is connected to a compressed air tank and the pressure is increased to about 5-6 bar.

Applying pressure

- Leave the pressure reactor inside of the ice bath in the fridge overnight (with the pressure still at 5-6 bar).

- Next day open the valve (VENT) a tiny bit to decrease the pressure. Mix detergent with water to create soapy water. Put some on the inlet of the pressure device. Open the valve a little bit and you can see bubbles forming. This should happen very slowly, only one bubble every 5-10 seconds. If this happens faster the gel will contain a lot of bubbles and the detector will not be good.

- Pressure is lowered slowly to avoid droplet vaporization.

- At the end of the day the pressure should be almost atmospheric pressure, if not leave it overnight. Open the valve completely to remove all the pressure and leave it for some time.

- Transfer the gel to a glass bottle, use the sides of the bottle to poor the gel in (otherwise you create extra bubbles in the gel).

- Leave the glass bottle in the fridge before making the detectors (best case: 1 or 2 weeks).

- Use a small syringe to transfer the gel from the glass bottle to the small glass vials. Very slowly push the gel out of the syringe to avoid air bubble formation.

Syringes and glass vials

- Put the vials in the pressure reactor (remove the lid of the vial) and then increase the pressure to 5-6 bar. This should remove the bubbles from the small vials. Wait for 30 minutes before releasing the pressure (for 1 hour or so back to atmospheric pressure).

Glass vials in pressure reactor

Appendix C: Block diagram of 'Data_Acquire_2.vi'

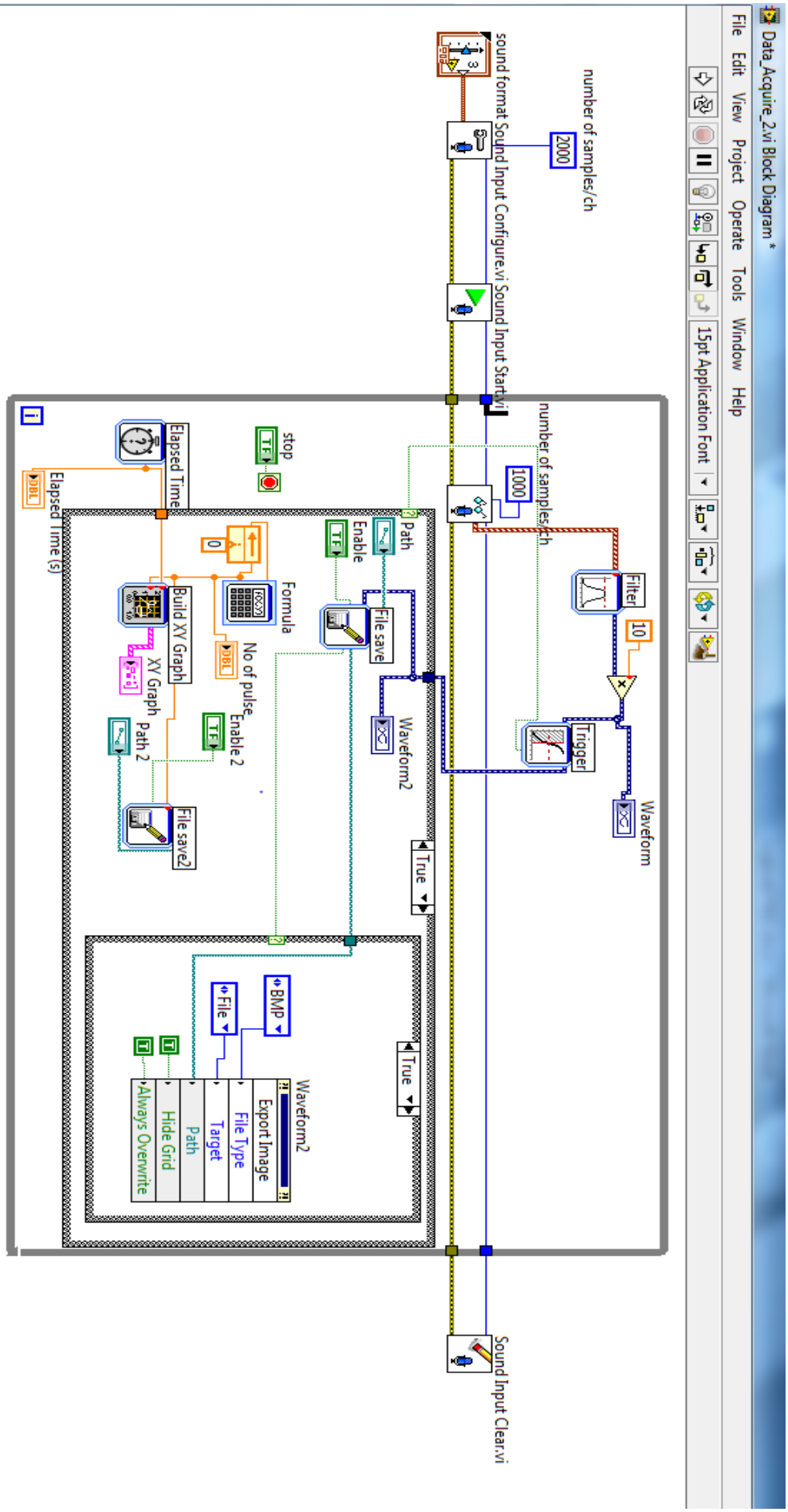

Appendix D: Block diagram of 'Hilbert transform & envelope auto.vi'

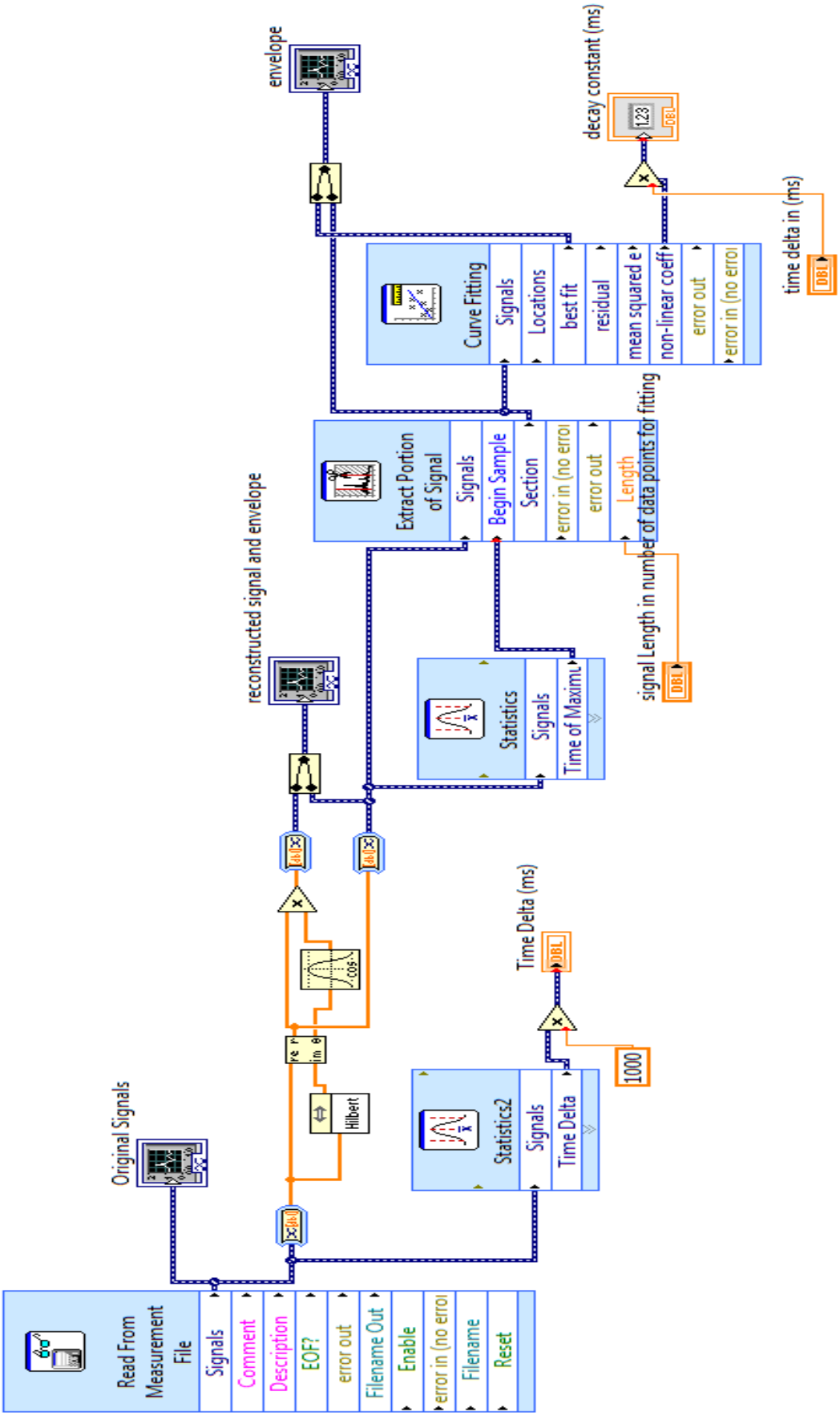

Appendix E: Block diagram of 'Pulse power spectra FFT.vi'

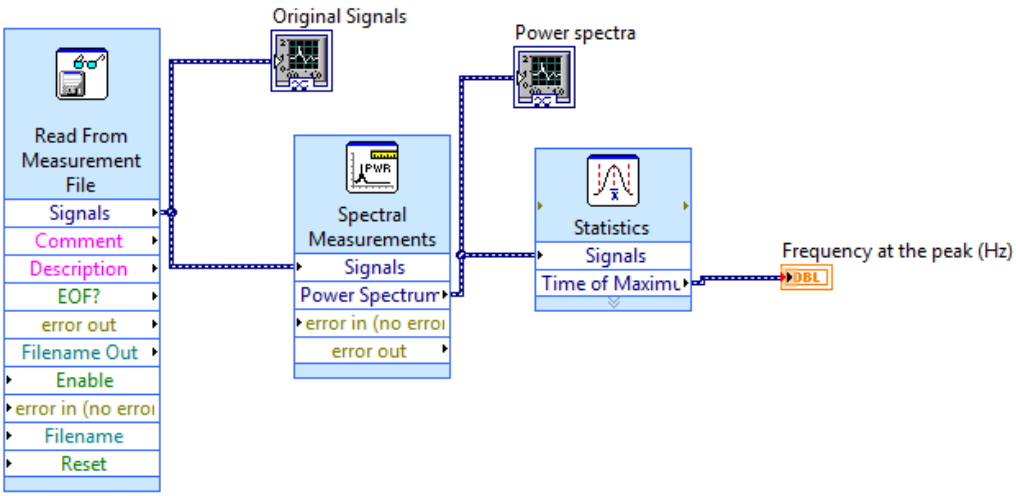

Appendix F: Block diagram of 'Data_Acquire_2 Full.vi'

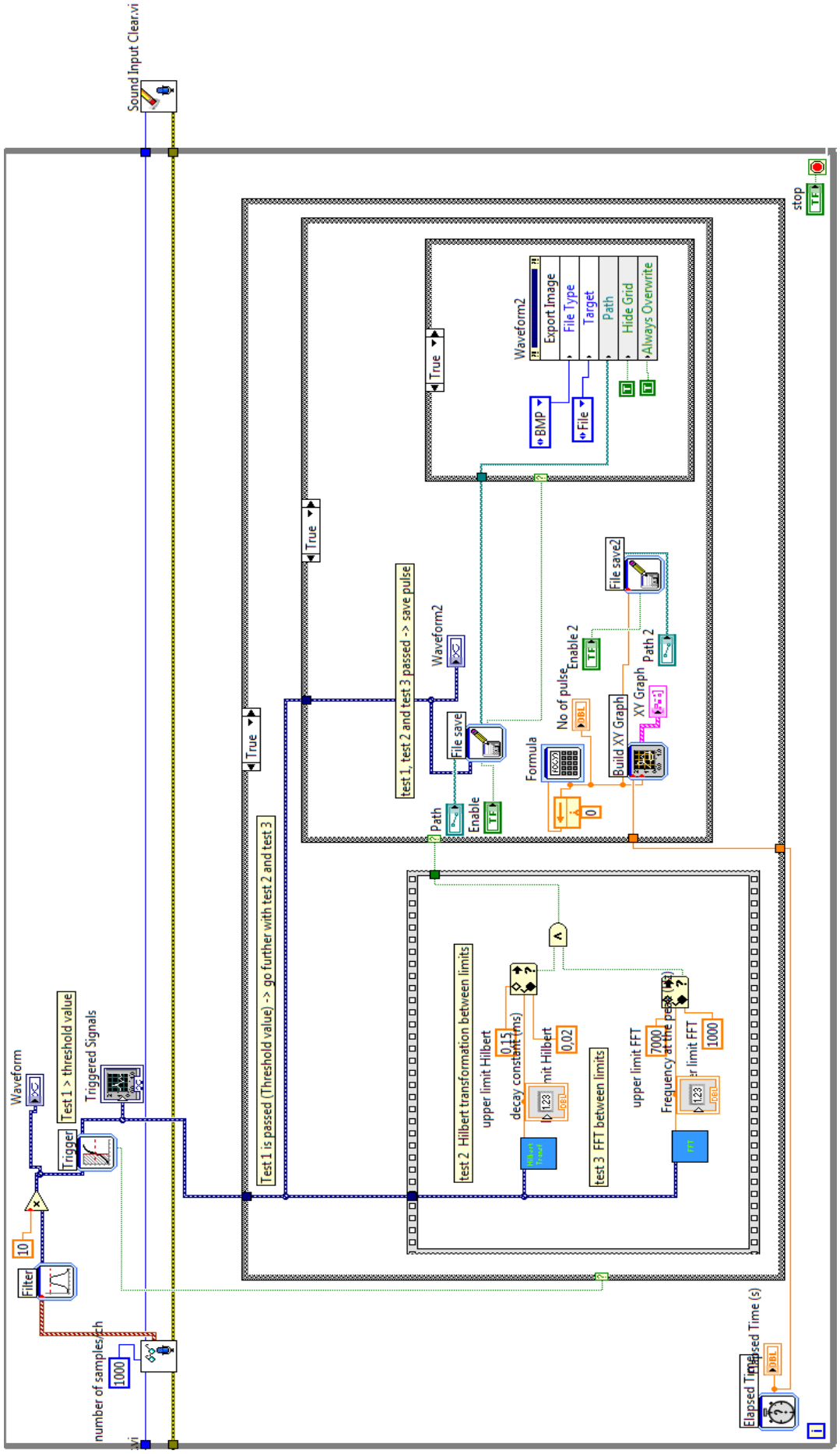

Auteursrechtelijke overeenkomst

Ik/wij verlenen het wereldwijde auteursrecht voor de ingediende eindverhandeling:
Fabrication and calibration of superheated droplet detectors (SDDs) for neutron dosimetry

Richting: **master in de industriële wetenschappen: nucleaire technologie-nucleaire technieken / medisch nucleaire technieken**
Jaar: **2017**

in alle mogelijke mediaformaten, - bestaande en in de toekomst te ontwikkelen - , aan de Universiteit Hasselt.

Niet tegenstaand deze toekenning van het auteursrecht aan de Universiteit Hasselt behoud ik als auteur het recht om de eindverhandeling, - in zijn geheel of gedeeltelijk -, vrij te reproduceren, (her)publiceren of distribueren zonder de toelating te moeten verkrijgen van de Universiteit Hasselt.

Ik bevestig dat de eindverhandeling mijn origineel werk is, en dat ik het recht heb om de rechten te verlenen die in deze overeenkomst worden beschreven. Ik verklaar tevens dat de eindverhandeling, naar mijn weten, het auteursrecht van anderen niet overtreedt.

Ik verklaar tevens dat ik voor het materiaal in de eindverhandeling dat beschermd wordt door het auteursrecht, de nodige toelatingen heb verkregen zodat ik deze ook aan de Universiteit Hasselt kan overdragen en dat dit duidelijk in de tekst en inhoud van de eindverhandeling werd genotificeerd.

Universiteit Hasselt zal mij als auteur(s) van de eindverhandeling identificeren en zal geen wijzigingen aanbrengen aan de eindverhandeling, uitgezonderd deze toegelaten door deze overeenkomst.

Voor akkoord,

Mommen, Stef

Datum: **18/08/2017**